# Impact of Renewable Energy Sources on Powers System Stability

**A Thesis Submitted**
**In Partial Fulfillment of the Requirements**
**for the Degree of**

# DOCTOR OF PHILOSOPHY

**in**

## Electrical Engineering

**by**

**Nitisha Sudhir Darwade**
**(Roll No. 2K21/Ph.D./EE/11)**

**Under the Supervision of**
Prof. S. T. Nagarajan




**Department of Electrical Engineering**

**DELHI TECHNOLOGICAL UNIVERSITY**
**(Formerly Delhi College of Engineering)**
**Shahbad Daulatpur, Main Bawana Road, Delhi-110042. India**

**December, 2025**

# ACKNOWLEDGEMENT

I would like to express my sincere gratitude to my supervisor, **Prof. S. T. Nagarajan**, for his invaluable guidance, motivation, and continuous support throughout my Ph.D. research. His insightful advice, patience, and encouragement have been instrumental in shaping this work.

My heartfelt thanks to my **husband, Mr. Chandramani Shahare**, for his constant support, understanding, and encouragement. His unwavering belief in me has been my greatest source of strength during challenging times.

Special love and gratitude to my **children, Arhant and Saisha**, for their patience and for filling my life with joy and inspiration. Their smiles gave me the strength to persevere and complete this journey.

I owe my deepest appreciation to my **parents** for their blessings, sacrifices, and unconditional love, which have been the foundation of all my achievements.

I also thank my **colleagues and friends** for their cooperation, encouragement, and insightful discussions that enriched my research experience.

Finally, I am grateful to the **Department of Electrical Engineering, Delhi Technological University**, for the academic support and conducive research environment provided throughout my doctoral studies.

(Nitisha Sudhir Darwade)

**DEHI TECHNOLOGICAL UNIVERSITY**
(Formerly Delhi College of Engineering)
Shahbad Daulatpur, Main Bawana Road, Delhi-42

## CANDIDATE'S DECLARATION

I **NITISHA SUDHIR DARWADE** hereby certify that the work which is being presented in the thesis entitled **Impact of Renewable Energy Sources on Power System Stability** in partial fulfillment of the requirements for the award of the Degree of Doctor of Philosophy, submitted in the Department of **Electrical Engineering**, Delhi Technological University is an authentic record of my own work carried out during the period from **2021** to **2025** under the supervision of **Prof S. T. Nagarajan**

The matter presented in the thesis has not been submitted by me for the award of any other degree of this or any other Institute.

**Candidate's Signature**

# DELHI TECHNOLOGICAL UNIVERSITY

(Formerly Delhi College of Engineering)
Shahbad Daulatpur, Main Bawana Road, Delhi-42

## CERTIFICATE BY THE SUPERVISOR(s)

Certified that **NITISHA SUDHIR DARWADE** (enrollment no **2K21/Ph.D./EE/11**) has carried out her research work presented in this thesis entitled **"Impact of Renewable Energy Sources on Power System Stability"** for the award of **Doctor of Philosophy** from Department of Electrical Engineering, Delhi Technological University, Delhi, under my supervision. The thesis embodies results of original work, and studies are carried out by the student herself and the contents of the thesis do not form the basis for the award of any other degree to the candidate or to anybody else from this or any other University/Institution.

Signature

Prof. S.T. Nagarajan

(Professor)

(Supervisor)

Department of Electrical Engineering
DELHI TECHNOLOGICAL UNIVERSITY
Shahbad Daulatpur, Main Bawana Road, Delhi-110042. India

Date:

# Impact of Renewable Energy Sources on Power System Stability

**Nitisha Sudhir Darwade**

## ABSTRACT

Ongoing global transition to sustainable and low-carbon energy systems has accelerated the integration of inverter-based resources (IBRs) including photovoltaic (PV) systems, wind turbines (WT), and battery energy storage systems (BESS) into modern power grids. This transition introduces new technical challenges for system operation, stability and protection. Traditionally, power systems relied on synchronous generators (SGs) as the primary sources of electricity generation. SGs inherently provide several advantageous characteristics including significant rotational inertia, robust fault current characteristics and predictable electromechanical dynamics. These properties ensured stable system operation and reliable coordination of protection schemes. In contrast, IBRs are grid-interfaced through power electronic converters, which do not contribute physical inertia and exhibit fundamentally different dynamic behavior during both normal and faulted conditions. IBRs fast control-based responses alter system frequency dynamics of conventional stability assessment tools and compromise the effectiveness of impedance and directional based protection schemes.

As the share of IBRs increases, power systems exhibit accelerated frequency excursions, higher rates of change of frequency (ROCOF), reduced frequency nadirs, altered inter-area oscillatory behavior and heightened vulnerability to transient and small-signal instability. These changes disrupt the assumptions supporting conventional protection schemes such as distance relays, directional relays, differential relays and power swing blocking (PSB) functions. Protection elements designed for predictable voltage and current responses may maloperate when exposed to converter-driven fault currents, distorted waveforms, or rapidly evolving system impedances. Specifically, negative-sequence relays lose dependability under IBR-driven fault characteristics, while distance relays exhibit reach inaccuracies due to distorted apparent impedance. The PSB function also becomes less effective, as it finds difficulty to distinguish true power swings from IBR-induced oscillations. Together, these factors necessitate a comprehensive re-evaluation of power system stability and protection under high renewable penetration, supported by advanced measurement and control methods.

The work carried out addresses these challenges through three primary contributions. First, it systematically assesses the impact of IBR integration on power system stability across transient, small-signal, and frequency domains. The research quantifies how reduced inertia and altered fault contributions affect stability margins, oscillatory behavior and wide-area interactions, with particular emphasis on inter-area oscillations, converter-driven modes, and spatial distribution of renewable generation.

Second, it investigates the performance of key protection schemes under high IBR penetration. The study evaluates negative-sequence-impedance-based directional relaying (67Q) under unsymmetrical fault conditions, analyzing negative sequence voltage ($V_2$), current ($I_2$), and their phase relationships to determine fault direction. In parallel, it examines the vulnerability of impedance-based distance relays and PSB functions to distorted or limited fault currents and accelerated power swings. By modelling both fault and swing scenarios, the research highlights under-reaching, over-reaching, delayed operation, and misclassification risks that arise when traditional relay logic interacts with low-inertia systems.

Third, the thesis develops and validates a novel methodology for real-time system inertia estimation. Recognizing that inertia is not directly measurable, the approach leverages phasor measurement units (PMUs) to capture synchronized, high-resolution bus voltage phase angles. Exploiting the close relationship between generator rotor angle oscillations and bus voltage phase angle oscillations, the derivative of phase angle is extracted and processed through a fuzzy logic inference system to estimate system inertia (Hsystem). This technique achieves high estimation accuracy (96.13%–99.98%) without relying on assumptions about frequency behavior, enabling effective inertia tracking under varying IBR penetration levels and providing actionable insights for adaptive protection, frequency control and emergency response.

Simulation studies employ benchmark power system models including the IEEE nine-bus system, the single-machine infinite bus system, and Kundur's two-area system, all modified to incorporate PV-based renewable generation. High-fidelity electromagnetic transient (EMT) simulations are performed in real time using OPAL-RT's HYPERSIM environment with a simulation step size of 50 microseconds, capturing fast transient phenomena occurring within microseconds to milliseconds. Time-domain simulations using PMU data further evaluate system response and protection behavior under various fault conditions.

Collectively, the results highlight that IBRs significantly alter the fault characteristics observed by conventional protection schemes, especially under negative sequence components. Directional overcurrent relays based on negative sequence impedance exhibit reduced sensitivity and accuracy, potentially leading to delayed or incorrect fault identification. Similarly, distance relays experience degraded performance under high IBR penetration, as reduced fault current levels and altered apparent impedance measurements can cause under-reach or over-reach conditions. Consequently, these relays may operate incorrectly or fail to detect faults within their intended protection zones. In addition, distance relay equipped with conventional PSB functions fail to differentiate between stable power swings and faults in low-inertia systems, increasing the risk of relay maloperation and system instability. The proposed inertia estimation technique, by contrast, provides a reliable and adaptive foundation for future protection and control schemes, offering system operators real-time visibility of inertia variations.

This thesis establishes a comprehensive framework for evaluating stability, protection challenges, and inertia estimation in contemporary power systems. By implementing real-time simulations and adopting PMU-based techniques on standard benchmark models, this thesis provides enhanced insights into wide-area monitoring and supports secure operation in renewable integrated power systems. The insights gained underscore the urgent need to redesign and adapt existing protection algorithms and stability assessment tools to accommodate the growing presence of IBRs and to develop resilient, flexible, and sustainable electric grids capable of withstanding disturbances as the energy transition accelerates.

**Key Contributions of the Thesis**

- **Comprehensive Stability Assessment:** Systematic evaluation of transient, small-signal, and frequency stability in benchmark test systems under varying levels of IBR penetration.

- **Protection Scheme Analysis:** In-depth investigation of negative-sequence-impedance-based directional relaying (67Q) performance under various faults with IBR integration.

- **Distance Relay and PSB Evaluation:** Detailed study of impedance-based distance protection and power swing blocking (PSB) functions under reduced inertia and distorted fault currents, identifying maloperation risks.

- **Novel Real-Time Inertia Estimation Method:** Development of a PMU-based technique using bus voltage phase angle derivatives and fuzzy logic to estimate system inertia online.

- **Real-Time Validation:** Implementation and testing of the proposed methods in the OPAL-RT HYPERSIM environment, providing high-fidelity validation under realistic conditions.

# List of Publications

**Journal Publication**

1. Darwade, N.S., Nagarajan, S.T. Investigation on Impact of Inverter-Based Resources on Power System Using Phasor Measurement Unit. *Arab J Sci Eng* (2025). https://doi.org/10.1007/s13369-025-10114-z.

**2.** Darwade, N., Nagarajan, S. Voltage Angle Based Power System Inertia Estimation Using Synchrophasor Technology. *J. Electr. Eng. Technol.* 20, 3925–3941 (2025). https://doi.org/10.1007/s42835-025-02305-3

**International Conference Publications**

1. N. S. Darwade and S. T. Nagarajan, "Investigation on Impact of Inverter Based Renewable Energy Sources on Distance Relaying," in *Proceedings of the 3rd IEEE International Conference on Power Electronics, Intelligent Control and Energy Systems, ICPEICES 2024*, Institute of Electrical and Electronics Engineers Inc., 2024, pp. 684–689. doi: 10.1109/ICPEICES62430.2024.10719278.

2. N. S. Darwade and S. T. Nagarajan, "Investigation on Impact of IBR on Negative Sequence Impedance Based Directional Protection," in *Proceedings of the 3rd IEEE International Conference on Power Electronics, Intelligent Control and Energy Systems, ICPEICES 2024*, Institute of Electrical and Electronics Engineers Inc., 2024, pp. 615–620. doi: 10.1109/ICPEICES62430.2024.10719257.

*3.* N. S. Darwade and S. T. Nagarajan, "Estimating Power System Inertia: A Study with Renewable Energy Integrated Power Networks." Presented in *IEEE 4th International Conference Smart Technologies for Power, Energy and Control December 10-13, 2025 | NIT Goa, India*

# CONTENTS

**Title** **Page No.**

**ACKNOWLEDGEMENT** ..... **ii**

**CANDIDATE'S DECLARATION** ..... **iii**

**CERTIFICATE BY THE SUPERVISOR(s)** ..... **iv**

**ABSTRACT** ..... **v**

**List of Publications** ..... **viii**

**List of Figures** ..... **xiii**

**List of Tables** ..... **xvi**

**List of Symbols and Abbreviations** ..... **xvii**

**CHAPTER 1 INTRODUCTION** ..... **1-13**

1.1 Power System Stability: Concept and Classification ..... 1

1.2 Significance of Power System Inertia ..... 4

1.2.1 System Inertia Calculation ..... 5

1.3 Impacts Of Renewable Energy Integration On Stability And Protection ..... 6

1.3.1 Challenges In Power System Stability ..... 6

1.3.2 Challenges in Power System Protection with IBRs ..... 7

1.3.2.1 Directional Relaying Issues: ..... 7

1.3.2.2 Distance Protection Malfunction: ..... 7

1.3 Need For Inertia Estimation ..... 9

1.4 Research Motivation ..... 9

1.5 WAMS (Wide Area Measurement System) ..... 11

1.7 Research Objectives ..... 12

1.8 Scope of the Work ..... 13

1.9 Thesis Organization ..... 13

**CHAPTER 2 LITERATURE REVIEW** ..... **14-27**

2.1 Influence of IBR on Power System Stability ..... 14

2.2 Impact of IBR on Protection Schemes ..... 16

2.3 Inertia Estimation ..... 18

2.3.1 Offline Inertia Estimation Methods ..... 18

2.3.2 Online Inertia Estimation Methods Using PMU Data ..... 19

2.4.1 Influence of IBR on Power System Stability ..... 20

**CHAPTER 3 INVESTIGATION ON IMPACT OF IBR ON POWER SYSTEM STABILITY .....27-51**

3.1 Introduction ..... 27

3.1.1 Specific Objectives ..... 29

3.1.2 Contributions ..... 29

3.2 Relation Between Power System Inertia, Protection Setting And Stability ..... 29

3.2.1 Expression of Power System Inertia ..... 30

3.2.2 Relation of Inertia With Bus Phase Angle Difference of Voltages And Critical Clearing Time ..... 30

3.3 PV Farm Implementation and PMU ..... 32

3.3.1 Photovoltaic Farm Implementation ..... 32

3.3.2 Photovoltaic Inverter control structure and Parameters ..... 32

3.4 Case Studies: Impact of Reducing Inertia on System Stability ..... 36

3.4.1 CASE I: Role of Kinetic Energy on Load Changes ..... 36

3.4.1.1 SCENARIO I: Inertia Variation of SG2 ..... 37

3.4.1.2 SCENARIO II: Inertia Variation of SG3 ..... 39

3.4.1.3 Comparison for Scenario I And II ..... 39

3.4.1.4 SCENARIO III: Replacement of SG2 with PV ..... 42

3.4.1.5 SCENARIO IV: Replacement of SG3 with PV ..... 42

3.4.2.1 SCENARIO I: Effect of inertia on rotor angle stability ..... 44

3.4.2.2 SCENARIO II: Effect of IBR on Protection Setting ..... 45

3.4.3 CASE III: Impact of IBR on Small Signal Stability ..... 46

3.4.3.1 SCENARIO I: Without Connecting PV ..... 47

3.4.3.2 SCENARIO II: SG1 replaced with PV farm ..... 48

3.4.3.3 SCENARIO III: SG3 replaced with PV farm ..... 48

3.4.3.4 SCENARIO IV: SG1 & SG3 replaced with PV farm ..... 49

4. Conclusion ..... 49

**CHAPTER 4 IMPACT OF IBR ON DIRECTIONAL PROTECTION SCHEMES .....51-63**

4.1 Introduction ..... 51

4.1.1 Objectives ..... 53

4.1.2 Contributions ..... 53

4.2 Basics of Directional Overcurrent Relaying ..... 53

4.2.1 Conventional Directional Overcurrent Relaying ..... 53

4.2.3 Setting of Negative Sequence-based Impedance based Directional Overcurrent Relaying 67Q ..... 54

4.3 Case Study ..... 55
4.3.1 Case I: Fault analysis of Nine Bus System ..... 55
Scenario I: LG fault near PV bus ..... 55
Scenario II: LLG fault at remote location to PV bus ..... 55
4.3.1.1 Scenario I: LG fault near PV bus ..... 56
4.3.1.2 Scenario 2: LLG Fault at Remote Bus from PV ..... 57
4.3.2 Case II: Fault analysis of Six Bus System ..... 58
4.3.2.1 Scenario I: LLG fault near PV bus ..... 58
4.3.2.2 Scenario I: LLG Fault Remote to PV Bus ..... 59
4.4 Result and Discussion ..... 60
4.5 Conclusion ..... 62
**CHAPTER 5 IMPACT OF IBR ON DISTANCE PROTECTION ..... 63-82**
5.1 Introduction ..... 63
5.1.1 Objectives ..... 64
5.1.2 Contributions ..... 64
5.2 Theoretical background ..... 65
5.2.1 Distance Relay Working Operation ..... 65
5.2.2 Mho Relay Setting ..... 65
5.2.3 Blinder Schemes ..... 66
5.2.4 Mathematical Relationship Between Inertia and ROCI ..... 66
5.3 Case Study ..... 67
5.3.1 Case Study I ..... 68
5.3.1.1 Scenario I: LLL fault at 25km from bus 7 ..... 69
5.3.1.2 LLL Fault at 50km From Bus 7 ..... 71
5.3.1.3 Scenario III: LG Fault at 50km From bus 7 ..... 72
5.3.1.4 Scenario IV LLL Fault at 90km from bus 8 ..... 73
5.3.1.5 Scenario V LG Fault at 30km from bus 8 ..... 74
5.4.2 Case Study II ..... 76
5.4.2.1 Scenario 1 Clearance of Fault without Removing Line ..... 79
5.4.2.2 Scenario 2 Removal of line connected between bus 7-8-9 ..... 79
5.5 Conclusion ..... 81
**CHAPTER 6 ONLINE INERTIA ESTIMATION USING PMU ..... 82-105**
6.1 Introduction ..... 82
6.1.1 Specific Objectives ..... 83
6.1.2 Contributions ..... 84

6.2 Voltage phase angle for estimation of system inertia ..... 84
6.2.1 Mathematical background of proposed concept for Inertia Estimation .... 84
6.2.2 Relation between phase angle and inertia constant H..... 86
6.3 Proposed Procedure for System Inertia Estimation..... 86
6 3.1 Design of Fuzzy Logic Estimator..... 86
6.3.1.1 Fuzzification..... 87
6.3.1.2 Fuzzy Rule Base..... 88
6.3.1.3 Defuzzification..... 88
6.3.2 Proposed Algorithm ..... 88
6.4 Case Study..... 89
6.4.1 Case –I Nine bus system ..... 89
6.4.1.1 Stage I: Design of fuzzy logic estimator to estimate Hsys..... 90
6.4.1.2 Stage II: Hsys estimation with Photovoltaic farm..... 94
6.4.2 Case –II Two area system ..... 97
6.4.2.1 Stage I- Design of fuzzy logic to estimate inertia ($H_{sys}$) ..... 97
6.4.2.2 Stage II- $H_{sys}$ estimation with Photovoltaic farm ..... 100
6.5 Limitation of traditional methods of estimation of system inertia based on frequency response..... 102
6.6 Conclusion..... 103
**CHAPTER 7 CONCLUSION, FUTURE SCOPE AND SOCIETAL IMPACT .....104-108**
7.1 Conclusion..... 104
7.2 Future Scope..... 105
7.3 Societal Impact..... 106
**REFERENCES .....108-123**
**Appendix-I.....124**
**Appendix-II.....124**
**Appendix-III.....125**

## List of Figures

Fig. 1.1 Classification of Power System Stability [4] ..... 2
Fig. 1.2 Block diagram of WAMS [70] ..... 12
Fig. 3.1 Single machine infinite bus system ..... 31
Fig. 3.2 EAC for three phase fault ..... 32
Fig. 3.3a Block diagram of Photovoltaic generation system ..... 33
Fig. 3.3b Schematic diagram for PV farm connected to grid ..... 33
Fig. 3.4 Schematic diagram for PV generation system ..... 34
Fig. 3.5a Active Regulator inner block diagram ..... 34
Fig. 3.5b DC link voltage Regulator inner block diagram ..... 35
Fig. 3.5c Reactive Power Regulator inner block diagram ..... 35
Fig. 3.5d Current Regulator inner block diagram ..... 35
Fig. 3.6 Functional PMU block diagram ..... 37
Fig. 3.7 Nine bus systems ..... 38
Fig. 3.8 Frequency plot at Bus 8 with respect to time ..... 39
Fig. 3.9 Frequency plot at Bus 8 with respect to time ..... 40
Fig. 3.10 Nadir Frequency with respect to time for G2 & G3 ..... 41
Fig. 3.11 Nadir Frequency with respect to Hsystem ..... 42
Fig. 3.13 PV Farm connected with G2 ..... 43
Fig. 3.13 PV Farm connected with G3 ..... 44
Fig. 3.14 Single machine infinite Bus model ..... 45
Fig. 3.15 Voltage angle during LLL Fault ..... 46
Fig. 3.17a Response of current during LLL Fault near Bus 2 ..... 47
Fig. 3.17b Response of current during LLG Fault near Bus 2 ..... 47
Fig. 3.18 Kundur's two area system ..... 48
Fig. 3.19 Power Flowing through Tie line with SG ..... 49
Fig. 3.20 Power Flowing through Tie line with PV in Area 1 ..... 49
Fig. 3.21 Power Flowing through Tie line with PV in Area 2 ..... 50
Fig. 3.22 Power Flowing through Tie line with PV in both Areas ..... 50
Fig. 4.1 Two source system with directional relay 67Q ..... 55
Fig. 4.2 Operating Area of Impedance base directional Overcurrent Relay 67Q ..... 56
Fig. 4.3 Nine bus system ..... 57
Fig. 4.4 Response of R78 for forward direction ..... 58
Fig. 4.5 Response of R78 for Reverse direction ..... 58
Fig. 4.6 Response of R96 for forward direction ..... 59
Fig. 4.7 Response of R96 for Reverse direction ..... 59
Fig. 4.8 Six Bus System ..... 60
Fig. 4.9 Response of 67QF connected at bus 4 ..... 60
Fig. 4.10 Response of 67QR connected at bus 4 ..... 61
Fig. 4.11 Response of 67QF connected at bus 8 ..... 61
Fig. 4.12 Response of 67QR connected at bus 8 ..... 62
Fig. 4.13 Response of Negative Sequence Voltage ..... 62
Fig. 4.14 Response of Negative Sequence Voltage Phase Angle ..... 63
Fig. 4.15 Response of Negative Sequence Current ..... 63
Fig. 4.16 Response of Negative Sequence Current Phase Angle ..... 63
Fig. 4.17 Response of Negative Sequence Impedance Phase Angle ..... 64

Fig. 5.1 Zones of Distance Relay ..... 67
Fig. 5.2 Characteristics of Mho relay ..... 67
Fig. 5.3 Blinder scheme adopted to analyze PSB ..... 68
Fig. 5.4 Single machine infinite bus model ..... 69
Fig. 5.5 Nine bus system ..... 70
Fig. 5.6 Mho relay operation during LLL fault at 25km ..... 71
Fig. 5.7 Response of circuit breaker post action from relay ..... 71
Fig. 5.8 Response of current during LLL fault ..... 72
Fig. 5.9 Impedance locus observed by Relay R78 during LLL fault at 25km ..... 72
Fig. 5.10 Mho relay operation during LLL fault at 50km ..... 72
Fig. 5.11 Response of circuit breaker post action from relay ..... 73
Fig. 5.12 Response of current during LLL fault ..... 73
Fig. 5.13 Impedance locus observed by Relay R78 during LLL fault at 50km ..... 74
Fig. 5.14 Mho relay operation during LG fault at 50km ..... 74
Fig. 5.15 Response of circuit breaker post action from relay ..... 74
Fig. 5.16 Response of current during LG fault ..... 75
Fig. 5.17 Impedance locus observed by Relay R78 during LLL fault at 25km .....75
Fig. 5.18 Mho relay operation during LLL fault at 90km from bus 8 ..... 76
Fig. 5.19 Response of current during LLL fault ..... 76
Fig. 5.20 Impedance locus observed by Relay R89 during LLL fault at 90km .....76
Fig. 5.21 Mho relay operation during LG fault at 30km from bus 8 ..... 77
Fig. 5.22 Response of circuit breaker post action from relay ..... 77
Fig. 5.23 Response of current during LG fault ..... 77
Fig. 5.24 Impedance locus observed by Relay R89 during LG fault at 30km .....77
Fig. 5.25 Kundur's Two area model ..... 79
Fig. 5.26 Impedance viewed by Relay at bus 7 ..... 83
Fig. 5.27 Impedance trajectories on RX plane ..... 83
Fig. 5.28 Rate of change of Impedance (ROCI) viewed by relay at bus 7 ..... 83
Fig. 5.29 Voltage angle difference between the buses 7 and 9 ..... 84
Fig. 6.1 Derivative of generator bus voltage phase angle for different inertia constant ..... 89
Fig. 6.2 Derivative of generator bus voltage phase angle for different types of loads 89
Fig. 6.3 Block diagram representation of Fuzzy logic ..... 90
Fig. 6.4 Membership function developed for fuzzy logic toolbox ..... 90
Fig. 6.5 Proposed algorithm for inertia estimation ..... 92
Fig. 6.6 Nine bus system ..... 93
Fig. 6.7 Response of derivative of generator bus voltage phase angle at bus 2 ..... 94
Fig. 6.8 Nine bus system with implementation of PV farm ..... 98
Fig. 6.9 Response of derivative of generator bus voltage phase angle at bus 2 ..... 98
Fig. 6.10 Response of derivative of generator bus voltage phase angle at bus 3 ..... 99
Fig. 6.11 Graphical representation of Theoretical Inertia and Inertia estimated ..... 100
Fig. 6.12 Two area system .....103
Fig. 6.13 Graphical representation of Theoretical Inertia and Estimated Inertia of Two Area System..... 100
Fig. 6.14 Frequency response during addition of different types of loads in the system for constant inertia ..... 105

Fig. 6.15 Frequency response during addition of load in the system for various values of inertia ..... 106

## List of Tables

Table 2.1 Comparison of algorithms available in literature with proposed method... 25
Table 3.1 Parameters of PV generation system ..... 36
Table 3.2 Nadir frequency and time to reach Nadir frequency ..... 39
Table 3.3 Hsystem with variation of individual generator's inertia ..... 42
Table 3.4 Nadir frequency with respect to time after implantation of PV at bus2 ..... 43
Table 3.5 Nadir frequency with respect to time after implementation of PV at bus3 .....44
Table 3.6 Effect of inertia for a fault duration of 0.39415 seconds ..... 46
Table 5.1 Summary of all performed scenarios ..... 78
Table 5.2 Hsys for the different generation share of PV ..... 81
Table 5.3 Variation in the response of impedance for different Hsys..... 82
Table 5.4 Variation in the response of impedance for different Hsys ..... 84
Table 6.1 Truth table for fuzzy logic development ..... 91
Table 6.2 Input data for fuzzy logic design ..... 94
Table 6.3 Membership function data for fuzzy logic ..... 95
Table 6.4 PV implementation to 9 bus system ..... 96
Table 6.5 Input data to design fuzzy logic for two area system ..... 98
Table 6.6 Membership function data for fuzzy logic ..... 99
Table 6.7 PV Farm addition to Two Area System ..... 101

## List of Symbols and Abbreviations

| | |
|---|---|
| RES | Renewable Energy Sources |
| SG | Synchronous Generator (SG); |
| PV | Photovoltaic |
| IBR | Inverter Based Resources |
| WT | Wind Turbine |
| BESS | Battery Energy Storage System |
| TSO | Transmission System Operators TSO |
| K.E | Kinetic energy |
| WAMS | Wide-Area Measurement System |
| PMU | Phasor Measurement Unite |
| PDC | Phasor Data Concentrator |
| ROCOF | Rate of change of frequency |
| V2 | Negative Sequence Voltage |
| I2 | Negative sequence Current |
| Z2 | Negative sequence impedance |
| 67Q | Negative Sequence impedance based directional relay |
| 21 | Distance Relay |
| ROCI | Rate of change of impedance |
| PSB | Power Swing Blocking |

# CHAPTER 1

# INTRODUCTION

Modern power system is undergoing a profound transformation driven by the global transition toward clean and sustainable energy. Increasing integration of renewable energy sources, has significantly altered the operational dynamics of conventional power grids. In introductory section of this thesis the background of power system stability, detailing its classification, significance, and the traditional methodologies used for inertia estimation is presented. This section further explores the challenges arising from reduced system inertia particularly its impact on stability and the performance of protection schemes. Finally, this chapter emphasizes the critical need for accurate inertia estimation in modern power systems to ensure reliable and resilient grid operation.

## 1.1 Power System Stability: Concept and Classification

Global transition toward sustainable and environmentally friendly energy generation has led to the widespread integration of Renewable Energy Sources (RES) such as solar photovoltaics (PV) and wind energy (WE) into modern power systems. These sources are typically connected to the grid through power electronic interfaces, commonly referred to as Inverter-Based Resources (IBRs). While IBRs play a crucial role in reducing carbon emissions and meeting global energy demand, their increasing penetration introduces new technical challenges in power system operation, stability, and protection[1], [2], [3]. According to the IEEE, "Power system stability is the ability of an electric power system, for a given initial operating condition, to regain a state of operating equilibrium after being subjected to a physical disturbance, with most system variables bounded so that practically the entire system remains intact"[4]. The stability of power systems has always been a critical area of focus to ensure uninterrupted and secure operation, especially when the system experiences disturbances such as faults, load changes, or switching actions.

In classical power systems, stability is fundamentally categorized into three major forms, as illustrated in Figure 1.1 [4]. These are voltage stability, frequency stability, and rotor angle stability, each addressing a distinct aspect of the system's ability to maintain equilibrium under various operating and disturbance conditions.

Voltage stability refers to the capability of a power system to maintain acceptable voltage magnitudes at all buses under normal operating conditions as well

as following a disturbance. It is primarily influenced by the balance between reactive power supply and demand. When the reactive power support in the system becomes inadequate, voltage levels begin to fall, which may eventually lead to voltage collapse or widespread system instability. The problem becomes more critical in heavily loaded networks or long transmission systems where reactive power losses are high[4].

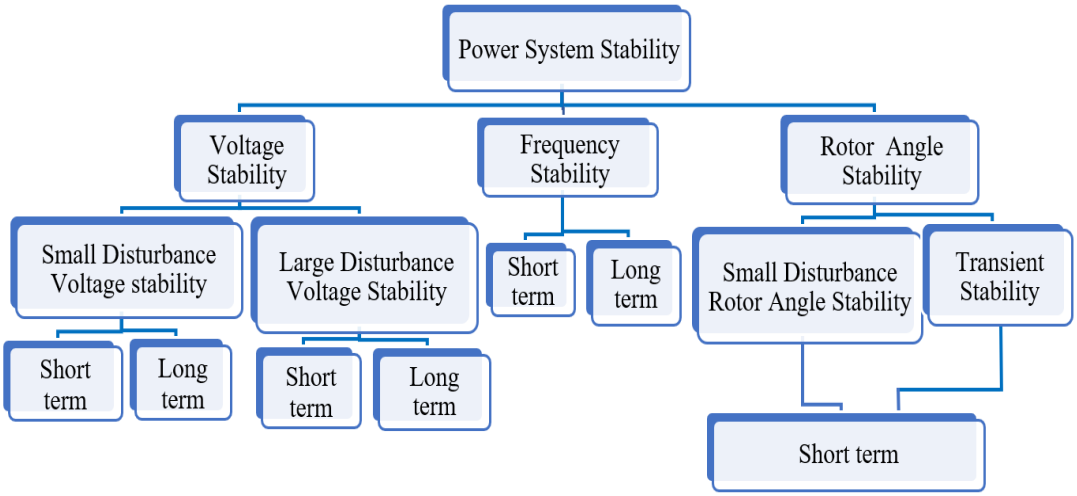


Fig 1.1 Classification of Power System Stability[4]

Frequency stability, on the other hand, concerns the system's ability to maintain a steady-state frequency following a significant disturbance, such as a sudden loss of generation or a large load increment. It arises from the imbalance between active power generation and demand. If the imbalance persists, system frequency deviates from its nominal value, potentially triggering under-frequency or over-frequency protection mechanisms. Hence, frequency stability depends on the system's inherent inertia and the dynamic performance of its primary and secondary control mechanisms[4].

Rotor angle stability is related to the maintenance of synchronism among interconnected synchronous generators during and after disturbances. It is governed by the electromechanical dynamics of generator rotors and the active power transfer between machines. When the accelerating and decelerating torques among generators are not balanced, the relative rotor angles may diverge, leading to a loss of synchronism and, in severe cases, system separation or blackout events[4].

The system's response to disturbances can further be classified based on the magnitude and duration of those disturbances. Transient stability deals with the ability of the system to maintain synchronism following large and sudden disturbances such as three-phase short circuits, the sudden tripping of a large generator, or the loss of a major transmission line. It involves highly nonlinear system dynamics and typically requires detailed time-domain simulations for assessment. In contrast, small-signal stability focuses on the system's ability to sustain stable operation under small, continuous perturbations, such as minor load fluctuations or gradual changes in control

settings [4]. Small-signal instability is often manifested through low-frequency oscillations that can deteriorate system performance over time.

Historically, these stability concepts were developed for conventional power systems dominated by large, rotating synchronous generators. In such systems, the physical inertia of rotating masses inherently supported the stability of both frequency and rotor angles. Initially, Inverter-Based Resources (IBRs) such as solar photovoltaic (PV) systems, wind turbines, and energy storage units were connected primarily at the distribution level, having minimal influence on the overall dynamic performance of the transmission system[5], [6], [7], [8].

However, with the rapid growth of renewable energy deployment, large-scale IBRs are now being integrated directly into transmission networks. This paradigm shift is transforming the fundamental dynamic behaviour of modern power systems. Unlike synchronous generators, IBRs are interfaced through fast-acting power electronic converters that lack physical inertia. Consequently, the traditional stability framework, which assumes inertia-based electromechanical dynamics, is no longer adequate for accurately characterizing system behaviour under high IBR penetration levels. As a result, new categories of stability phenomena have emerged that are not captured by classical classifications. Among these, converter-driven stability has gained attention, which arises from complex interactions among multiple power electronic converters and their associated control systems. Such interactions can lead to oscillations or instability, especially under weak grid conditions or in systems with high converter density. Another emerging form is resonance stability, characterized by high-frequency oscillations or control-loop instabilities that result from the coupling between inverter control dynamics and grid impedance[9].

The emergence of these new stability modes has necessitated a revision of traditional stability frameworks to incorporate the fast, nonlinear, and control-dependent behaviour of converter-dominated power systems.

Maintaining system stability under these new conditions poses several significant challenges:

1. The displacement of synchronous machines significantly reduces system inertia, resulting in rapid frequency deviations during disturbances. This shortens operator response time and increases the risk of frequency instability.

2. Protection and control schemes originally developed for synchronous generator–based systems may not operate reliably in IBR-rich grids. The fast electronic interfaces of IBRs alter fault current characteristics, delay detection, and weaken the coordination of traditional protection mechanisms.

3. Existing modelling frameworks require major revisions to accurately represent IBR dynamics. Conventional models based on swing equations and mechanical inertia fail to capture the fast, control-driven behaviour of converter-dominated systems. [10], [11], [12]

Given these emerging challenges, there is a growing need to develop new approaches for real-time system monitoring, inertia estimation, and adaptive protection. Advanced analytical and data-driven techniques are being explored to characterize system inertia, assess dynamic behaviour, and ensure stable operation under varying renewable penetration levels [13], [14].

These evolving conditions and challenges form the foundation and motivation for the research presented in this thesis, which aims to systematically investigate the impact of inverter-based resources on power system stability and propose methodologies to enhance the resilience, reliability, and secure operation of future converter-dominated grids.

Considering these emerging issues, the study of power system inertia becomes particularly essential, since it determines how quickly the system reacts to disturbances and is highly sensitive to the transition from synchronous machines to inverter-based resources.

## 1.2 Significance of Power System Inertia

Traditionally, power systems were predominantly powered by large Synchronous Generators (SGs), which inherently contribute inertia by the kinetic energy stored in the rotating masses, along with a minor contribution from frequency responsive loads[15], [16], [17]. Since the rotational speed of these generators is synchronized with the system frequency which resists abrupt frequency deviations by releasing or absorbing kinetic energy during system disturbances. This dynamic response plays a vital role in maintaining the grid frequency within acceptable operational limits. Globally, grid operators enforce strict frequency regulation usually maintaining frequency within ±0.05 Hz of the nominal value to preserve system stability and prevent under-frequency or over-frequency protection actions[18], [19], [20]. A stable operation of an AC power grid hinges on the continuous real-time balance between power generation and consumption. The stored kinetic energy in synchronous machines supports in maintaining this balance, particularly during the initial seconds of a contingency, such as a generator tripping or sudden loss of load. This immediate support provided by system inertia slows down the rate of change of frequency (ROCOF), facilitating short-term resilience for secondary control systems such as governor response to activate[21], [22].

The inertia constant (H), expressed in seconds, quantifies the duration a machine can supply its rated power using only its stored kinetic energy[15]. For synchronous machines, this constant typically ranges from 2 to 10 seconds, varying based on machine type and capacity. At the system level, the combined inertia constant reflects the overall capability of the grid to sustain power through kinetic energy alone in case of sudden imbalances[21], [23]. However, with the growing penetration of renewable energy sources especially those interfaced via power electronic inverters there is a significant reduction in system inertia. IBRs do not possess rotating masses that can store and release energy in the same way as synchronous machines. As a result,

the grid becomes more sensitive to disturbances, leading to faster frequency deviations and a higher risk of instability[24], [25]. This reduction in inertia poses new challenges for grid operators. Accurate real-time estimation and monitoring of system inertia are becoming increasingly important to ensure system reliability. Unfortunately, inertia is not a directly measurable parameter, which complicates its assessment. The need to develop reliable techniques for estimating system inertia under varying operational conditions has therefore become a key research area in modern power system engineering[26] [27]

### 1.2.1 System Inertia Calculation

The inertia of power systems is represented through the inertia constant (H), measured in seconds. For an individual synchronous generator, the inertia constant represents the amount of time the generator could supply its rated power using its stored kinetic energy, assuming no external energy input. Mathematically, it is expressed as equation 1.1:

$$\mathbf{H} = \frac{\mathbf{1}}{\mathbf{2}} \frac{\mathbf{J}\boldsymbol{\omega}_{\mathbf{n}}^{\mathbf{2}}}{\mathbf{S}_{\mathbf{n}}} \quad [\mathrm{s}] \tag{1.1}$$

Where J is the moment of inertia of a generator and turbine [kg/m2],
$\boldsymbol{\omega}_{\boldsymbol{n}}$ is the rated mechanical angular velocity of the rotor [rad/s],
Sn is the rated apparent power of the generator [VA].

Similarly, for a power system comprising multiple generators, an aggregate inertia constant can be defined to reflect the collective kinetic energy of all online generating units relative to the system's total rated capacity.

The aggregate equivalent inertia $\mathbf{H}_{\mathbf{sys}}$ of power system can be defined as time for which system can supply its rated power from its stored kinetic energy in the rotor. Aggregated Inertia of power system can be calculated by equation 1.2 utilizing inertia of individual turbine generator ,

$$\mathrm{H}_{\mathbf{sys}} = \frac{\sum_{\mathbf{i=1}}^{\mathbf{N}} \mathbf{S}_{\mathbf{ni}} \mathbf{H}_{\mathbf{i}}}{\mathbf{S}_{\mathbf{n,sys}}} \ [\mathrm{s}] \tag{1.2}$$

Where $\mathbf{S}_{\mathbf{n,sys}}$ given by,

$$\mathbf{S}_{\mathbf{n,sys}} = \sum_{\mathbf{i=1}}^{\mathbf{N}} \mathbf{S}_{\mathbf{ni}} [\mathrm{MVA}]$$

Sni is the rated apparent power of generator i [MVA],
Hi the inertia constant of turbine-generator i [s],
i is the number of synchronous generators [13], [15]

While the theoretical definition of inertia provides useful insight, in practical operation, the actual duration over which a generator or system can rely solely

on stored kinetic energy is constrained by protection settings. These include frequency thresholds and ROCOF limits that trigger automated actions such as generator tripping or load disconnection to protect equipment and system integrity[15], [28].

## 1.3 Impacts Of Renewable Energy Integration On Stability And Protection

### 1.3.1 Challenges In Power System Stability

The growing integration of IBRs is reshaping the dynamics of modern power systems. Unlike conventional synchronous generators, IBRs does not contribute physical inertia. This reduction in system inertia has emerged as a critical challenge for maintaining the stability and security of the grid, particularly during disturbances or sudden imbalances between generation and demand[21], [29].

A major consequence of reduced system inertia is the deterioration of frequency stability. When a disturbance occurs, low-inertia systems experience faster ROCOF and a deeper frequency nadir compared to conventional high-inertia systems[30], [31]. These conditions increase the likelihood of false or premature operation of underfrequency relays, which can unnecessarily disconnect loads and further destabilize the grid. As renewable penetration continues to rise, ensuring reliable frequency protection and control has become increasingly complex[32], [33].

Inertia reduction also impacts directly to the critical clearing time (CCT) for faults. In high-inertia systems, synchronous machines provide a natural buffer that allows protective devices sufficient time to isolate the fault while maintaining system stability[34], [35]. However, in IBR-dominated grids, this margin is significantly reduced, leaving the system more vulnerable to transient instability if faults are not cleared within a much shorter time[34].

Another important challenge is the intensification of inter-area oscillations. In traditional power systems, synchronous inertia provides effective damping of oscillatory modes between interconnected regions. With low inertia, however, the damping of these oscillations is weakened, increasing the risk of poorly damped or unstable modes. Such oscillations, if not controlled, can spread widely across the network and trigger large-scale instability or even blackouts[36]. In addition to these issues, IBR integration alters fault current characteristics, reduces available short-circuit strength, and modifies impedance profiles[37]. These changes reduce the effectiveness of traditional protection schemes such as distance relays, negative-sequence impedance-based relays, and power swing blocking functions. Therefore, the challenges posed by IBRs demand new approaches for system monitoring, protection, and control. Advanced solutions such as online inertia estimation, adaptive relay settings, and wide-area protection schemes are essential to ensure reliable and stable operation of future power systems dominated by renewable energy[3].

### 1.3.2 Challenges in Power System Protection with IBRs

The integration of IBRs significantly affects power system protection. Conventional protection schemes such as distance protection, directional protection, and differential protection assume predictable fault current characteristics, which are largely determined by the physical properties of SGs. However, IBRs produce controlled fault current responses limited by their protection systems, current-limiting features, and converter controls[1], [38], [39].

As a result, the following protection challenges have been observed:

#### 1.3.2.1 Directional Relaying Issues:

Directional relays (e.g., 67Q relays using negative sequence components) rely on phase relationships between voltage and current[40]. These relationships change with IBR integration, resulting in incorrect direction detection. IBRs exhibit distinct behavior during failures owing to their rapid control loops, restricted current contribution, and integrated protective features like current limitation. This challenges the core concepts of traditional protection systems. Fault current contributions from IBRs are often smaller in size, decrease rapidly, and frequently deviate from the sinusoidal patterns anticipated by conventional relays[41], [42].

The directional features of IBR-generated currents are significantly influenced by the kind of inverter control either grid-following or grid-forming as well as the position and intensity of the disturbance[8]. Consequently, traditional directional overcurrent relays (67Q) may inadequately detect faults or malfunction, resulting in erroneous trips or a failure to trip during actual failures. The negative sequence component of current and voltage is crucial for determining fault direction and system imbalance[43]. In traditional systems, this component serves as an input to relays such as overcurrent relay, directional overcurrent relay 50Q/51Q and directional relay 67Q for the detection of imbalanced failures. The angular relationship between the voltage and current negative sequence components is crucial for appropriate directed decision making. IBRs may induce negative sequence currents via various mechanisms, influenced by their control techniques, fault ride-through capabilities, and grid connection configurations. The inconsistency in negative sequence response hinders the dependable functioning of directional protection strategies [12], [44], [45], [46], [47], [48], [49]

#### 1.3.2.2 Distance Protection Malfunction:

Distance protection is a frequently used protection scheme to protect transmission line which evaluates the apparent impedance between the relay site and the fault location. If the calculated impedance falls inside the designated zones, the relay generates a trip signal. A specific distance relay, known as the mho relay, is especially useful on long lines owing to its circular working characteristic in the impedance plane[50], [51]. However, the integration of IBRs creates major hurdles to

traditional distance relays[38]. Traditional protection methods depend on three essential assumptions:

1. High and sustained fault current levels provided by synchronous generators.
2. Consistent impedance trajectory during faults for relay operation.
3. Sufficient system inertia, [52]

These assumptions enable moderate changes in frequency and voltage during disruptions. These assumptions do longer hold in power networks with substantial IBR penetration. IBRs do not offer physical rotational inertia and frequently restrict their fault current contribution via built-in protective features in the converter. As a consequence, the size and shape of fault current waveforms are drastically altered often restricted in amplitude, swiftly curtailed, and occasionally even non-sinusoidal. This shift in fault current characteristics might lead distant relays to alter fault location or fail to work entirely[53], [54], [55]. Furthermore, the dynamic response of IBRs during transients is generally driven by rapid digital control systems rather than the electromechanical behavior of synchronous generators. These differential effects the impedance trajectory recorded by distance relays, making them more prone to malfunction under both t fault circumstances and non-fault disturbances, such as power fluctuations[56].

Conventional distance protection solutions are not intrinsically built to manage the fast-changing dynamics provided by IBRs. For example, relays may wrongly perceive transitory impedance behavior during a power swing or inverter fault ride-through event as a line fault, resulting to unintended tripping[3], [57], [58].

Power swings are oscillations in power flow caused by disturbances such as generator disconnections, sudden load variations, or network switching. During these events, the internal voltages of generators across different parts of the grid can differ, resulting in dynamic fluctuations in active and reactive power flow. In conventional systems, these swings occur in a relatively stable and damped manner due to high system inertia. The Power Swing Blocking (PSB) function in modern distance relays is designed to detect such swings and block relay operation when the impedance enters tripping zones due to swing rather than an actual fault[59]. PSB algorithms work on the principle that power swings cause slow impedance movement across the relay characteristic, while faults result in abrupt impedance changes. This temporal distinction allows relays to differentiate between swings and genuine fault conditions. However, with the integration of IBRs, the nature of power swings and fault dynamics has changed considerably. IBRs typically respond to system disturbances via fast-acting control systems rather than physical inertia, resulting in altered swing trajectories and faster frequency variations. The lack of mechanical coupling and reduced inertia make the system more susceptible to transient instability, especially under large disturbances. Consequently, the behavior of apparent impedance during swings becomes less predictable, challenging the effectiveness of traditional PSB mechanisms[60].

## 1.3 Need For Inertia Estimation

The accurate estimation of system inertia has become a fundamental necessity in the operation and planning of modern electric power systems. As power systems transition from conventional centralized generation to distributed, inverter-based renewable generation, the traditional assumptions regarding system inertia no longer hold. Historically, inertia has been provided by the large rotating masses of synchronous generators where the rotational kinetic energy inherent in these machines plays a crucial role in stabilizing the system frequency during disturbances. However, unlike other physical quantities such as voltage, current, or frequency that can be measured directly using conventional sensors like Phasor Measurement Units (PMUs), system inertia is an abstract and indirect parameter. It depends on the aggregate physical properties mainly the moment of inertia and rated power of all online synchronous machines, and on how these machines are operated at any given time. Moreover, inertia is inherently dynamic, varying with changes in generator dispatch, system topology, and operational conditions[61], [62].

The growing integration of RES has significantly altered the inertial behavior of power systems. Unlike synchronous generators, inverter-based resources (IBRs) do not have rotating masses that are electromagnetically coupled to grid frequency. Consequently, they do not naturally contribute to system inertia. In power systems with a high penetration of IBRs, this leads to reduced total system inertia and, therefore, a greater sensitivity to frequency disturbances[63], [64]. Furthermore, the complexity is the decentralized and variable nature of modern power generation. Inertia can no longer be assumed constant over time or uniform across the network. The generation mix is now highly dynamic, with RES output fluctuating due to weather conditions, and with synchronous units being frequently brought online or taken offline depending on system needs and market conditions. As a result, real-time knowledge of system inertia is critical for maintaining frequency stability, designing protection schemes, and configuring automatic controls such as governor response and under-frequency load shedding (UFLS). This has created a growing demand for online or real-time inertia estimation methods, particularly those that can leverage high-resolution, time-synchronized measurements provided by PMUs[65], [66].

Addressing this challenge is essential for enhancing system visibility, informing operational decisions, supporting frequency regulation services, and safeguarding power system stability in the face of rapid structural transformations driven by renewable energy integration.

## 1.4 Research Motivation

With the increasing penetration of IBR, introduces new and complex challenges for both power system dynamics and protection. Specifically, two major issues have emerged as critical concerns:

(1) The instability of power system frequency and dynamics due to the reduction in system inertia, and

(2) The declining reliability of conventional protection schemes due to the altered fault current behavior introduced by power electronic interfaces.

These interlinked challenges pose serious hazards to the stability, security, and resilience of future power systems especially those with high levels of renewable energy integration. With lower inertia, the system experiences a higher rate of change of frequency (ROCOF), leading to sharper and more severe frequency dips during events such as generator trips or sudden load changes. This necessitates real-time awareness of the system's inertia level so that appropriate control or mitigation strategies can be applied in time. However, inertia is not a directly measurable quantity, and conventional methods for its estimation rely heavily on offline system models and assumptions. These methods may not be effective in modern, dynamically changing power systems with variable operating conditions. Therefore, there is a strong need for real-time, measurement-based methods of inertia estimation, particularly those that can leverage high-resolution, time-synchronized data provided by Phasor Measurement Units (PMUs). Such techniques must be robust enough to account for variations in system topology, load demand, and generation mix.

Simultaneously, the shift in generation technology has also affected the behavior of fault currents, presenting serious challenges to conventional protection schemes. Protective devices such as directional overcurrent relays and distance relays are designed based on the predictable, high-magnitude fault current contributions from synchronous machines. In contrast, IBRs owing to their power electronic interfaces and control limits contribute much lower and more variable fault currents, typically governed by internal control logics and current-limiting mechanisms. As a result, traditional protection functions may fail to detect faults accurately or may mis operate under normal or slightly disturbed conditions. For instance, the directionality logic used in 67Q (negative-sequence directional overcurrent) relays may become unreliable when the magnitude and angle of negative-sequence components are affected by the control strategies of IBRs. Similarly, distance relays 21, especially those employing impedance-based measurements such as the Mho relay, may operate incorrectly due to altered voltage-current relationships during IBR-dominated faults.

An additional complexity arises in the operation of power swing blocking (PSB) functions, which are commonly employed in distance relays to differentiate between faults and power swings. In high-inertia systems, power swings are generally slow and well-damped, allowing PSB functions to distinguish them from faults effectively. However, in low-inertia systems, power swings tend to be faster and less predictable due to the reduced electromechanical damping and the dynamic control actions of IBRs. This can lead to misclassification of fast power swings as genuine faults, causing unnecessary tripping of transmission lines and compromising grid reliability. Such unintended relay operations during fast transient events are of growing concern, particularly as the grid becomes more converter dominated.

This thesis is therefore motivated by the need to develop a complete framework that addresses the combined impact of IBRs on system dynamics and protection. The research aims to propose a real-time method for system inertia estimation using PMU-based phase angle data, and investigate the behavior of protection functions such as distance and directional relays in low-inertia, IBR-rich environments, with a specific focus on the operation and maloperation of PSB schemes. By bridging the gap between system dynamics and protective relaying, this research seeks to contribute toward the design of future-ready, resilient power systems that can ensure stability and security in the face of growing renewable integration.
The increasing integration of IBRs presents three challenges:

(1) Instability in power system dynamics due to reduced inertia,
(2) Unreliable operation of protection schemes due to altered fault current profiles.
(3) Online inertia estimation

These challenges are critical in the context of large-scale renewable deployment and can significantly affect power system reliability and security.

The motivation for this research arises from the following observations:

- There is a lack of effective real-time methods for estimating system inertia that utilize PMU data and are robust under varying operating conditions.

- Conventional protection functions such as directional overcurrent relays and distance relays are prone to maloperation under high IBR penetration.

- Power swing blocking functions may misclassify fast power swings as faults in low-inertia systems.

- Existing studies often focus on one aspect (e.g., either inertia or protection), but an integrated perspective is needed to understand the cross-domain interactions between protection and system dynamics.

## 1.5 WAMS (Wide Area Measurement System)

With the advancement of synchrophasor technology, extensive research has been directed toward the development and application of Wide Area Measurement Systems (WAMS). A WAMS is a coordinated network of Phasor Measurement Units (PMUs) connected through a high-speed communication infrastructure. All PMUs installed at various substations transmit synchronized data to a Phasor Data Concentrator (PDC) as presented in block diagram 1.2. Super PDC serves as a central computing unit that collects, aligns, and stores information from all PMUs for real-time monitoring and future analysis of network performance. The PDC can

continuously observe system conditions, issue warnings to operators, or trigger control actions in response to disturbances. The key feature of this technology is the GPS-based synchronization of PMUs, which enables accurate, time-stamped phasor measurements across wide geographic areas. PMUs typically operate at reporting rates of 10, 30, 60, or 120 frames per second, converting instantaneous voltage and current signals into synchronized phasor data. This capability provides a precise, real-time view of system dynamics, making WAMS an indispensable tool for stability assessment, fault detection, and advanced grid control in modern power systems [67], [68], [69]

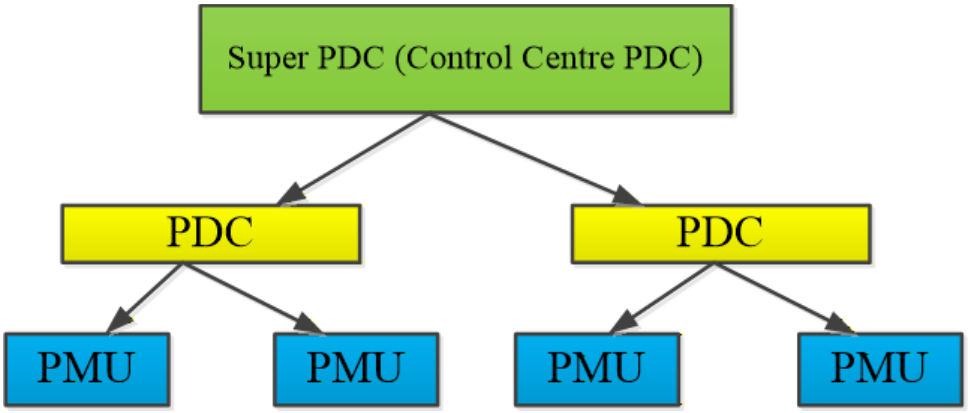


Fig.1.2 Block diagram of WAMS[70]

## 1.7 Research Objectives

This thesis addresses the above challenges through a comprehensive study that combines system modelling, real-time simulations, and data-driven estimation techniques. The specific objectives of the research are:

1. To analyze the impact of IBR integration on power system stability, including frequency, rotor angle, and small signal stability, through time-domain simulations on standard test systems.

2. To investigate the behavior and limitations of conventional protection schemes (directional overcurrent relays and distance relays) in IBR-dominated power systems, particularly under negative sequence and power swing conditions.

3. To develop and validate a novel fuzzy logic-based inertia estimation method using bus voltage phase angle derivatives measured from PMUs.

4. To evaluate the performance of the proposed estimation and protection approaches using real-time simulation platforms like OPAL-RT and HYPERSIM, ensuring high-fidelity testing of transient behaviors.

## 1.8 Scope of the Work

This research considers benchmark power systems such as the IEEE nine-bus system, a single-machine infinite bus system, and Kundur's two-area system. These systems are modified to incorporate PV-based IBRs. Simulation studies are conducted using OPAL-RT's HYPERSIM platform with a 50 μs time step, allowing the analysis of fast transients and detailed relay responses. The work focuses on:

- Dynamic system response under different fault conditions.
- Protection maloperations due to IBR characteristics.
- Validation of real-time inertia estimation using PMU-based signals.

## 1.9 Thesis Organization

This thesis is structured as follows:

- **Chapter 2:** Literature Review – Provides a review of existing work on power system stability, protection schemes, and inertia estimation in IBR-integrated systems.

- **Chapter 3:** Investigation on Impact of IBR on power system stability- Presents detailed analysis of impact of IBR on inertia, frequency stability,

- **Chapter 4:** Impact of IBR on Directional Protection Schemes– Presents the simulation results and analysis of relay behavior under various fault scenarios.

- **Chapter 5:** Impact of IBR on Distance protection Schemes- Investigates Impact of IBR on performance of distance relay 21 and Power Swing Blocking. Function in distance relays.

- **Chapter 6**: Online Inertia Estimation using PMU- Details the proposed algorithm, its implementation using PMU data, and performance validation.

- **Chapter 7:** Conclusion, Future scope and Societal impact– Summarizes the key findings and suggests directions for future research

# CHAPTER 2

# LITERATURE REVIEW

Transition of power systems toward renewable and inverter-based generation has stimulated extensive research in power system stability, protection coordination, and inertia estimation. A comprehensive review of the existing literature is essential to identify the current state of knowledge, highlight technical gaps, and justify the need for the present research.

This literature survey aims to systematically explore and analyses prior work related to the impact of inverter-based resources (IBRs) on system dynamics, the limitations of protection schemes in low-inertia environments, and emerging techniques for real-time inertia estimation.

The discussion is organized systematically to provide clarity and coherence, covering three major areas:

## 2.1 Influence of IBR on Power System Stability

The conventional classification of power system stability is currently undergoing significant revisions to account for the emerging challenges posed by the integration of Inverter-Based Resources (IBRs) Initially, IBRs were primarily integrated at the distribution level, where their impact on overall system stability was relatively negligible. As RES integration have driven large-scale deployment, particularly at the transmission network level, the influence of IBRs on power system behavior has become more pronounced. A key concern is the absence of synchronous generator-like characteristics in IBRs during disturbances, which impairs the system's ability to respond effectively and maintain equilibrium [3], [10]. Moreover, the integration of IBRs directly affects several parameters critical to system stability. These include system inertia, fault current levels, oscillatory behavior, and power quality issues such as voltage flicker and harmonic distortion [11], [12], [71]. These changes undermine the essential presumptions on which traditional protection and control strategies were developed.

A comprehensive survey of literature reveals several efforts to assess the influence of IBRs on various aspects of power system stability. The predominant areas of focus include frequency stability, rotor angle dynamics, voltage control [44], [72], [73]. Among these, the impact of IBRs on system inertia, power oscillations, and

reliability has emerged as a particularly critical concern. Earlier studies emphasized that one of the most consequential effects of IBR integration is the reduction in system inertia, which weakens the system's capability to resist sudden frequency deviations during disturbances [21] [74]. This degradation of inertial support once inherently provided by the rotating masses of synchronous generators poses significant challenges to both operational stability and protective coordination in low-inertia grids.

Further in the literature, the critical importance of inertia in power system stability has been widely recognized, its role in resisting frequency deviations and supporting the system during disturbances has been comprehensively addressed. Studies such as those in [11], [21] have thoroughly investigated the implications of inverter-based resource (IBR) integration on system stability. Specifically, the influence of IBRs has been analyzed either by directly modifying the inertia of synchronous generators or by introducing IBRs into simulation models to observe the resulting dynamic behavior. Several researchers have examined how reduced system inertia, caused by displacement of conventional generators with IBRs, influences frequency response under under-frequency load-shedding (UFLS) scenarios [11], [75] Andreas et al. [76] highlighted the significant reduction in system inertia due to extensive IBR integration over recent years. The resulting decline in frequency support capabilities has become a key issue, especially during disturbances that demand immediate system response. Much of the following literature explores the relationship between reduced inertia and the frequency dynamics of power systems, including nadir frequency, rate of change of frequency (ROCOF), and inter-area oscillations. Son et al. [77] proposed a Frequency Nadir Index (FNI) to quantify the relationship between inertia and frequency nadir, providing an analytical approach to evaluate system resilience. Atia and Jovica [78] modelled multiple IEEE standard benchmark systems incorporating IBRs to study the effects of energy storage and synthetic inertia on frequency response characteristics. In a two-area test system, Andreas et al. [76]investigated the evolution of inter-area oscillations as generator inertia was systematically reduced, showing increased system vulnerability. Liu et al. [79] focused on virtual inertia networks, analyzing the influence of various IBR types connected at different nodes in a two-area system, and how these affect power oscillations. Their findings demonstrate that virtual inertia implementation through control strategies has a significant impact on damping and oscillation modes. Similarly, Xu et al. [80]demonstrated how decreased inertia alters primary frequency response and local oscillation modes, using both small-scale systems and large synthetic models. You et al. [81] investigated the impact of photovoltaic (PV) integration on inter-area mode oscillations, revealing that as PV penetration increases, oscillating frequencies rise and mode shapes evolve, potentially introducing new oscillatory modes into the system. Zhou et al. [82] examined low-frequency oscillations in PV-based power systems and proposed the integration of Virtual Synchronous Generators (VSGs) to introduce virtual inertia and damping, improving system stability. Agrawal et al. [83]analyzed the frequency response and oscillatory behavior in a modified power system where synchronous generators were replaced by wind turbines. Their findings underscore the degradation in primary frequency response and mode stability as system inertia decreases.

Collectively, these studies cover a wide range of IBR-related stability concerns in addition to exploring inertia-related effects, Yijing Liu et al. [84] investigated the ACTIVSg200 synthetic power system to analyze the impact of system inertia on the critical clearing time (CCT) during fault conditions. Their work highlights how variations in inertia can significantly influence system transient stability. Furthermore, Phasor Measurement Units (PMUs) have demonstrated the capability to monitor dynamic responses of power systems under both steady-state and transient scenarios [85]. With the growing integration of Inverter-Based Resources (IBRs), which introduces variability in system inertia, it has become increasingly important to estimate inertia accurately in grids comprising diverse generation technologies. Accordingly, recent research efforts have focused on developing techniques to assess inertia and its subsequent impact on overall power system performance and stability.

## 2.2 Impact of IBR on Protection Schemes

Transition of power generation with IBR has introduced significant challenges to the protection mechanisms of modern power systems. IBRs are typically interfaced through power electronic converters, which differ fundamentally from conventional synchronous generators (SGs) in their operational dynamics as well as fault response characteristics. One of the primary concerns arising from high IBR penetration is the compromised performance of traditional protection schemes, such as distance protection, directional protection, and differential protection. These schemes were originally designed with the assumption of predictable fault current contributions from rotating machines. However, IBRs often do not produce fault currents of the same magnitude or phase characteristics as synchronous generators. Their current-limiting controls, lack of rotational inertia, and fast converter control response lead to reduced and distorted fault currents, making it difficult for conventional protection relays to detect and isolate faults accurately. As a result, the reliability and selectivity of protection systems are being challenged, potentially leading to maloperation or failure to operate under fault conditions[38], [56].

Upon literature survey, reference [86], [87] highlighted the maloperation of transmission line protection schemes in systems with significant penetration of Inverter-Based Resources (IBRs). The study in predicts that multiple transmission line protection schemes, including distance and overcurrent protection may fail to operate reliably in IBR-dominated networks. Similarly, Haddadi et al.[38], [42], observed that the integration of IBRs adversely affects the performance of conventional distance and differential protection methods, potentially leading to incorrect relay operation. Hooshyar et al. [72] investigated the impact of IBRs on short-circuit current behavior and system impedance, which in turn contributes to protection failures. Mishra et al. [88] analyzed the analyzes the behavior of positive and negative sequence components during faults, highlighting how their magnitudes and phase angles deviate in the presence of IBRs. In addition, proposed an improved distance protection strategy to address associated challenges. In addition, Grande et al. [89]demonstrated the altered voltage and current response resulting from the integration of IBRs, underscoring the need for adaptive protection approaches suited to these new system dynamics. Several

studies in the literature have comprehensively addressed the challenges posed to various protection schemes due to the integration of Inverter-Based Resources (IBRs) in modern power systems. The impact of IBRs on traditional protection mechanisms has been extensively discussed by the authors in [90] [91], [92] research outline the limitations of conventional relaying techniques under altered system dynamics. Reference further elaborates on the malfunctioning of distance and differential protection in transmission systems with high levels of inverter-based generation.

To address these challenges, researchers have proposed modifications and alternatives. For instance,[87] investigates the limitations of distance protection and introduces an improved detection strategy to enhance fault identification accuracy. The authors of [72]examine how IBR integration affects impedance-based distance relaying under various types of balanced faults. Meanwhile, reference [93] explores the impedance angle characteristics under varying fault resistance values, providing insights into relay performance under different fault scenarios. In [94], the focus shifts to analyzing negative sequence power during unbalanced faults, offering a method to assess system response and improve fault detection reliability.

Further in literature numerous studies addressing the challenges faced by distance relays and the broader protection schemes due to the integration of Inverter-Based Resources (IBRs) in modern power systems. The authors in [90]examine various protection system challenges introduced by IBRs, emphasizing the limitations of conventional relaying methods under altered grid dynamics. Similarly, [95] demonstrates that the variation in fault current contribution from IBRs leads to failures in distance relay operation, particularly due to reduced fault current magnitudes. In[96], the researchers show that the positive and negative sequence currents generated during faults in IBR-connected systems are significantly lower than those produced by conventional synchronous generators, which affects the reliability of relay operation. Reference [97] presents a simulation-based analysis of Mho relay behavior under varying fault resistance conditions, showing that IBR integration often leads to undetected faults. Finally, in [72], the authors analyze how the variation in system impedance response caused by IBRs leads to failures in distance relay performance, further underscoring the need for protection system enhancements in evolving grid environments.

The integration of Inverter-Based Resources (IBRs) in modern power systems introduces dynamic and programmable characteristics that can rapidly alter system behavior, significantly impacting the effectiveness of conventional protection schemes [21] Unlike traditional synchronous generators, IBRs contribute considerably lower fault currents, thereby reducing the sensitivity of protective relays and undermining their ability to detect faults accurately [86]. One of the key challenges posed by IBR integration is its impact on line current differential protection (87L), where the traditional assumptions regarding fault current magnitudes no longer hold true, leading to maloperation or failure of protection schemes [93],[42] Furthermore, negative sequence-based directional relays may also become ineffective in fault detection when IBRs are present, as observed in [98].

During balanced fault conditions, the performance of distance relays is significantly affected by the fault current characteristics of squirrel cage induction generators (SCIGs), which may under-reach due to inadequate voltage support and reduced fault current magnitudes. Similarly, the fault current contributed by doubly-fed induction generators (DFIGs) contains frequency components that deviate from the nominal system frequency, as a result of rotor speed fluctuations. These variations in frequency disrupt accurate impedance calculation, leading to maloperation of distance relays [72].[99] Studies also report that mho relays fail to detect faults accurately during different fault scenarios applied on transmission lines with IBRs, resulting in delayed tripping actions [100].

While Power Swing Blocking (PSB) is a critical concept in ensuring protection stability during stable oscillations, [60], [101], limited research has been conducted on its performance in systems with high IBR penetration. For instance, the methodology proposed in [102]utilizes local measurements to block the operation of third-zone distance relays during power swings. However, the study does not account for the presence of IBRs, limiting its applicability in modern grid environments. More recent investigations have begun to explore the challenges posed by IBRs on PSB. Reference [103]simulates power swings in a transmission system and establishes a relationship between the rate of change of impedance and system inertia. Nonetheless, the absence of fault scenarios and lack of an IBR representation reduce the practical relevance of the study for real-world power system conditions.

## 2.3 Inertia Estimation

Inertia estimation methods are broadly classified as offline and Online inertia estimation methods.

### 2.3.1 Offline Inertia Estimation Methods

Offline inertia estimation is typically referred to as post-disturbance analysis, where the estimation is performed only after a major event such as a fault or a frequency dip has occurred. These methods are rooted in the classical swing equation, and rely on parameters like frequency deviation, change in active power, Rate of Change of Frequency (ROCOF), or the second derivative of the rotor angle at the time of disturbance [104][105], [106], [107], [108]

One of the major challenges in offline methods is the noise and oscillatory behavior associated with direct measurements of frequency transients. This noise often arises due to the synchronizing power effect of generators. To address this, researchers have proposed various signal-processing techniques such as curve fitting and the use of different low-pass filters, including Butterworth filters and filters with 0.5 Hz and 5 Hz cutoffs, to suppress unwanted noise components in frequency signals [107], [108], [109], [110].

Moreover, direct measurement of ROCOF and active power variation at individual generator locations during a disturbance is not only technically challenging

but often infeasible in real-time environments. In many cases, frequency is measured from a single system location, or an average system frequency is used—both of which are not always reliable for accurate ROCOF estimation [111]. Another critical factor is the timing of the disturbance. Since ROCOF is time-sensitive, knowing the exact moment when a disturbance begins is essential. Some studies have addressed this issue by adopting Detrended Fluctuation Analysis (DFA), which helps identify the precise timing of an event and therefore improves the reliability of the inertia estimation process [104],[110]. Additionally, the location of the disturbance and the quality of measurements recorded from that location play a crucial role in the accuracy of the inertia estimation. These considerations make it clear that while offline methods are informative, they face significant practical challenges when applied to complex, real-world power systems.

### 2.3.2 Online Inertia Estimation Methods Using PMU Data

With the advent of Wide Area Measurement Systems (WAMS), Phasor Measurement Units (PMUs) have become central to real-time power system monitoring. These devices provide high-resolution time-synchronized data, enabling real-time estimation of system dynamics including inertia [85]. A number of recent studies have capitalized on PMU data to develop online inertia estimation techniques. Ariff et al. [112] proposed a method using PMU measurements coupled with an Unscented Kalman Filter (UKF). This approach allows for accurate estimation of dynamic model parameters, even in the presence of noise. Another significant contribution by Wall et al.[113] introduced a Sliding Window Method (SWM) for inertia estimation. This technique employs a sequence of data windows immediately following a disturbance to simultaneously estimate both the system inertia and the precise time of the event.

Petra et al. [114]adopted a more model-based approach using the magnitude and phase angle of load bus voltages. Their technique involves solving differential-algebraic equations (DAEs) that describe the dynamic behavior of generators and network components. These equations are embedded within a Bayesian framework, and two distinct estimation techniques adjoint-based and stochastic spectral were applied. Tuttleberg et al. [115] developed a method that estimates online inertia using PMU-based active power and frequency data, highlighting the practicality of using operational measurements in real-time. Tan et al. [116] proposed a decentralized, data-driven estimation approach grounded in Thevenin's Theorem. Their methodology identifies a mathematical correlation between generator terminal voltage, current, and internal rotor speed to estimate inertia. Cao et al. [117]leveraged steady-state and low-frequency variation data recorded over two years from three geographically dispersed PMU locations. They employed Switching Markov Gaussian Models trained on this dataset to estimate system inertia in real time. This approach reflects the growing trend of applying machine learning and statistical models in power system estimation. Furthermore, Andreas and Byongjun [118]implemented Artificial Neural Networks (ANNs) to train the system frequency response under varying conditions, thereby enabling an adaptive, data-driven approach to online inertia estimation. However, despite these advancements, limitations remain. Kerdphol et al.

[109] pointed out that not all PMU locations provide equally reliable data. In particular, inter-area oscillations can distort local frequency measurements, leading to inaccurate inertia estimates.

In summary, while offline methods provide a classical foundation for inertia estimation, they are limited by challenges in real-time application, especially due to issues related to noise, ROCOF timing, and localized measurements. On the other hand, online methods, particularly those using PMU technology, offer promising avenues for real-time and decentralized inertia estimation. Nonetheless, achieving consistent accuracy remains a challenge, especially under complex dynamic conditions and non-uniform PMU coverage.

## 2.4 Identified Research Gaps

### 2.4.1 Influence of IBR on Power System Stability

Despite extensive research efforts, the existing literature addressing the impact of Inverter-Based Resources (IBRs) on power system stability reveals several critical limitations. A majority of these studies have primarily focused on microgrid-level systems, where the scale, complexity, and operational dynamics differ significantly from those encountered in large-scale transmission and interconnected grids. Consequently, the extrapolation of findings from microgrids to real-world bulk power systems remains questionable, limiting practical applicability of such results.

Furthermore, available studies fail to capture the true dynamics of real power systems. Realistic modelling of factors such as load variations, grid topology changes, intermittent generation from renewables, and interaction among different system elements are often simplified or ignored. As a result, these models do not accurately represent system behaviors under actual grid disturbances or transient events.

Most of the simulations have been conducted in offline platforms, and real-time validation is rarely addressed. Additionally, most of the research isolates IBRs from synchronous machines rather than considering hybrid systems comprising both. Therefore, a gap remains in understanding the composite dynamics and interaction effects in real power systems, which this research aims to address.

This research proposes a systematic methodology to evaluate the influence of system inertia on power system stability, protection schemes, and inter-area oscillation modes using synchrophasor measurements from Phasor Measurement Units (PMUs). A comprehensive set of simulation studies has been carried out on multiple standard benchmark systems under a variety of operating conditions. These simulations were conducted in real time using EMTP-RV and the OPAL-RT real-time simulator. Additionally, HYPERSIM was employed to model and analyze the IEEE 9-bus system, the single-machine infinite bus (SMIB) system, and Kundur's two-area system. The central concept underlying this research is the broader impact of system inertia on both dynamic stability and protective device performance. The study

specifically investigates how the system's inertia constant (Hsystem) affects critical parameters such as system frequency, bus voltage phase angle, fault current, and inter-area oscillations. These dynamic responses were captured and analyzed through high-resolution PMU data to derive meaningful insights into inertia-driven behavior in modern power systems.

To summarize,

- This research study examines the impact of reduced system inertia $H_{system}$ on frequency response,
- The impact of low inertia on critical clearing time has been experimentally validated
- Fault current for different values of power generation from IBR under different fault conditions has been investigated.
- Further, this study analyzes the inter-area mode oscillation of power in the presence of IBR in the system
- Overall, a comprehensive study on the impact of IBR interaction in power systems on major aspects of stability has been carried out.

### 2.4.2 Impact of IBR on Protection

The scope of analysis often remains restricted to systems either entirely dominated by IBRs or completely based on conventional synchronous machines. The realistic scenario, that modern power systems are rapidly transitioning into hybrid system, where IBRs coexist with traditional synchronous generators. This hybrid nature introduces new challenges in terms of protection coordination, inertia variability, fault current behavior, and dynamic response, which are not comprehensively addressed in current studies. In addition, lacks a systematic exploration of protection strategies across diverse hybrid configurations involving varying proportions of RES and SGs. The interaction effects, contribution to fault currents, and impact on relay settings in such configurations require detailed study. Without such insights, existing research falls short of delivering comprehensive and validated protection solutions that are suitable for modern and future power systems. while valuable contributions have been made in understanding the behavior of IBRs within power systems, the literature remains deficient in providing a complete framework for protection studies in hybrid systems. There is a persistent need for more realistic, large-scale, and practically validated research that encompasses the full range of grid components, including renewables and conventional systems.

Despite extensive advancements in power system protection, several critical research gaps remain unaddressed in the context of modern grids with high penetration of inverter-based resources (IBRs). One of the major concerns is the

performance degradation of directional relays. These relays traditionally rely on the phase angle relationship between current and voltage, which is significantly altered by the fast, low-inertia dynamics of IBRs. Especially in weak grid conditions or during unbalanced faults, negative sequence-based directional relays fail to correctly identify the fault direction due to the low magnitude and distorted waveform of fault currents injected by IBRs. Additionally, most existing directional schemes are not adaptive to the time-varying fault current behavior characteristic of converter-dominated systems, leading to frequent maloperations in hybrid networks that combine synchronous machines and IBRs.

Motivated by the challenges posed by the integration of Inverter-Based Resources (IBRs) on conventional power system protection schemes, this research investigates the impact of IBRs on negative sequence impedance-based directional relaying (67Q) during unsymmetrical fault conditions. Two benchmark models of 230 kV HVAC transmission systems have been developed and simulated in the OPAL-RT HYPERSIM real-time environment under two distinct fault scenarios to evaluate the relay's ability to accurately determine fault direction. The presence of IBRs is incorporated into the system to assess their influence on the performance and reliability of the 67Q directional protection scheme.

Contribution of this research work is summarized as,

- Analyzing the impact of IBR on Negative sequence Impedance based directional overcurrent relay 67Q.
- The result of the analysis shows that with the increasing penetration of IBR in the system impact on the negative sequence impedance based relaying increases.
- Comprehensive analysis of negative sequence voltage $V_2$, negative sequence current $I_2$ and its corresponding phase angle before and after incorporating IBR in the system

Similarly, distance protection schemes undergo serious challenges in the presence of IBRs. These relays estimate fault location by calculating impedance between the relay location and the fault, but IBRs produce non-sinusoidal, frequency-varying, and rapidly fluctuating fault currents, which disrupt the accuracy of impedance estimation. This results in either overreach or underreach of the distance protection zone. Moreover, conventional distance relay algorithms often ignore the impact of control strategies in IBRs, such as current limiting and fast current injection, which further slopes impedance trajectory during faults. Most literature lacks real-time validation of modified distance relays under dynamic conditions and fails to model hybrid systems comprehensively, where traditional generators and IBRs co-exist.

Motivated by the literature to enhance the research on impact of IBR on Mho relay has been investigated by integrating IBR in the system. IEEE benchmark Nine bus system has been simulated in OPAL RT HYPERSIM real time simulator. Main contribution of this research study is as follows.

- Analyzing the operation of mho relay for different types of faults at different locations.

- Analyzing the operation of mho relay after implementing Photovoltaic farm (PV) in nine bus system at different locations for different types of fault.

- Analyzing the variation in current response with the integration of PV in the system

- Analyzing the behavior of impedance trajectory on RX plane for different fault cases.

- Result of the simulation study shows that with the increased share of PV farm in the system mho relay takes longer time to identify the fault or it fails to detect fault in the system which may cause instability of power system.

The Power Swing Blocking (PSB) function, an essential feature to distinguish between faults and stable power swings, also suffers from under-researched challenges in IBR-integrated systems. Since PSB logic is traditionally designed based on rotor angle stability and inertia-based system dynamics, it does not align with the behavior of IBRs that do not possess physical inertia. The fast control responses of IBRs during transient events alter the impedance trajectory and often resemble that of a fault rather than a swing, which significantly affects the impedance trajectory during swings making conventional PSB algorithms unreliable. The literature also lacks standardized modelling and validation frameworks to assess PSB reliability in practical hybrid grids, and there is minimal exploration of coordinated operation between PSB, distance, and directional functions under evolving grid conditions.

Overall, the existing body of research is limited by its focus on isolated microgrid studies or idealized simulation environments, often neglecting real-time validation, practical system dynamics, or hybrid grid configurations involving both conventional and renewable energy sources. These deficiencies highlight the urgent need for robust, adaptive, and coordinated protection strategies tailored for modern power systems with diverse generation sources, including IBRs and conventional synchronous machines.

This research focused on the power swing blocking function of blinder schemes in presence of IBR. Blinder scheme has been developed for the Kundur's two area model. Furthermore, power swing scenario and fault scenario have been considered to analyze response on rate of change of impedance. Photovoltaic farm model has been utilized as IBR which has been integrated into the two-area model reducing inertia of system which intern reduces rate of change of impedance. Simulation has been performed in OPAL RT real time simulator using HYPERSIM. Contribution of this paper:

• Hsystem has been calculated for the different proportion of generation shared by IBR

• Power swing scenario as well as fault scenario has been considered to investigate the response of rate of change of impedance.

• Rate of change of impedance ($\Delta z / \Delta t$) for different power swing scenarios. under blinder has been investigated for different values of Hsys

• Change in time (Δt) reduces to cross blinder impedance (Δz) for the same fault with the reduction in inertia of system Hsys.

### 2.4.3 Online Inertia Estimation

As research studies emphasize the importance of real-time inertia estimation methods. These methods help grid operators better understand the dynamic characteristics of the system at any given moment, enabling proactive control strategies and more effective deployment of synthetic inertia or fast frequency response from IBRs. Therefore, inertia estimation is not only a technical requirement but also a preparatory step to ensure system stability in future power grids with high renewable penetration. Although numerous techniques have been proposed for estimating system inertia, several critical research gaps still persist in the modern power systems experiencing a rapid shift from conventional synchronous generators to inverter-based resources (IBRs).

One major gap is the limited applicability of traditional inertia estimation methods both offline and online to IBR-dominated systems. Offline methods typically rely on post-disturbance analysis using classical swing equations and assume consistent, large-magnitude disturbances. These methods become less effective in present-day systems where disturbances can be of larger or smaller magnitude, inertia is low, and system responses are more dynamic. Similarly, many online inertia estimation methods are based on the rate of change of frequency (ROCOF), which becomes unreliable when frequency data is noisy or when measured from a single PMU location. Such approaches also fail to capture the spatial variability of frequency across the grid, especially in large systems with multiple asynchronous areas. Furthermore, ROCOF-based methods suffer from high sensitivity to noise and measurement delays, while frequency filtering techniques used to reduce noise may introduce phase lag, distorting the timing and magnitude of inertia-related events.

In addition, most of the literature assumes known and accurate disturbance timing and location, which is rarely the case in practical systems. While some studies use techniques like Detrended Fluctuation Analysis (DFA) to estimate the event timing, there remains a gap in methods that can simultaneously detect the disturbance and estimate inertia in real time, especially under ambient (non-event) conditions. Also, current techniques lack generalization across system sizes and topologies, often being tested only in small-scale or idealized systems. This makes it difficult to assess the robustness and reliability of proposed methods in practical scenarios, especially in hybrid systems that combine synchronous generators and IBRs.

In this research, bus voltage phase angles—rather than frequency—are utilized for the estimation of power system inertia, leveraging high-resolution measurements from Phasor Measurement Units (PMUs). The central concept of this approach is based on the strong correlation between generator rotor angle oscillations and the corresponding oscillations in bus voltage phase angles. Specifically, the time derivative of the phase angle is analyzed using artificial intelligence techniques, particularly fuzzy logic, to estimate the system inertia constant (Hsys). The proposed methodology has been validated using standard benchmark systems, and extensive simulations have been conducted in the OPAL-RT real-time simulation environment using HYPERSIM to ensure its accuracy and applicability under realistic operating conditions.

Comparison of different estimation techniques available in literature with proposed method are tabulated in Table 2.1.

Table 2.1 Comparison of algorithms available in literature with proposed method

| **References** | **Mode** | **Input Quantity/ Methodology** | **Error** |
|---|---|---|---|
| [104], [105], [106], [107], [109] | Offline | ROCOF and change in active power using Swing equation | Not investigated |
| [119] | Offline | Second derivative of frequency response | Not investigated |
| [120] | Online | Fourier Transform of swing equation | 4.09% |
| [113] | Online | Frequency response and active power using smooth window method | 5.43% |
| [117] | Online | Frequency response using Markov Gaussian models | Not investigated |
| Proposed method | Online | Bus voltage phase angle using Fuzzy logic | 0.023% - 3.869%. |

To summarize the Contributions in this thesis are

● A novel approach for online system inertia estimation has been proposed.

● Unique response of bus voltage phase angle derivative, with a given system inertia has been established.

● A new signal, based on bus voltage phase angle measured by the PMU has been explored for inertia estimation purpose.

● AI based fuzzy logic inertia estimator has been developed for online estimation of system inertia.

● The Proposed algorithm can estimate system inertia accurately in presence of renewable energy sources and does not get influenced by generation shared by RES.

● Proposed algorithm estimates system inertia with high accuracy irrespective of type of disturbance

# CHAPTER 3

# INVESTIGATION ON IMPACT OF IBR ON POWER SYSTEM STABILITY

This chapter discusses the influence of Inverter-Based Resources (IBRs) on power system stability, emphasizing the linkage between system inertia, protection coordination, and overall grid performance. It describes the modeling of a photovoltaic (PV) farm and the incorporation of phasor measurement units (PMUs) within the simulation setup. Additionally, it presents three case studies designed to evaluate the effects of IBR integration on frequency stability, rotor angle stability, and system oscillations.

## 3.1 Introduction

The stability of electric power systems has long been a foundation of secure and reliable operation. Traditionally, stability is defined as the ability of the system to return to an operating equilibrium following a disturbance, while maintaining continuous supply of power to consumers. Disturbances are further categorized by their magnitude: transient stability refers to large and severe events such as faults or generator outages, while small-signal stability describes the system response to minor perturbations such as load fluctuations[4], [9].

With the growing penetration of IBRs such as photovoltaic (PV) systems, wind farms, and battery storage the dynamics of the power grid have shifted significantly. Initially, IBRs were primarily connected to distribution networks, contributing only marginally to the overall generation mix. In that context, their impact on bulk system stability was negligible. However, as renewable penetration has scaled to transmission networks, displacing conventional synchronous generators, the fundamental characteristics of power systems are being reshaped[121], [122], [123].

One of the most critical differences between synchronous generators and IBRs is the absence of rotational inertia in the latter. The kinetic energy stored in the rotating masses of synchronous machines naturally resists rapid changes in frequency during a disturbance, providing what is known as inertial response. IBRs, by contrast, are electronically coupled to the grid and lack physical inertia, unless explicitly emulated through advanced control algorithms. As a result, systems with high IBR penetration exhibit faster frequency deviations, higher rates of change of frequency

(ROCOF), and reduced frequency nadirs after disturbances. This erosion of inertia has direct consequences for frequency stability, fault ride-through capability, and transient stability margins. Beyond inertia, IBRs also alter other critical aspects of stability. Their limited ability to provide fault current challenges conventional protection coordination schemes such as distance, differential, and overcurrent relays, which are traditionally designed for synchronous machine fault behavior. Similarly, IBRs affect oscillatory modes of the system. Conventional inter-area oscillations, typically damped by synchronous machines, can be amplified or reshaped in the presence of inverter controls, potentially leading to poorly damped or even unstable modes. Furthermore, the power electronic interface of IBRs introduces additional stability phenomena, such as converter-driven stability and resonance interactions, which were not relevant in systems dominated by synchronous generation[124], [125].

These changes necessitate a re-examination of power system stability in the context of high renewable integration. Stability is no longer influenced solely by the physical properties of machines and networks but also by the control strategies of converters, their interactions with synchronous generators, and the coordination of protective devices. Moreover, the spatial distribution of IBRs introduces complexities in inter-area oscillations and wide-area stability, requiring advanced monitoring and control[126], [127]. In this context, the control structure of the grid-following PV inverter has a significant influence on the dynamic stability of the power system. The PI-based current-control loop determines the dynamic response of the inverter, while the PLL provides synchronization with the grid voltage. The interaction of these control dynamics with the grid impedance can influence the damping and stability of the system, particularly under weak-grid conditions. The PLL and current-control dynamics may introduce poorly damped oscillations when the controller parameters and grid conditions are not appropriately selected. Therefore, appropriate tuning of the PI controller and PLL parameters is important for maintaining stable dynamic operation of the grid-following PV inverter[128], [129], [130]

Recent advancements in measurement technology, particularly the widespread deployment of Phasor Measurement Units (PMUs), provide new opportunities to address these challenges. PMUs offer time-synchronized, high-resolution measurements of voltage, current, frequency, and phase angle across large areas of the grid. They enable accurate detection of transient events, real-time monitoring of oscillations, and estimation of inertia by analyzing frequency and ROCOF responses. Leveraging PMU data thus allows a more accurate and dynamic assessment of how IBRs impact stability, bridging the gap between theoretical studies and practical system operation[131], [132], [133].

Motivated by these developments, this chapter focuses on systematically assessing the impact of IBR integration on power system stability and protection, with an emphasis on the role of system inertia. By combining benchmark test systems, real-time simulations, and PMU-based measurements, the work provides insights into how reduced inertia and altered fault current contributions affect stability margins, oscillatory behavior, and protective coordination.

### 3.1.1 Specific Objectives

The specific objectives of this chapter are:

- Analyze the effect of reduced system inertia H system on frequency dynamics, including frequency nadir and ROCOF.
- Investigate how inertia variations influence critical clearing time under fault conditions.
- Examine the contribution of IBRs to fault current characteristics under different operating conditions.
- Study the behavior of inter-area oscillations with varying levels of IBR penetration.
- Explore the role of PMU-based measurements in monitoring and quantifying stability dynamics in hybrid systems.

### 3.1.2 Contributions

This chapter presents the following key contributions:

- A comprehensive simulation-based analysis of IBR impacts on stability, focusing on frequency, rotor angle, and oscillatory dynamics.
- Verification of the relationship between reduced inertia and critical clearing times using real-time simulators.
- Detailed investigation of fault current contributions from IBRs and their implications for conventional protection schemes.
- Assessment of inter-area oscillatory modes in hybrid systems with varying levels of IBR penetration.

## 3.2 Relation Between Power System Inertia, Protection Setting And Stability

During active power disturbance in the power system, the frequency deviates from its nominal value. Normally, the frequency of the system shall be restored by governor control setting of the generator. However, response of the governor is normally delayed by few seconds to restore the system frequency.

Therefore, there is a steep change in the frequency of the system which is restricted by the release of kinetic energy from rotor masses of generator. In literature, kinetic energy of the system is represented in terms of generating capacity defined as the ratio of kinetic energy stored to the rating of generator denoted as H. The mathematical representation of H can be expressed in the following subsection.

### 3.2.1 Expression of Power System Inertia

The inertia constant H of a synchronous machine is defined as the time in seconds for which the machine can supply its rated power from its stored kinetic energy in the rotor [15]. Inertia can be calculated as expressed in equation 3.1,

$$\mathbf{H} = \frac{1}{2}\frac{\mathbf{J}\boldsymbol{\omega}_{\mathbf{n}}^{2}}{\mathbf{S}_{\mathbf{n}}} \quad [\mathrm{s}] \tag{3.1}$$

Where J is the moment of inertia of a generator and turbine [kg/m$^2$], $\boldsymbol{\omega_n}$ is the rated mechanical angular velocity of the rotor [rad/s], $S_n$ is the rated apparent power of the generator [VA].

The aggregate equivalent inertia $\boldsymbol{H_{sys}}$ of power system can be defined as time for which system can supply its rated power from its stored kinetic energy in the rotor. Aggregated Inertia of power system can be calculated by using inertia of individual turbine generator expressed in 3.2. [134]

$$\mathbf{H_{sys}} = \frac{\sum_{\mathbf{i=1}}^{\mathbf{N}} \mathbf{S_{ni}} \mathbf{H_i}}{\mathbf{S_{n,sys}}} \ [\mathrm{s}] \tag{3.2}$$

Where,

$$\mathbf{S_{n,sys}} = \sum_{\mathbf{i=1}}^{\mathbf{N}} \mathbf{S_{ni}} \ [\mathrm{MVA}] \tag{3.3}$$

$S_{ni}$ is the rated apparent power of generator i [MVA], $H_i$ the inertia constant of turbine-generator i [s], i is the number of synchronous generators mentioned in 3.3.

### 3.2.2 Relation of Inertia With Bus Phase Angle Difference of Voltages And Critical Clearing Time

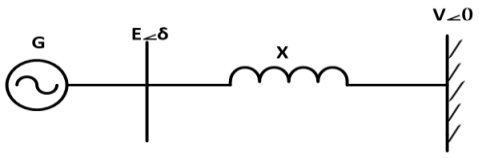


Fig. 3.1 Single machine infinite bus system

The impact of inertia in the power system can be observed from a system shown in fig. 1, where the power transfer through transmission line by a synchronous generator in terms of bus voltages and bus phase angle between the buses can be expressed as in equation 3.4. [70],

$$P = \frac{EV}{X} Sin\delta \quad (3.4)$$

Where, $\delta$ is phase angle difference of voltage. Generator rotor angle can be considered to be the same as generator bus voltage angle if the generator stator reactance is neglected. The Dynamics introduced in the system during disturbance in the system, can be expressed in terms of swing equation 3.5. It can be observed that the rate of change of generator rotor angle is dependent on the inertia H of the system.

$$\frac{d^2\delta}{dt^2} = \frac{\pi f}{2H}(P_m - P_e) \quad (3.5)$$

The critical clearing time can be evaluated by Equal area criterion (EAC) plotted in the figure 3.2,

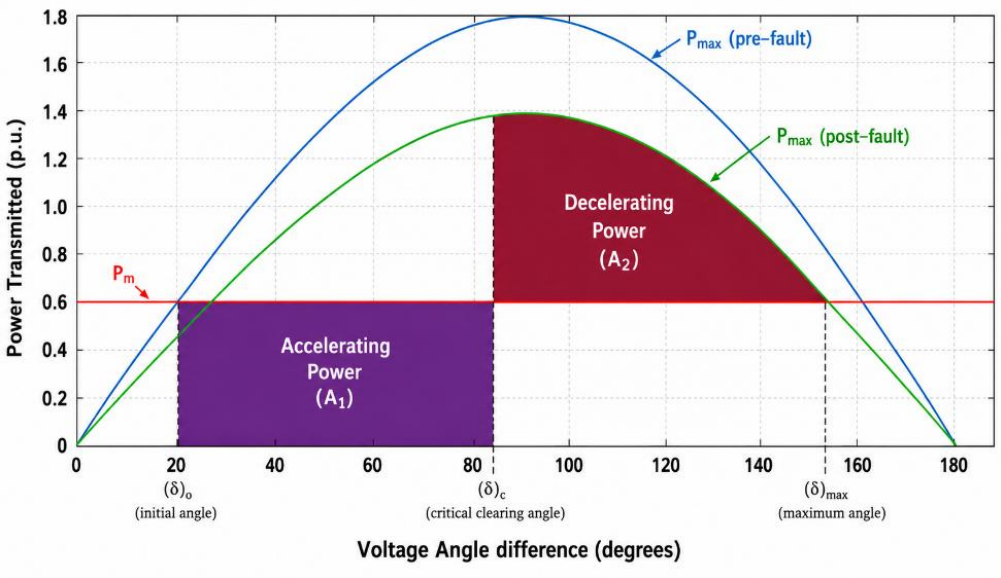


Fig.3.2 EAC for three phase fault

Critical clearing time to clear the fault can be deduced as 3.6 [33],

$$tc = \sqrt{\frac{2H(\delta_c - \delta_0)}{\pi f_0 P_m}} \quad (3.6)$$

Where,

$t_c$= critical clearing time, H=inertia of system, $\delta_c$=critical clearing angle, $\delta_0$= initial operating angle, $P_m$= Mechanical input power. Reduced inertia decreases critical clearing time which in turn affects the protection relay settings and stability. As the generation with IBR is largely intermittent in nature it is inconvenient to change setting of protection relays differently for conventional synchronous generator and IBR. Thus, protection of the system is one of the major concerns with IBR [42], [82], [84], [88].

## 3.3 PV Farm Implementation and PMU

### 3.3.1 Photovoltaic Farm Implementation

PV and wind farm has a large share in IBR generation of present power systems across the world. In this study only PV farms have been integrated in simulation studies as IBR generation. In simulation studies detailed representation of PV has been considered. Block diagram representation for PV generation system and Schematic diagram for PV farm connected to grid are as shown in figure 3.3a and 3.3b.

PV generating system block comprising of PV array connected to an inverter through a boost converter and RL choke filter which is used to limit total harmonic distortion as shown in figure 3.3a. This complete block is connected to step up transformers via point of common coupling PCC, then through a feeder line and three winding transformers to the grid as shown in figure 3b. This scheme has been developed and controlled on OPAL RT HYPERSIM and EMTP RV real time simulator to form a PV farm.

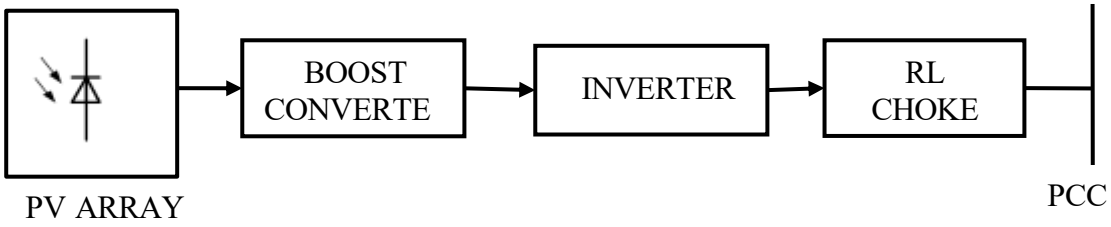


Fig. 3.3a Block diagram of Photovoltaic generation system

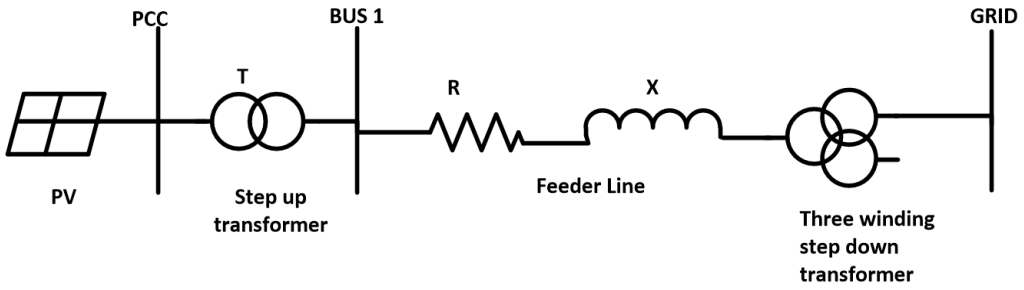


Fig. 3.3b Schematic diagram for PV farm connected to grid

### 3.3.2 Photovoltaic Inverter control structure and Parameters

IBR is interfaced with the power system through a grid-following (GFL) inverter. The adopted inverter model represents conventional inverter-based generation and does not employ synchronous-machine emulation or virtual synchronous-machine control. IBR model used in simulations is a Photovoltaic generation system model with rating of 750 kVA solar plant that extracts DC power from a PV array through an inverter and feeds AC power into the electrical grid presented in figure 3.4.

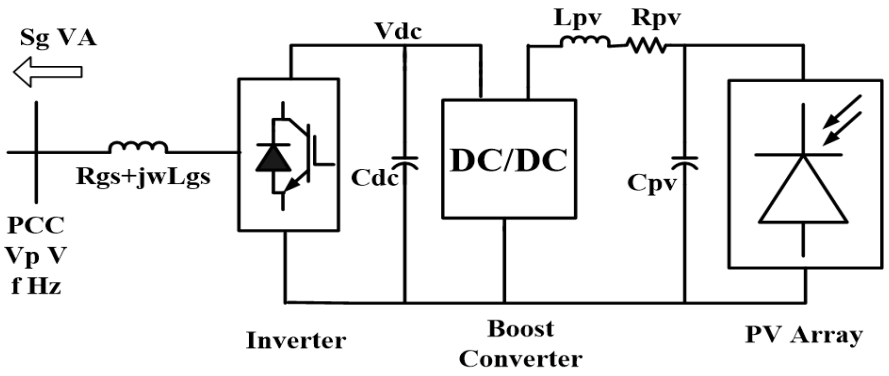


Fig.3.4 Schematic diagram for PV generation system

It uses a two-stage conversion process:

1) DC-DC Boost Converter: Operates in either MPPT mode (using a Perturb-and-Observe algorithm to maximize power output based on sunlight and temperature) or active power curtailment mode (limiting output power to follow a specified reference).

**Active Power Regulator**: The active power regulator shown in the figure 3.5 (a) is implemented as a PI controller in the boost-converter stage. It compares the measured PV active power with its reference value and generates the required duty-cycle command to regulate the power transferred from the PV array to the DC link. The duty-cycle limits, D_up and D_low, are imposed according to the operating constraints of the boost converter.

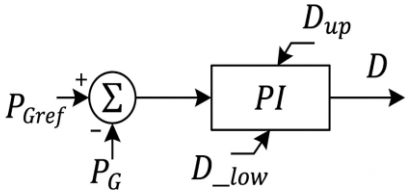


Fig 3.5a Active Regulator inner block diagram

2) DC-AC Grid Following Inverter: The grid-side inverter employs a cascaded control structure consisting of two loops, one outer-loop PI controller and an inner dq axis current controller. The outer-loop PI controller regulate the DC-link voltage and reactive power, generating the d and q axis current references for inner loop, respectively. The inner current controller tracks these current references and generates the corresponding inverter voltage commands for PWM generation. The controllers employed in the inverter are described below.

**DC link voltage regulator:** The DC-link voltage regulator presented in the figure 3.5(b) is implemented using a PI controller. The reference DC-link voltage, $V_{dcref}$, is compared with the measured DC-link voltage, $V_{dc}$, to obtain the voltage error. This error is supplied to the PI controller, which generates the reference $d$-axis current, $I_{dref}$. The generated $I_{dref}$ is then supplied to the inner current-control loop of the grid-

side inverter. Since the $d$-axis current primarily governs the active-power exchange between the PV generating system and the grid, regulation of $I_{dref}$ enables the grid-side inverter to maintain the DC-link voltage at its desired reference value. The output of the PI controller is also limited according to the allowable converter current rating.

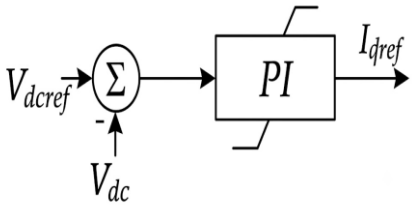


Fig 3.5b DC link voltage Regulator inner block diagram

**Reactive Power regulator:** The reactive power regulator presented in the figure 3.5 (c) is implemented using a proportional–integral (PI) controller. The reference reactive power, $Q_{Grid}$, is compared with the measured reactive power, $Q_G$, to obtain the reactive-power error. The resulting error is supplied to the PI controller, which generates the reference $q$-axis current, $I_{qref}$. This current reference is subsequently provided to the inner current-control loop of the grid-side inverter. The $q$-axis current primarily regulates the reactive-power exchange between the PV generating system and the grid. The generated current reference is constrained according to the maximum allowable converter current.

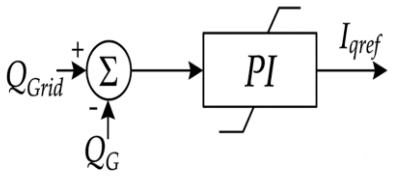


Fig 3.5c Reactive Power Regulator inner block diagram

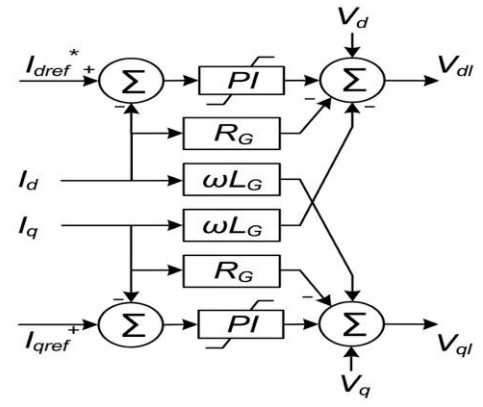


Fig 3.5d Current Regulator inner block diagram

**Current Regulator:** The $d$- and $q$-axis current references, $I_{dref}$and $I_{qref}$, generated by the DC-link voltage and reactive-power regulators, respectively, are compared with the corresponding measured grid currents, $I_d$and $I_q$. Separate PI controllers are

employed to regulate the $d$ and $q$-axis currents. The inner current controller also incorporates cross-coupling compensation terms involving $\omega L_G$ and grid-voltage feed-forward terms $V_d$ and $V_q$to improve current tracking and decouple the $d$- and $q$-axis dynamics. The resulting inverter voltage references, $V_{dl}$ and $V_{ql}$, are used for PWM generation and control of the grid-side inverter. The $d$-axis current primarily controls active-power exchange, whereas the $q$-axis current controls reactive-power exchange with the grid. Current Regulator is shown in the figure 3.5 (d).

Parameters considered for PV generation system are presented in table 3.1.

Table 3.1 Parameters of PV generation system

| **Regulator Category** | **Parameter** | **Notation** | **Value** |
|---|---|---|---|
| System Parameters | Nominal Power | Sg | 750KVA |
| | Nominal Voltage | Vp | 480V |
| | Nominal Frequency | f | 60Hz |
| | Nominal DC Link Voltage | Vdc | 1,050V |
| | DC Link Capacitance | Cdc | 0.012F |
| | Filter Resistance | Rgs | 0.01 Ω |
| | Filter Inductance | Lgs | 2.50E-04H |
| | Switching Frequency | Fsw | 1,620Hz |
| Active power regulator | Proportional gain | KpP | 0.20 |
| | Integral gain | KiP | 2 |
| Reactive power regulator | Proportional gain | KpQ | 1 |
| | Integral gain | KiQ | 25 |
| Current regulator | Proportional gain | KpI | 10 |
| | Integral gain | KiI | 300 |
| VDC regulator | Proportional gain | KpVDC | 1 |
| | Integral gain | KiVDC | 50 |
| Current limit | Limit | Ilim | 1.20p.u |

### 3.3.2 Phasor Measurement Unit (PMU)

Recently Phasor measurement unit (PMU) are being installed on large scale for wide area measurement systems (WAMS) to measure electrical quantities during steady and transient state[69]. As per IEEE C37.118.1-2011, PMU gets analog signals of voltage and current and estimates phasor, positive sequence component of

voltage and current, frequency and rate of change of frequency (ROCOF). All these electrical quantities are time stamped by referring to the Universal Time Coordinate (UTC) as a standard, GPS (Global Positioning satellite) communication is used to synchronize these time stamped data[67], [68]. Functional block diagram of a PMU is as represented in figure 3.6. In this study two PMU has been used to measure rotor angle in a single machine infinite bus model. Bus voltage phase angle difference can be measured by utilizing equation 3.7.

$$\delta = E\angle PMU1 - V\angle PMU2 \tag{3.7}$$

Where PMU1 is used to measure phase angle of generator side bus and PMU2 is used to measure load side bus.

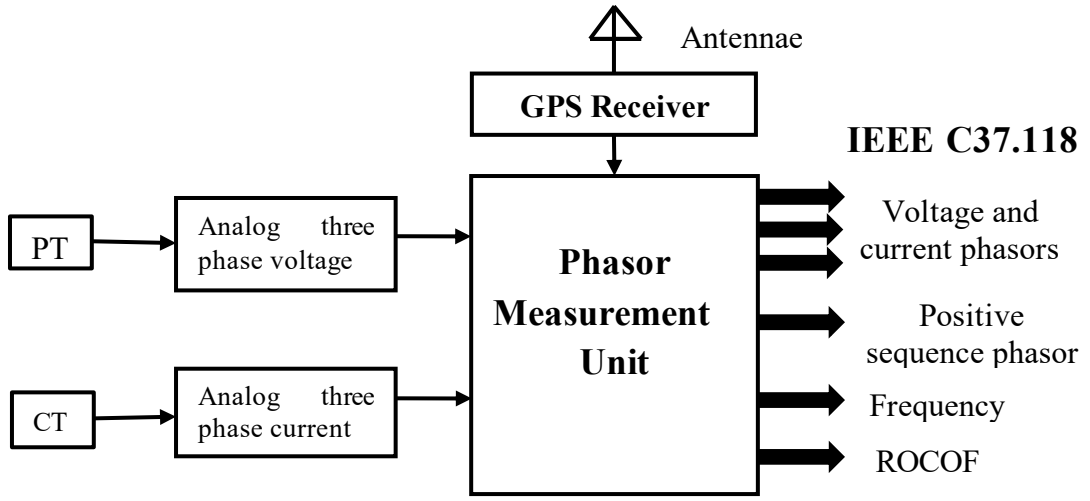


Fig. 3.6 Functional PMU block diagram

## 3.4 Case Studies: Impact of Reducing Inertia on System Stability

In this section, an investigation on the impact of inertia on power systems with three case studies has been performed considering various scenarios in each case.

Case I: The role of kinetic energy on load changes on nine bus benchmark systems has been investigated.

Case II: Impact of inertia on fault current & rotor angle on single machine infinite bus have been analyzed.

Case III: The impact of IBR on power oscillations in Kundur's two-area system has been studied.

### 3.4.1 CASE I: Role of Kinetic Energy on Load Changes

Nine bus benchmark system [15] shown in figure 3.7, has been simulated on OPAL –RT HYPERSIM Real time simulator. Nine bus system consists of three synchronous generators of rating 512MVA, 270 MVA and 125MVA respectively connected to three transformers to make the system operate at constant voltage of

230kV. Three loads A,B,C placed at bus respectively 5, 6 and 8 consumes 315MW. Generator 1 is considered to be swing bus inertia of which is assumed to be constant at 4.112s. Inertia of generator 2 and 3 have been varied step by step in the range of 1-9s to study its impact on the frequency response of the system. The same phenomenon has been verified by integration of PV in the system. The time step for simulation is kept at 50μseconds and sampling rate is 20000samples/seconds. Load flow has been performed for initialization and simulation has been carried for 50 seconds.

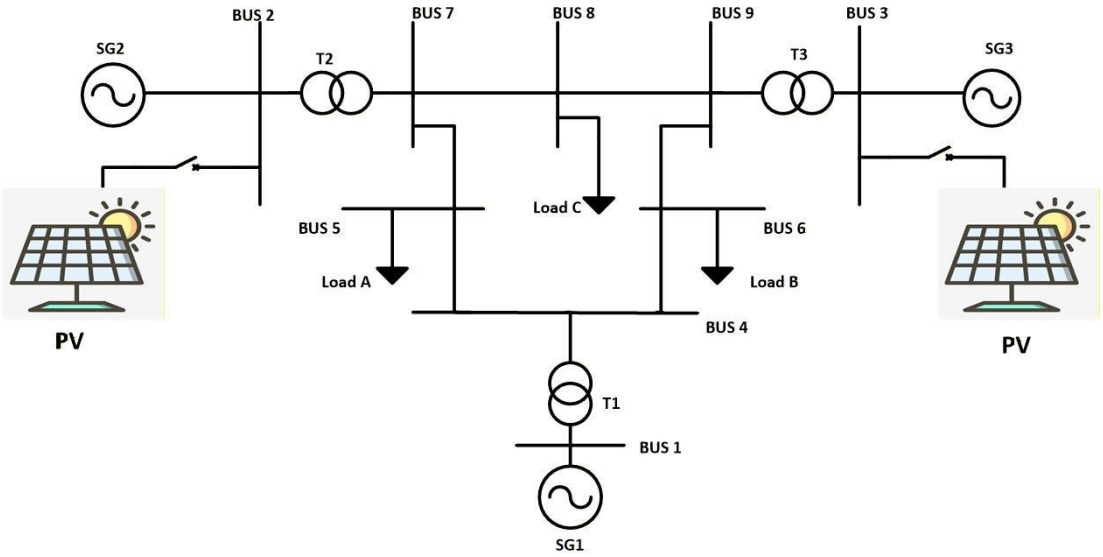


Fig. 3.7 Nine bus systems

Under this case four scenarios have been considered to analyze impact on kinetic energy in the system.

- In scenario I: Inertia of generator SG2 has been varied and frequency response has been studied.

- In scenario II: Inertia of generator SG3 has been varied and frequency response has been studied. A comparison study of frequency and time to reach nadir frequency for generators SG2 & SG3 have been performed.

- In scenario III & IV detailed PV farms have been incorporated at generator bus 2 and bus 3 to analyze and verify frequency response.

### 3.4.1.1 SCENARIO I: Inertia Variation of SG2

In this scenario, the inertia of SG1 and SG3 is considered at 4.112s, whereas inertia constant H of SG2 has been varied from 1-9s and an additional 50 MW load at bus 8 has been applied at 1 second to analyze its impact on frequency response. The frequency response of the system is plotted in the figure 3.8. It can be observed that, with the increase in load at 1 second, frequency drops till nadir frequency and

gets recovered. However, nadir frequency changes with respect to the magnitude of inertia constant H. It is clearly observable that nadir frequency decreases at faster rate with the reduction in inertia. Results of the simulation is taken to further explain the behavior of response from figure 3.5. Nadir frequency is the lowest point of frequency and Δt is time to reach nadir frequency after the application of disturbance. When H= 9 seconds, frequency drops to 58.7398 Hz and Δt9=5.79476 seconds while with H = 1 second frequency goes to 58.3479 Hz and Δt1= 4.24119seconds. Corresponding values for complete range of H for 1 – 9 seconds has tabulated in table 3.2.

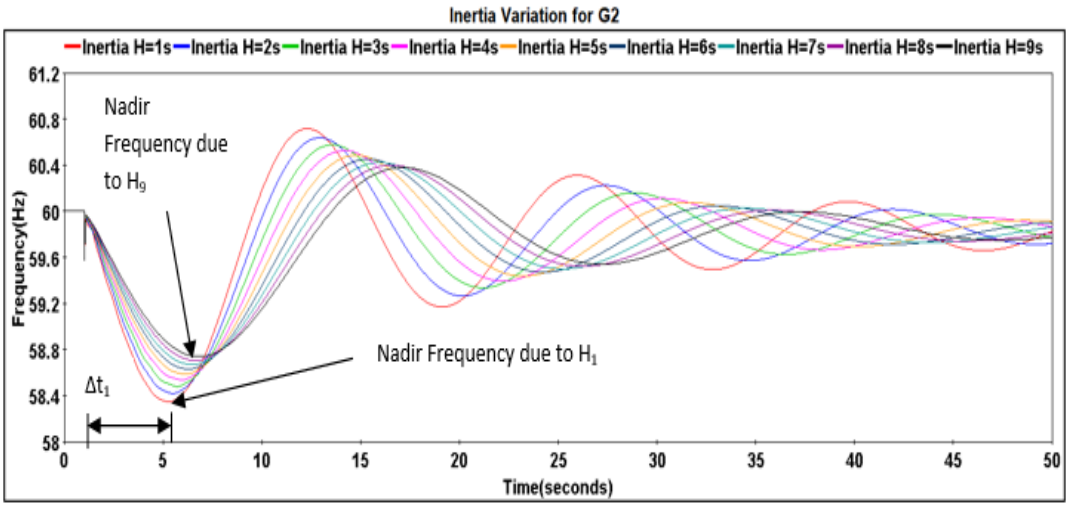


Fig. 3.8 Frequency plot at Bus 8 with respect to time

Table 3.2 Nadir frequency and time to reach Nadir frequency

| Sr. No | Inertia (s) | Scenario 1 | | Scenario 2 | |
|---|---|---|---|---|---|
| | G2 for scenario 1 and G3 for scenario 2 | Frequency Nadir (Hz) | Time to reach Nadir Frequency Δt(seconds) | Frequency Nadir (Hz) | Time to reach Nadir Frequency Δt (Seconds) |
| 1 | 1 | 58.3479 | 4.24119 | 58.4653 | 4.62766 |
| 2 | 2 | 58.4179 | 4.48543 | 58.4930 | 4.74511 |
| 3 | 3 | 58.4794 | 4.67941 | 58.5170 | 4.86318 |
| 4 | 4 | 58.5368 | 4.92199 | 58.5403 | 4.98433 |
| 5 | 5 | 58.5878 | 5.11465 | 58.5628 | 5.02803 |
| 6 | 6 | 58.6316 | 5.26944 | 58.5856 | 5.05994 |
| 7 | 7 | 58.6706 | 5.42420 | 58.6069 | 5.13875 |
| 8 | 8 | 58.7068 | 5.57900 | 58.6276 | 5.17682 |
| 9 | 9 | 58.7398 | 5.79476 | 58.6472 | 5.21732 |

### 3.4.1.2 SCENARIO II: Inertia Variation of SG3

Same type of disturbance as in scenario I has been applied to bus 8 at 1s. Here, inertia of SG1 and SG2 are assumed to be constant at 4.1112s. Whereas inertia of generator SG3 is varied from 1-9 seconds. Corresponding frequency response plot of the system has been observed in figure 3.9. For H = 9 seconds frequency drops to 58.6472 Hz and Δt 9= 5.21732 seconds. Whereas for H = 1 second frequency decreased to 58.4653Hz and time taken $\Delta t_1 = 4.62766$ seconds. Observed response data for H of 1-9 seconds are tabulated in table 1. In table 1, 2nd column indicates the value of inertia G2 for scenario 1 and that of G3 for scenario 2.

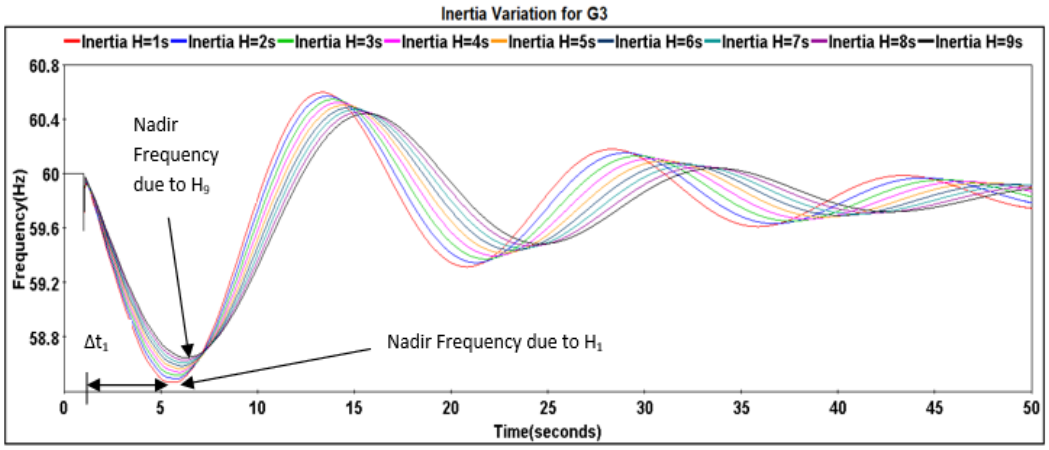


Fig. 3.9 Frequency plot at Bus 8 with respect to time

So, it is evident that when load increases on the system frequency drops but the system with higher inertia frequency decreases slowly. Nadir frequency and time to reach nadir frequency depend on inertia of the system.

### 3.4.1.3 Comparison for Scenario I And II

A comparison plot of frequency response of SG2 & SG3 for inertia variation, nadir frequency & time to reach nadir frequency is in the figure 3.10.

For the same inertia value, the frequency responses of SG2 and SG3 are different because of the different MVA ratings of individual generators. The MVA rating of SG2 is 270 MVA, and SG3 is 125 MVA, so the effect on $H_{system}$ by generator SG2 will be more impactful on the system than SG3. Therefore, the nadir frequency variation response is wider in the case of SG2. Hence, it can be augmented that frequency response doesn't depend only upon the inertia of an individual generator, but it responds according to the whole inertia of the system.

Table 3.3 represents total inertia of the system for 18 combinations in which MVA rating and inertia is constant for G1 while inertia of G2 and G3 varied one at a time accordingly inertia of the whole system has been calculated. From table

3.2, When, G1= 512MVA, G2=270MVA, G3=125MVA, H1 = 4.112s, H2=1s, H3=4.112s, So, H1G1= 2105. 34MVA.s, H2G2=270, MVA.s, H3G3=514 MVA.s, $H_{system}$=3.1856s In a similar manner $H_{system}$ has been estimated for the rest of combinations.

Data from Table 3.2 has been utilized to plot figure 3.11. Plot represents nadir frequency with respect to $H_{system}$, nadir frequency decays with respect to $H_{system}$. So, it can be augmented that $H_{system}$ changes not only with respect to inertia of an individual generator but with inertia of whole system. If the inertia of each individual generator is known, $H_{system}$ can be estimated for the whole system which will be useful to prevent Under Frequency Load shedding (UFLS).

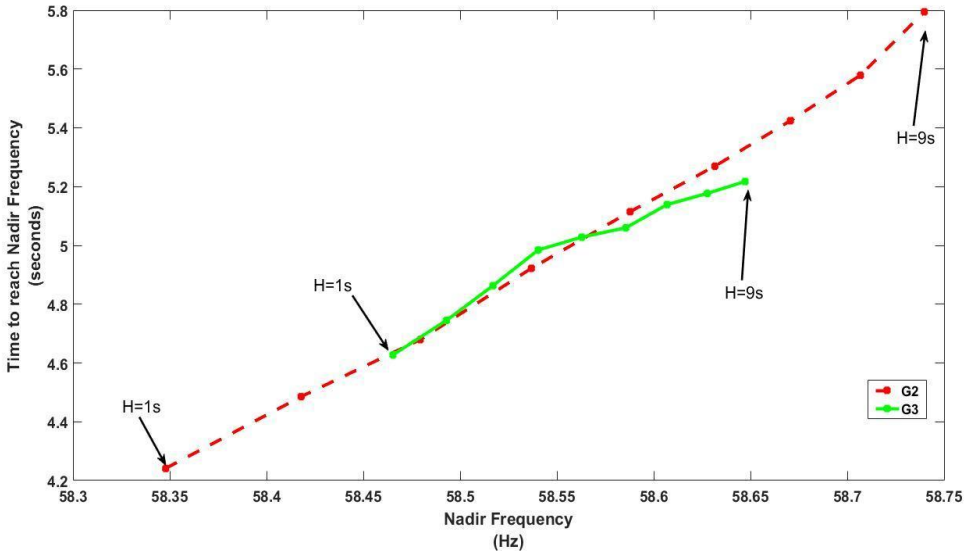


Fig. 3.10 Nadir Frequency with respect to time for G2 & G3

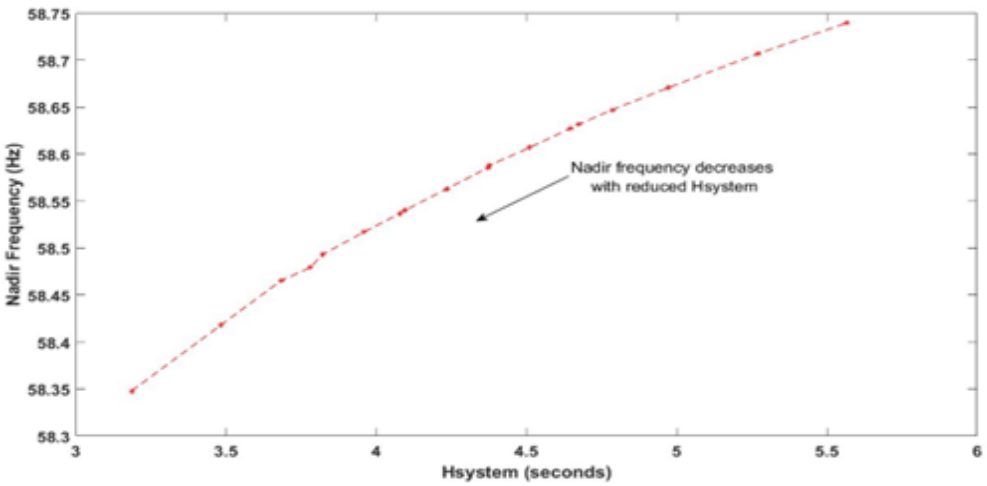


Fig. 3.11 Nadir Frequency with respect to $H_{system}$

Table 3.3 $H_{system}$ with variation of individual generator's inertia

| Sr. No | G1 (MVA) | G2 (MVA) | G3 (MVA) | $H_1$ (s) | $H_2$ (s) | $H_3$ (s) | $H_1G_1$ MVA.s | $H_2G_2$ MVA.s | $H_3G_3$ MVA.s | $H_{system}$ (s) |
|---|---|---|---|---|---|---|---|---|---|---|
| 1 | 512 | 270 | 125 | 4.112 | 1 | 4.112 | 2105.34 | 270 | 514 | 3.1856 |
| 2 | 512 | 270 | 125 | 4.112 | 2 | 4.112 | 2105.34 | 540 | 514 | 3.4823 |
| 3 | 512 | 270 | 125 | 4.112 | 3 | 4.112 | 2105.34 | 810 | 514 | 3.781 |
| 4 | 512 | 270 | 125 | 4.112 | 4 | 4.112 | 2105.34 | 1080 | 514 | 4.0786 |
| 5 | 512 | 270 | 125 | 4.112 | 5 | 4.112 | 2105.34 | 1350 | 514 | 4.3763 |
| 6 | 512 | 270 | 125 | 4.112 | 6 | 4.112 | 2105.34 | 1620 | 514 | 4.674 |
| 7 | 512 | 270 | 125 | 4.112 | 7 | 4.112 | 2105.34 | 1890 | 514 | 4.9717 |
| 8 | 512 | 270 | 125 | 4.112 | 8 | 4.112 | 2105.34 | 2160 | 514 | 5.2693 |
| 9 | 512 | 270 | 125 | 4.112 | 9 | 4.112 | 2105.34 | 2430 | 514 | 5.567 |
| 10 | 512 | 270 | 125 | 4.112 | 4.112 | 1 | 2105.34 | 1110.24 | 125 | 3.6831 |
| 11 | 512 | 270 | 125 | 4.112 | 4.112 | 2 | 2105.34 | 1110.24 | 250 | 3.8209 |
| 12 | 512 | 270 | 125 | 4.112 | 4.112 | 3 | 2105.34 | 1110.24 | 375 | 3.9587 |
| 13 | 512 | 270 | 125 | 4.112 | 4.112 | 4 | 2105.34 | 1110.24 | 500 | 4.0966 |
| 14 | 512 | 270 | 125 | 4.112 | 4.112 | 5 | 2105.34 | 1110.24 | 625 | 4.2343 |
| 15 | 512 | 270 | 125 | 4.112 | 4.112 | 6 | 2105.34 | 1110.24 | 750 | 4.3722 |
| 16 | 512 | 270 | 125 | 4.112 | 4.112 | 7 | 2105.34 | 1110.24 | 875 | 4.51 |
| 17 | 512 | 270 | 125 | 4.112 | 4.112 | 8 | 2105.34 | 1110.24 | 1000 | 4.6478 |
| 18 | 512 | 270 | 125 | 4.112 | 4.112 | 9 | 2105.34 | 1110.24 | 1125 | 4.7856 |

### 3.4.1.4 SCENARIO III: Replacement of SG2 with PV

In order to verify the observations of scenario I & scenario II, a PV farm has been implemented at bus 2. SG2 has been replaced with five small generators of equal rating and one small generator has been tripped off at a time to reduce power flow of synchronous generator and generate the same power flow in the system through PV. 50MW load at bus 8 is added at 5 seconds and its frequency response has been plotted in figure 3.13. PV has been incorporated in the range of 20-80% share of SG2.

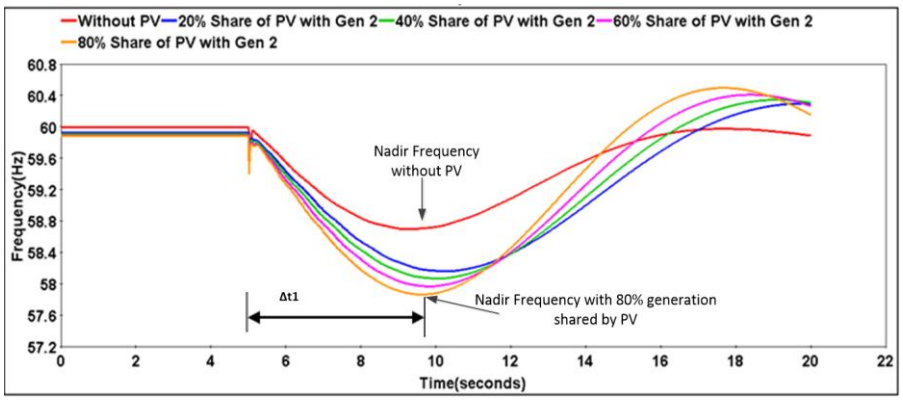


Fig. 3.13 PV Farm connected with G2

It can be analyzed from the figure 3.12 as the percentage of PV farm share is increased, nadir frequency decreases accordingly Δt increases and vice versa. Table 3.3 presents detailed study of frequency response for the given percentage share of PV with SG2. For 20% share by PV with SG2 frequency reduced to 58.3108Hz in 5.5325seconds and with the increase in share of PV frequency decreases at faster rate.

Table 3.3 Nadir frequency with respect to time after implantation of PV at bus2

| Sr. No | % share of PV | MVA Rating of Synchronous Generator SG2 (MVA) | Power of SG2 Synchronous Generator (MW) | MVA Rating of PV (MVA) | POWER of PV at Bus 2 (MW) | Nadir Frequency (Hz) | Time to reach Nadir Frequency Δt (s) |
|---|---|---|---|---|---|---|---|
| 1 | 20% | 216 | 130.4 | 54 | 32.6 | 58.3108 | 5.5325 |
| 2 | 40% | 162 | 97.8 | 108 | 65.2 | 58.3063 | 5.5553 |
| 3 | 60% | 108 | 65.2 | 162 | 97.8 | 58.2994 | 5.5909 |
| 4 | 80% | 54 | 32.6 | 216 | 130.4 | 58.2965 | 5.6027 |

### 3.4.1.5 SCENARIO IV: Replacement of SG3 with PV

SG3 has been replaced with five small generators of equal rating and PV has been implemented at bus 3. 50MW additional load has been added at bus 8 at 5 seconds. SG3 has been reduced percentage wise and PV has been increased in the system in order to analyze its impact on frequency response. Frequency with respect to time for the percentage share of PV has been plotted in figure 3.13.

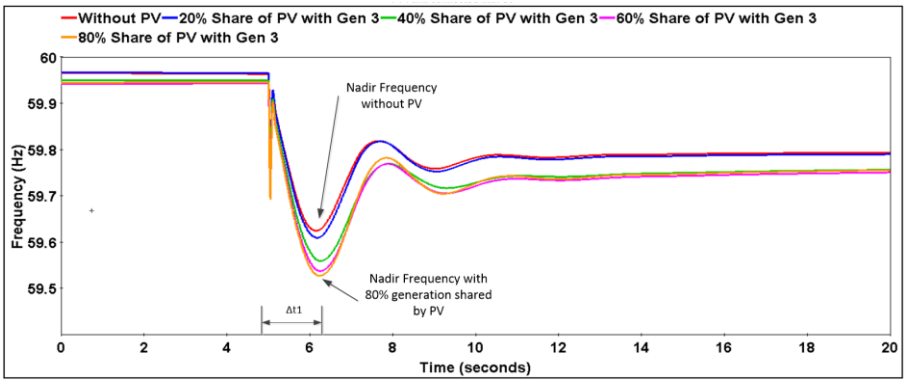


Fig. 3.13 PV Farm connected with G3

Table 3.4 presents MVA rating of SG3 and PV and its response on frequency. When the percentage share of PV is 20% of total 125 MVA of SG3 frequency reduces to 59.6092 Hz in 5.28290 s as PV share increases and power supply from SG3 reduces frequency decreases at faster rate. By studying above scenarios, as load on the system increases frequency reduces but reduction in frequency is lesser with synchronous generator as compared with PV. Hence it can be concluded that synchronous generator prevents abrupt change in frequency drop during disturbed condition and attempts to maintain frequency stability however with PV frequency deviates instantly. In the grid load deviates often thus frequency stability is major concern in case of PV. Integration of IBR to power system form more unstable and complicate power system.

Table 3.4 Nadir frequency with respect to time after implementation of PV at bus3

| Sr. No | % share of PV | MVA Rating of Synchronous Generator SG3 (MVA) | Power of SG3 Synchronous Generator (MW) | MVA Rating of PV (MVA) | POWER of PV at Bus 3 (MW) | Nadir Frequency (Hz) | Time to reach Nadir Frequency Δt (s) |
|---|---|---|---|---|---|---|---|
| 1 | 20% | 100 | 68 | 25 | 17 | 59.6092 | 5.2829 |
| 2 | 40% | 75 | 51 | 50 | 34 | 59.5589 | 5.26425 |
| 3 | 60% | 50 | 34 | 75 | 51 | 59.5372 | 5.24885 |
| 4 | 80% | 25 | 17 | 100 | 68 | 59.527 | 5.2432 |

### 3.4.2 CASE II: Impact of IBR on Rotor Angle Stability and Protection Relay Setting

In this case a single machine of 100 MVA feeds active power of 60MW and reactive power 45MVAR to infinite bus through two parallel transmission lines of 100 km is shown in the figure 3.14 [33]. Phasor measurement units (PMU) have been placed across transmission lines to measure bus voltage angle. Three phase fault (LLL) and double phase to ground fault (LLG) has been considered in this case to study the impact of inertia on generator rotor angle and protection relay settings. The data of the system is given in the appendix I.

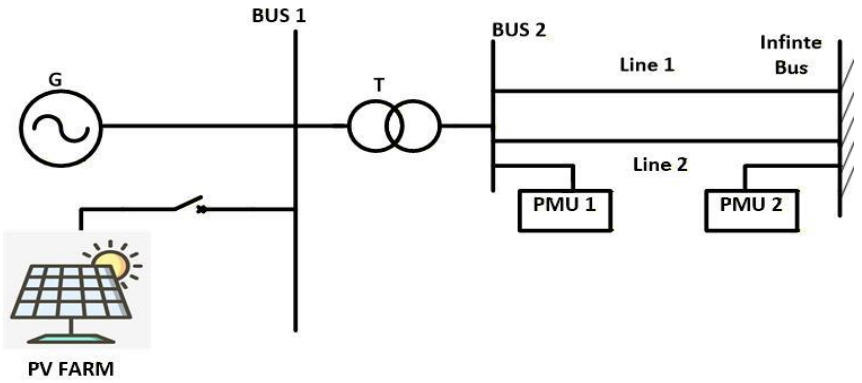


Fig. 3.14 Single machine infinite Bus model

Two scenarios have been considered in this case to analyze rotor angle oscillations and fault current.

- Scenario I: Rotor angle oscillations has been observed after a three-phase fault with different inertia values.

- Scenario II: Influence of Fault current variations has been studied due to IBR on protection relay settings.

### 3.4.2.1 SCENARIO I: Effect of inertia on rotor angle stability

To analyze rotor angle behavior with variation in inertia this scenario has been performed. The inertia of the generator is considered as 6.112s and a three phase (LLL) fault has been applied at 1 second at line 2 near bus 2. Fault is cleared after 0.39415s with tripping of Line 2. Voltage bus angle of the generator has been plotted in figure 3.15. The inertia of the generator is then reduced to 3.112s assuming a system equivalent to operating with IBR and the bus voltage angle has been plotted in comparison with the previous case. With H=6.112s when fault occurs rotor angle oscillates and settles down after few seconds whereas with H=3.112s rotor angle increases beyond180° and goes out of step.

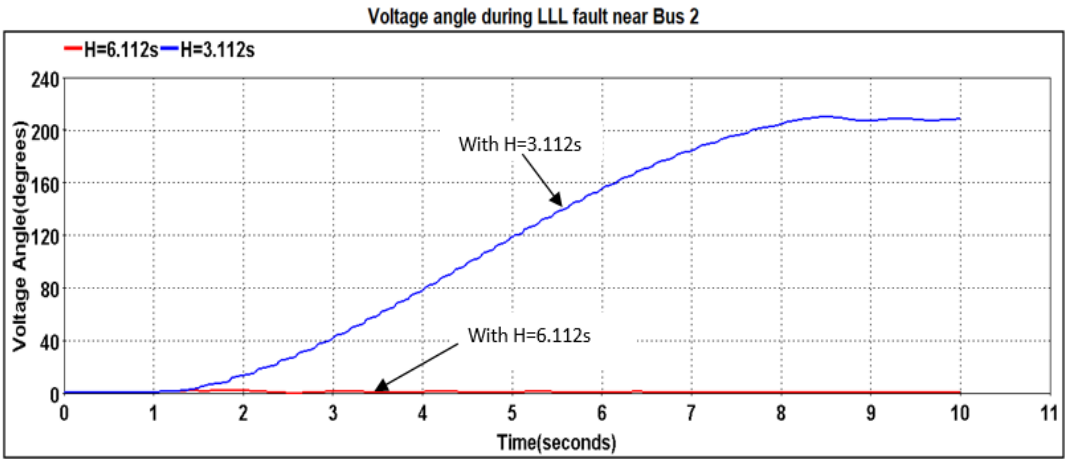


Fig. 3.15 Voltage angle $\delta$ during LLL Fault

Table 3.5 Effect of inertia for a fault duration of 0.39415seconds.

| Sr. No. | Inertia | Critical clearing time (observed value) | Critical clearing time (calculated value) | Rotor angle |
|---|---|---|---|---|
| 1 | 6.112s | 0.4600s | 0.347s | Stable |
| 2 | 3.112s | 0.3283s | 0.247s | Unstable |

Critical clearing time observed from the figure 3.15 and calculated using equation 6.6 tabulated in table no. 3.5. Critical clearing time for a fault decreases with reduced inertia. If fault clearing time is less than critical clearing time, the rotor angle is stable, but if fault clearing time is more than critical clearing time, the rotor angle gets unstable. Thus, the change in the system's inertia could lead to an unstable condition due to the change in critical clearing time.

### 3.4.2.2 SCENARIO II: Effect of IBR on Protection Setting

To analyze the effect of IBR on relay setting a three-phase fault (LLL) and double phase to ground fault (LLG) has been applied on a single machine infinite bus at line 2 near bus 2 at 1 second and fault cleared at 1.017 seconds. As shown in the figure 3.14.a LLL fault is applied at 1 second, fault current starts to flow goes beyond peak up value and just after clearance short circuit current goes to zero. While with the integration of 40% and 80% of PV short circuit current shall not reach to pick up current setting due to which fault may not get clear and persists in the system for long duration. From the figure 3.17a it can be observed that system consists of only synchronous generator magnitude of short circuit current reaches to 2864A. However, with 40% share of PV short circuit current attains 2321A and with sharing of 80% short circuit current reaches to 1685A which is much lesser than short current response of conventional generators.

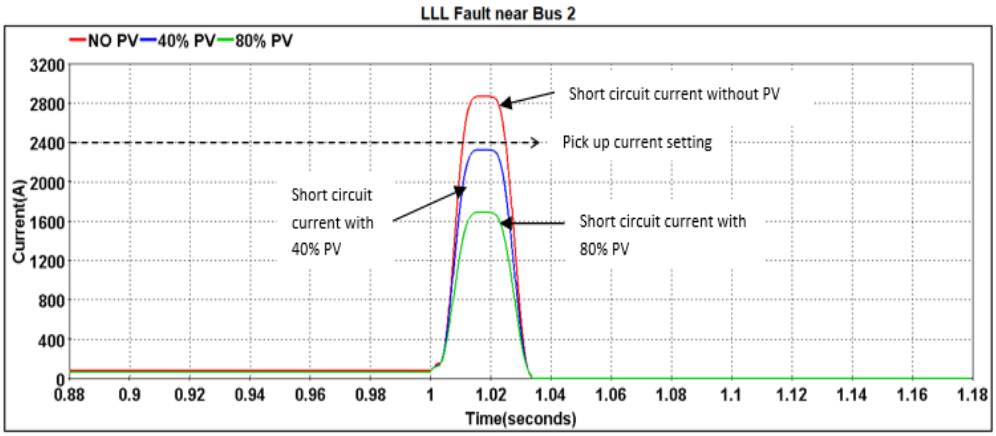


Fig. 3.17a Response of current during LLL Fault near Bus 2

LLG fault is applied at line 2 near bus 2 at 1 second and fault has been cleared at 1.017 seconds. As shown in the figure 3.17.b without PV in the system magnitude of short circuit current reaches to 3391A. However, with 40% integration of PV short circuit current attains 2835A and with 80% integration of PV short circuit current reaches to 2118A. If pick up current setting is 2400A as shown in figure 3.14a

& 3.17b fault current with integrating PV in the system shall not reach to pick up value of current in case of LLL fault while in case of LLG it shall reach to pick up value with 40% but fails in case of 80% integration of PV.

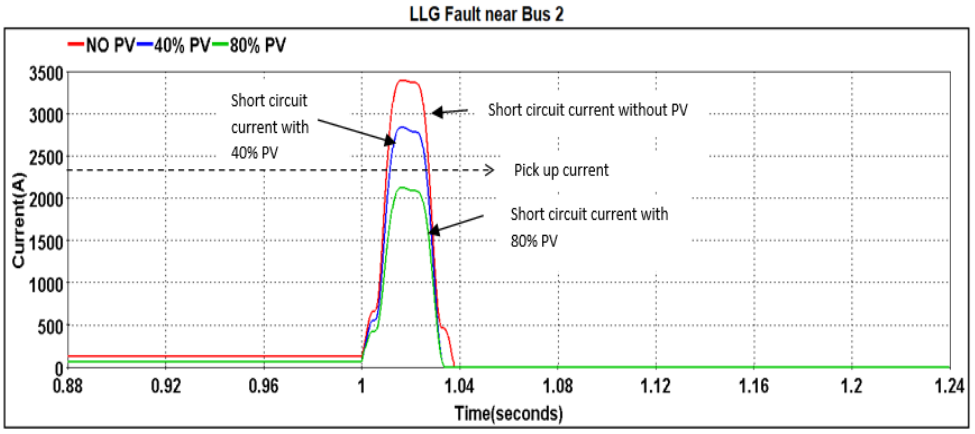


Fig. 3.17b Response of current during LLG Fault near Bus 2

By analyzing above scenarios, it can be concluded that reduction of inertia affects rotor angle stability. With reduced inertia, critical clearing time reduces thus system can gets unstable before clearance of fault. Besides, integration of IBR affects amplitude of short circuit current. As the penetration of PV increases into the grid and power sharing of synchronous generator decreases than the magnitude of short circuit current decreases. Resulting fault current shall not reach to pick up value of protective relay and doesn't get cleared, due to which the fault sustains for longer duration of time damaging the system and equipment.

### 3.4.3 CASE III: Impact of IBR on Small Signal Stability

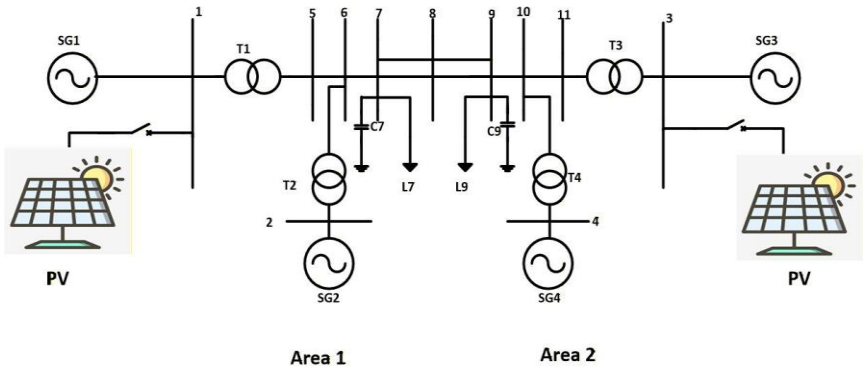


Fig. 3.18 Kundur's two area system

Kundur's two area system [32] with 75 MW PV farm as shown in the figure 3.18 has been simulated in EMTP RV real time simulator. Results have been analyzed for the effect of inertia reduction by IBR. In two area system two modes of oscillations occur prominently. Local area mode and Inter area mode of oscillation. In this study inter area mode oscillation has been observed. The system has been

initialized with a transfer of 400 MW from area 1 to area 2. A three phase to ground fault has been applied on a tie line near the terminal of area 1 at 3.0 sec and the fault is cleared at 3.01 sec by tripping the faulted line from both the ends resulting in only one transmission line connected between the two areas.

In this case four scenarios have been studied to observe power oscillations.

- Scenario I: Without integrating PV inter area mode oscillation has been observed.
- Scenario II: SG1 has been replaced with PV farm to observe inter area mode oscillation.
- Scenario III: SG3 has been replaced with PV farm to observe inter area mode oscillation.
- Scenario IV: Both SG1 & SG3 have been replaced with PV farm to observe inter area mode oscillation

### 3.4.3.1 SCENARIO I: Without Connecting PV

Two area system as shown in the figure 3.18 has been simulated. Tie line carries 400MW power sharing equal amount of power before fault is shown in the figure 3.19. After the occurrence of fault one line gets tripped off than power on another line oscillates for few seconds then after get stabilize transmitting full amount of 400MW power from area 1 to area 2.

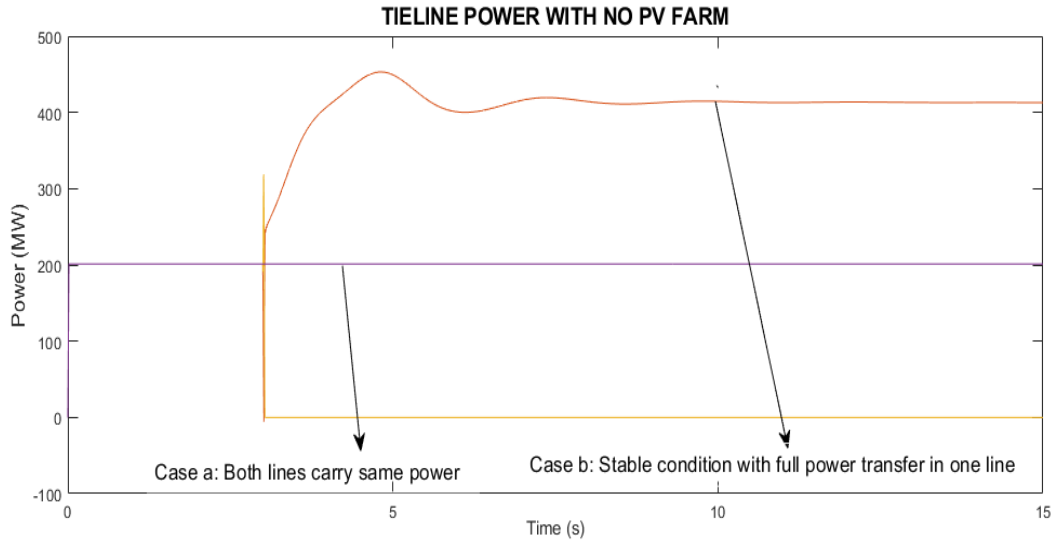


Fig. 3.19 Power Flowing through Tie line with SG

### 3.4.3.2 SCENARIO II: SG1 replaced with PV farm

Here, SG1 has been replaced with PV in area 1 while remaining three generators supply power as previously. It has been observed that before fault both the line carries equal amount of power as in scenario 1. After the application of fault power increases drastically on one line after clearance of fault one line gets tripped off while power of another one causes unstable oscillations and leads to instability as shown in the figure 3.20.

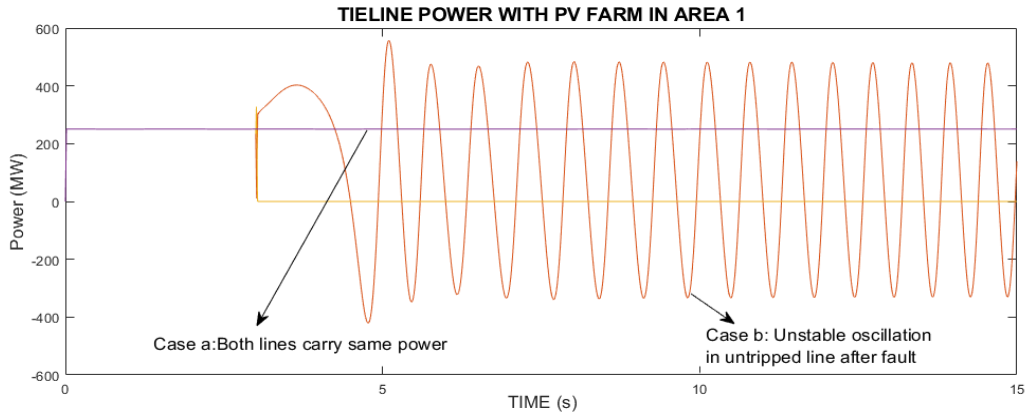


Fig. 3.20 Power Flowing through Tie line with PV in Area 1

### 3.4.3.3 SCENARIO III: SG3 replaced with PV farm

In this scenario in area 2, G3 has been replaced with PV farm. Load in area 2 has been shared by PV hence tie line power shall not get affected by it causing stable power flow from area 1 to area 2 after the clearance of fault is shown in the figure 3.21.

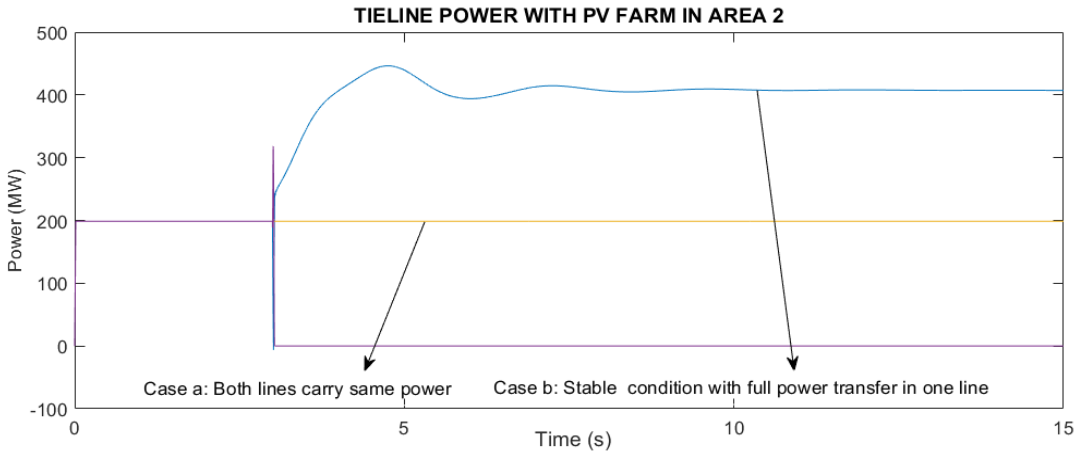


Fig. 3.21 Power Flowing through Tie line with PV in Area 2

### 3.4.3.4 SCENARIO IV: SG1 & SG3 replaced with PV farm

In both the area SG1 and SG3 are replaced by PV farm. Power of uninterrupted line oscillates after the clearance of fault leads to instability as shown in figure 3.22.

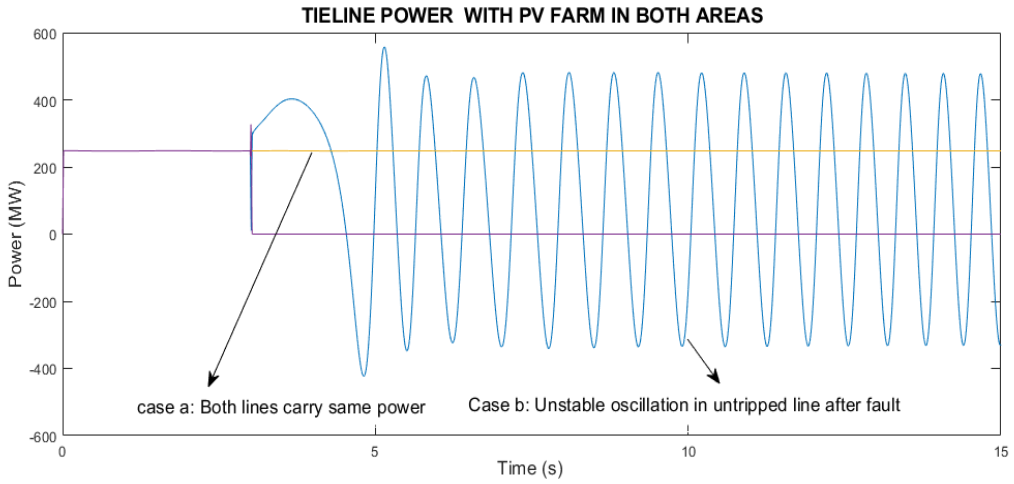


Fig. 3.22 Power Flowing through Tie line with PV in both Areas

By analyzing the above scenarios, it can be concluded that the tie line transmits an equal amount of power from area 1 to area 2 before the fault, even in the presence of PV. While after clearing the fault by tripping of one line another line carries full amount of power from area 1 to area 2 in absence of PV or if PV is in area 2. When PV is in area 1 power oscillates and leads to instability [135]. With the lower inertia damping ratio gets reduced which causes more power oscillation in the tie line. The frequencies of the oscillations depend on the strength of the system and the moments of inertia of the generator rotors. Fault in area 1 causes more oscillation in area 1. Post fault in two area system causes inter-area oscillation due to the flow on uninterrupted line, voltage at tie line bus near area 1 being reduced which causes a reduction in load hence generator power gets reduced. Since the torque applied to the generator rotors is constant, the torque imbalance causes the generator rotors to accelerate increase in the rotor speed renders the system stable. The absence of inertia in the system fails to increase the speed of the rotor, leading to the instability of the system.

## 4. Conclusion

This research presents a comprehensive analysis on impact of the IBR on power system with various benchmark models along with different types of disturbance.

It can be concluded from the analysis that:

- Integration of IBR in power system results in reduction in system inertia.

- Reduction in system inertia results in a reduced frequency nadir, increasing the likelihood of false triggering of under frequency relay.

- A decrease in system inertia reduces the critical clearing time, heightening the risk of system instability.

- Low system inertia intensifies inter-area oscillations, potentially causing instability.

- In addition to reduction in inertia controllers in IBRs decreases short-circuit current during faults, potentially leading to maloperation of protective devices.

Overall, the conclusion of the above analysis suggests that the integration of IBR in power system decreases power system lesser stability margin.

# CHAPTER 4

# IMPACT OF IBR ON DIRECTIONAL PROTECTION SCHEMES

This chapter discusses directional protection schemes used in power systems to protect transmission lines, feeders, and generators, with particular emphasis on the negative-sequence impedance-based directional overcurrent relay. However, the increasing integration of Inverter-Based Resources (IBRs) has affected the performance of these relays due to significant changes in fault current characteristics. To assess this impact, the study implements IBRs within standard IEEE benchmark models and evaluates their influence on relay operation.

## 4.1 Introduction

The electrical power system is undergoing continuous transformation with the large-scale integration of inverter-based resources (IBRs). While IBRs enhance sustainability and reduce dependency on fossil fuels, their integration presents new challenges for power system protection. IBRs are interfaced with the grid through power electronic converters, which significantly alter their dynamic response during disturbances. This has direct implications on conventional protection schemes such as directional protection, distance protection and differential protection, many of which rely on well-established current and voltage characteristics that are no longer valid under high IBR penetration[1], [71].

One of the most critical differences is the behavior of fault currents. In traditional systems dominated by synchronous generators, fault currents are large, predictable, and sustained long enough to be effectively detected by protective devices. In contrast, IBRs contribute fault currents of reduced magnitude, limited duration, and strongly dependent on control algorithms and protection mechanisms inherent in the converter[47], [136]. This deviation challenges the proper operation of protective relays, particularly in large, interconnected grids where accurate fault detection and coordination are vital for system security.

Negative sequence quantities have long been employed in protection schemes to detect unbalanced operating conditions. In particular, negative sequence current is used in overcurrent relays (50Q/51Q) and directional overcurrent relays (67Q), with the latter utilizing the angular relationship between negative sequence

voltage and current to determine fault direction. However, in the presence of IBRs, the magnitude and phase of negative sequence currents vary depending on the type of IBR and its control strategy, which may compromise the reliability of such relays. Given that directional relays are essential in transmission networks for distinguishing between forward and reverse faults especially when overcurrent and distance relays alone may not provide sufficient discrimination it is crucial to understand how IBRs affect the performance of these schemes. Motivated by these challenges, this research investigates the impact of IBR integration on negative sequence impedance-based directional relaying (67Q) under unsymmetrical fault conditions. Two benchmark 230 kV HVAC transmission system models have been developed and simulated using the OPAL-RT HYPERSIM real-time environment, with and without IBR integration. By analyzing negative sequence voltage $V_2$, current $I_2$ and their phase relationships, the study assesses the effectiveness of directional relays in maintaining reliable protection under varying levels of IBR penetration.

The capability limit of the IBR considered in this study is defined by the converter current limiter. The adopted Photovoltaic generation system model has a maximum converter current limit of 1.20p.u., corresponding to approximately 1.08 kA for the 750 kVA, 480 V IBR system. The existing simulations therefore evaluate the protection performance of power system relays under this limited fault-current capability.

The power system relay settings were intentionally kept unchanged when the synchronous generator was replaced by the IBR, in order to evaluate the impact of the altered fault-current characteristics on the existing protection system. With increasing PV penetration, the total fault current contribution also depends on the number and rating of IBR units connected to the system.

Defining a universal minimum IBR capability for safe relay operation is not straightforward because different protection functions depend on different electrical parameters. For example, overcurrent protection depends primarily on current magnitude, overvoltage/undervoltage protection on voltage magnitude, distance protection on apparent impedance, differential protection on the difference between currents, directional and negative-sequence protection on the magnitude and phase relationship of sequence components, and oscillation-related protection on phasor measurements.

Therefore, the impact of IBR on power system relays settings depends upon the relation between IBRs contribution to the variables upon which the conventional relay settings has been made. Further the impact of IBRs on conventional power system relay settings depends on the number of IBR units.

A universal minimum short-circuit current requirement cannot consequently be established without a dedicated analysis involving different IBR current limits and protection settings of given system.

### 4.1.1 Objectives

The specific objectives of this chapter are as follows:

- To investigate the effect of IBR integration on negative sequence current and voltage characteristics under unsymmetrical fault conditions.
- To analyze the performance of negative sequence impedance-based directional overcurrent relay (67Q) in systems with varying IBR penetration.
- To evaluate how the phase angle relationship between $V_2$ and $I_2$ is influenced by IBRs and its impact on fault direction identification.
- To utilize real-time simulation platforms (OPAL-RT HYPERSIM) for validating the effectiveness of 67Q relaying in hybrid systems.

### 4.1.2 Contributions

The contributions of this chapter can be summarized as:

- A systematic analysis of the impact of IBRs on negative sequence impedance-based directional relays (67Q).
- A comprehensive evaluation of negative sequence voltage (V2), current (I2), and corresponding phase angles, highlighting their variation before and after IBR integration.

## 4.2 Basics of Directional Overcurrent Relaying

This section discusses about the conventional directional overcurrent relaying followed by negative sequence impedance based directional overcurrent relaying 67Q adopted for this study.

### 4.2.1 Conventional Directional Overcurrent Relaying

Traditionally directional element of the relay evaluates the directional component of the system fault with negative sequence measurements in the system. Conventional Directional overcurrent relay 67Q detects the direction of fault using phase relationship of voltage V and current I. Modern microprocessor base relay uses phase angle of positive sequence impedance $Z_1$, negative sequence impedance $Z_2$ and zero sequence impedance $Z_0$ to detect the direction of fault. Negative sequence current $I_2$ and voltage $V_2$ occurs only during unbalanced fault. While zero sequence current

I0 and V0 occurs only with the involvement of ground in case of fault. Hence, this parameter makes an ease in detecting the direction of fault quickly[62], [137], [138].

### 4.2.2 Negative Sequence-based Impedance based Directional Overcurrent Relaying 67Q

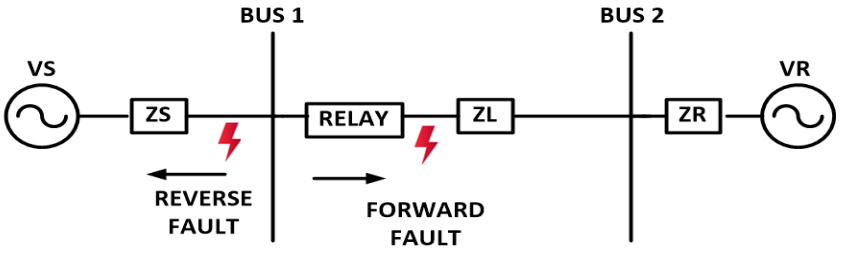


Fig. 4.1 Two source system with directional relay 67Q

Directional relaying does not play significant role for system with single source. For the two-source system shown in the figure 4.1 to detect a fault in forward direction and that of reversed direction impedance observed by the relay is different Negative sequence impedance base directional relay 67Q uses phase angle relationship of voltage $V_2$ and current $I_2$. For detecting fault in forward direction $Z_2$ measures impedance behind the relay which is equal to $ZS_2$ can be represented as in equation 4.1.

$$Z_{2F} = -ZS_2 \tag{4.1}$$

For the fault in reverse direction $Z_2$ measured is equal to the addition of line impedance ZL and impedance of remote source ZR represented in the equation below. [15-17].

$$\mathrm{Z}_{2\mathrm{R}} = ZS_2 + ZLINE_2 \tag{4.2}$$

### 4.2.3 Setting of Negative Sequence-based Impedance based Directional Overcurrent Relaying 67Q

Negative Sequence impedance relay measures negative sequence impedance Z2 by equation in 4.3,

$$Z_2 measured = \frac{Re[\,V_2(1\angle Z_1 ANG \times I_2)^*]}{|I_2|^2} \tag{4.3}$$

Where, $V_2$ is Negative Sequence Voltage

$I_2$ is Negative Sequence current

$\angle Z_1 ANG$ is Positive sequence line angle

* Sign indicates complex conjugate

Operating area based on $Z_2$ is presented in figure 4.2.

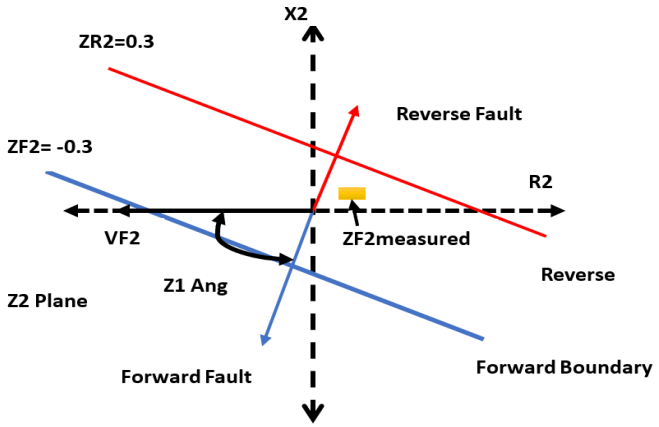


Fig. 4.2 Operating Area of Impedance base directional Overcurrent Relay 67Q

$Z_2$ measured detects the direction of fault. If $Z_2$ measured is lower than $ZF_2$ than fault shall be detected in forward direction. In case of $Z_2$ more than $ZR_2$ fault shall be detected in reverse direction.

## 4.3 Case Study

In this research study two benchmark models are considered for two different unsymmetrical fault scenarios.

Case I: Fault analysis of nine bus system.

Case I: Fault analysis of six bus system.

### 4.3.1 Case I: Fault analysis of Nine Bus System

Nine bus system [62], [135]consists of three generators of rating 512MVA, 270MVA, 125 MVA is shown in the figure 4.3 has been simulated on opal RT HYPERSIM real time simulator. In this study 270 MVA synchronous generator has been replaced with five small generators of equivalent rating. To incorporate PV in the system PV farm is connected at bus 2 which has been added in the system such that at a time it can replace one small synchronous generator which could be tripped off. Likewise, PV is increased in the system and synchronous generator reduced. Negative sequence-based impedance directional relays 67Q are connected at each end of a transmission line to identify the direction of fault.

Two fault scenarios have been tested on the system with and without PV in the system.

Scenario I: LG fault near PV bus

Scenario II: LLG fault at remote location to PV bus

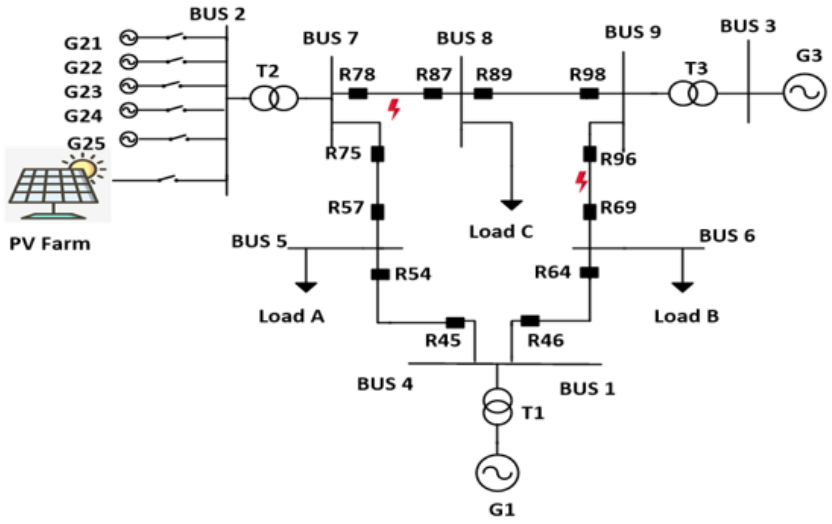


Fig. 4.3 Nine bus system

### 4.3.1.1 Scenario I: LG fault near PV bus

In this scenario LG Fault has been applied at 2 seconds in line between bus 7 and 8. For this line relay R78 (Negative sequence impedance base directional relay) detects the fault in forward direction hence relay gets trip while relay shows no fault in reverse direction. Response of the relay R78 for both the direction are presented in the figures below 4.4 and 4.5 which shows relay is working properly.

The same relay has been tested further by integrating PV in the system. PV has been replaced in the system by tripping off G21 and incorporating the same amount of power of G21. Response of R78 has been plotted in the figure 4.4 and 4.5 which shows relay operating accurately. Further, more amount of PV in the system has been replaced by tripping off synchronous generators G22, G23, G24 simultaneously. The response of which is also plotted in the figure 4.4 and 4.5. With the increases of PV in the system response of relays R78 get more disturbed signal of relay leads to maloperation of the relay.

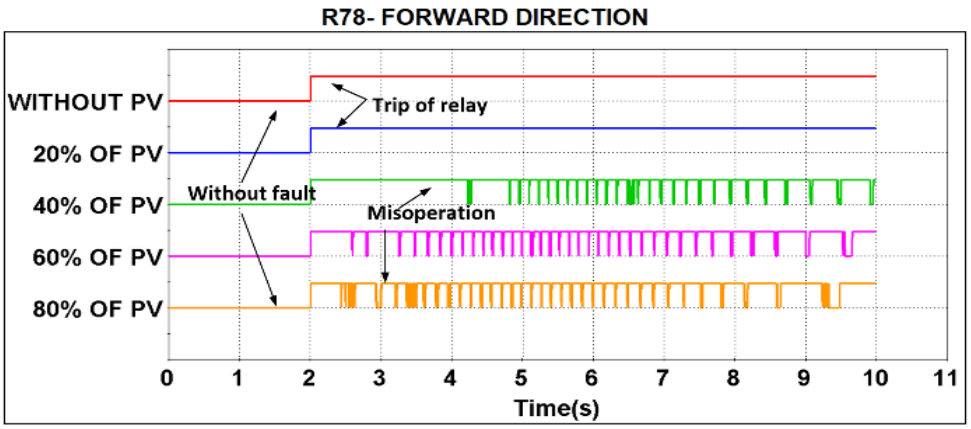


Fig.4.4. Response of R78 for forward direction

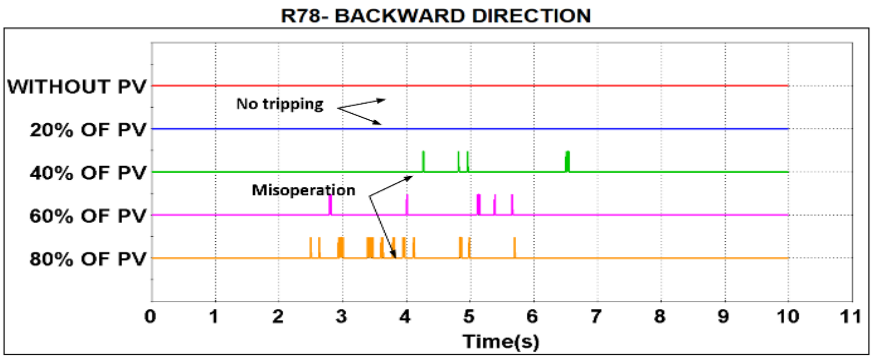


Fig.4.5 Response of R78 for Reverse direction

### 4.3.1.2 Scenario 2: LLG Fault at Remote Bus from PV

In this scenario LLG fault has been applied at 2 seconds at line between bus 7 and 8 which is far away from PV bus and response of relays R96 were analyzed for forward and reverse direction. Without PV in the system relay operates properly and gets trip as the fault occurred in the system. However, with integration of PV in the system till 20% of G2 the relay operates normally while PV power goes beyond 20% of G2 maloperation has been observed in both the direction. Response of the relay R96 is plotted in the figure below 4.6 and 4.7.

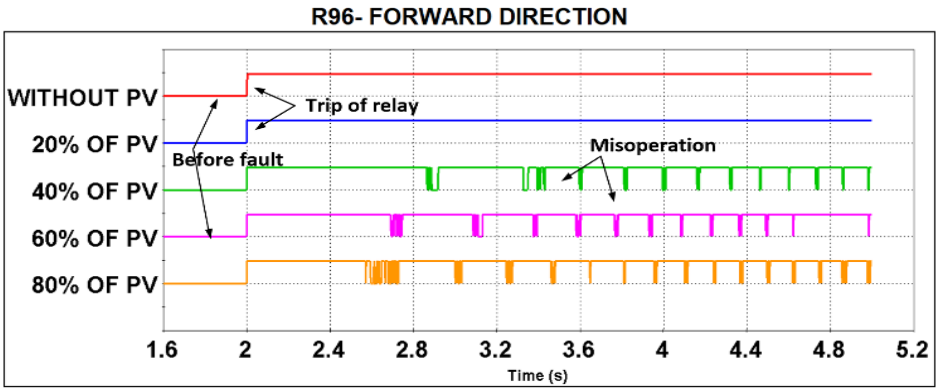


Fig.4.6. Response of R96 for forward direction

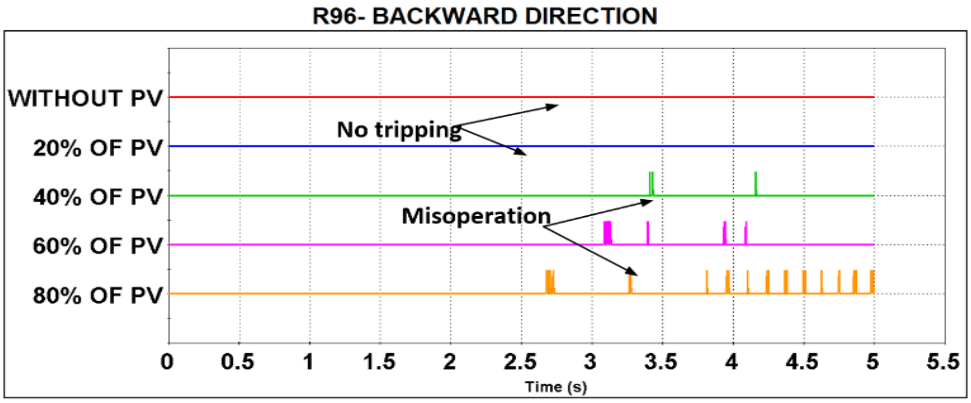


Fig.4.7. Response of R96 for Reverse direction

### 4.3.2 Case II: Fault analysis of Six Bus System

To validate the result obtained by nine bus system six bus 230 kV HVAC system is shown in the figure 4.8 has been considered for simulation [21]. Six bus HVAC 230 transmission line benchmark model consists of two synchronous generators of rating 1000MVA each. 67Q relay connected at each end of transmission line. G1 and G2 (G21and G22) supplies active power of 25MW. Efficacy of 67_Q has been tested for LLG fault without integrating PV in the system. Then after PV of 12.5 MW has been incorporated in the system by tripping off G21 in first step. Further, G21 and G22 both tripped off and 25 MW supplied by PV alone.

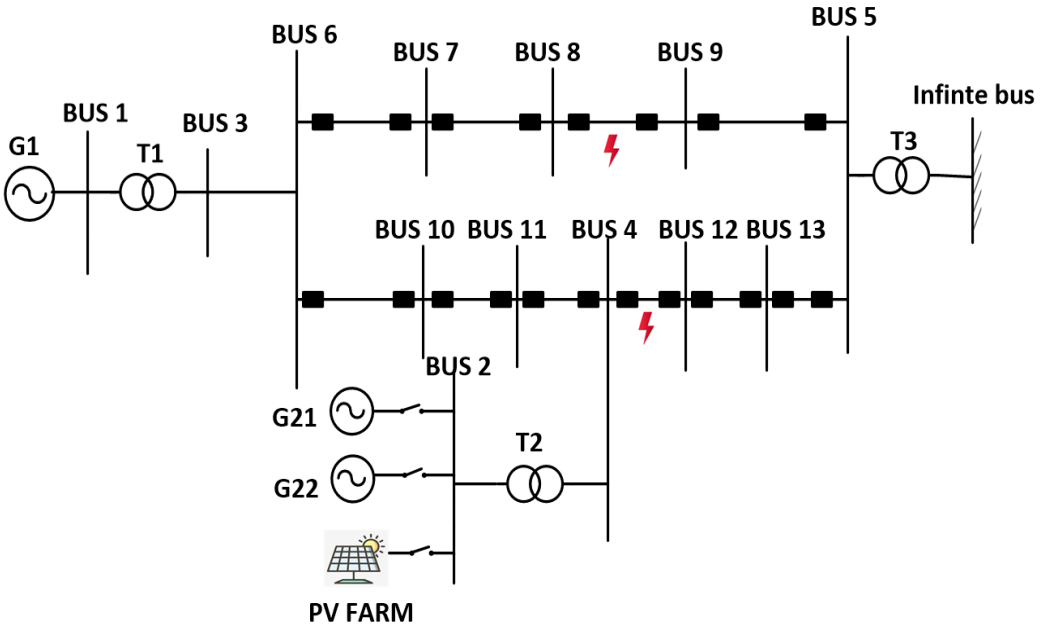


Fig.4.8. Six Bus System

Two fault scenarios have been considered to analyze response of relay

- Scenario I: LLG fault near PV bus
- Scenario II: LLG fault at remote location to PV bus

#### 4.3.2.1 Scenario I: LLG fault near PV bus

LLG fault has been applied at 2 seconds at line between bus 4 and 12. Negative sequence impedance based directional relay 67Q detects the direction of fault in forward direction and gets trip, no fault has been detected by relay in backward direction is shown in the figure below 4.9 and 4.10. With the replacement of G21 by PV (50% of G2), relay 67Q operates correctly while with the replacement of G21 and G22 (100% of G2) by PV relay malfunctioning occurs as indicated in the figures below 10 and 11. With the increase in PV generation in the system disturbance in relay increases for forward as well as reverse direction.

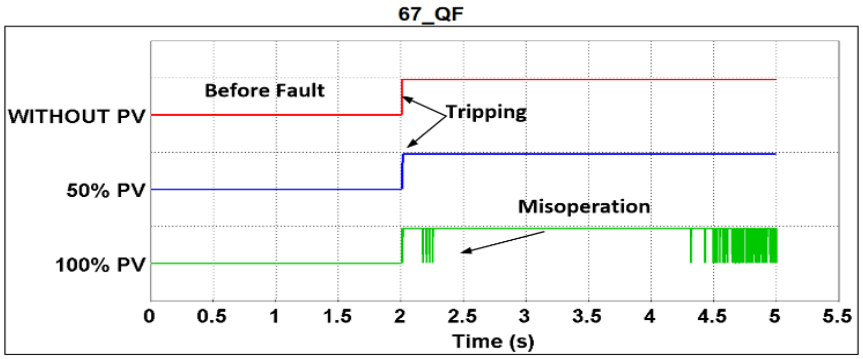


Fig.4.9. Response of 67QF connected at bus 4

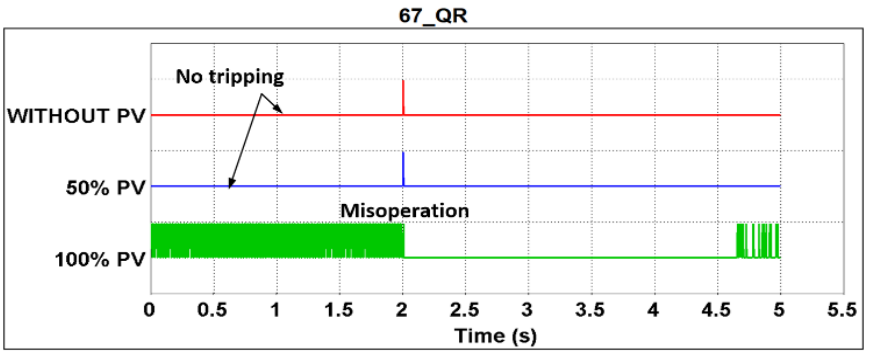


Fig.4.10 Response of 67QR connected at bus 4

### 4.3.2.2 Scenario I: LLG Fault Remote to PV Bus

LLG fault has been applied at line between bus 8 and 9. 67Q directional relay connected at bus 8 detects the fault in forward direction whereas the no fault has been detected in reverse direction. With integration of PV in the system when G21 has been tripped off 67Q relay connected at bus 8 works properly detecting direction of fault in forward direction and no fault in backward direction. Further, by tripping off G21 and G22, 25MW (100% of G2) power supplied by PV alone relay operates properly in forward direction getting relay getting trip signal indicated in figure 4.11 while in reverse direction maloperation occurs is indicated in figure below 4.12.

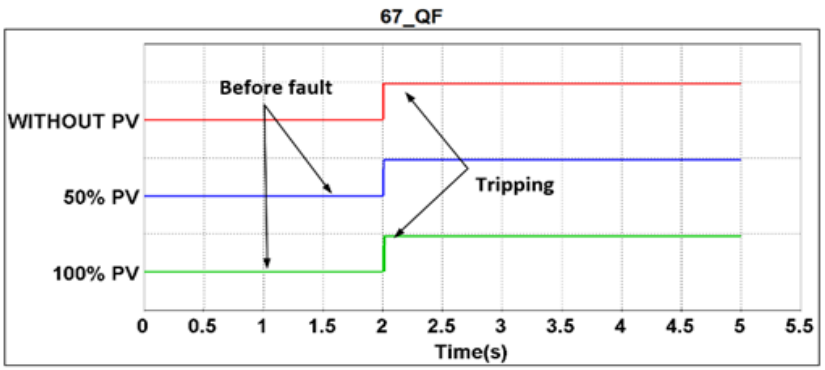


Fig.4.11 Response of 67QF connected at bus 8

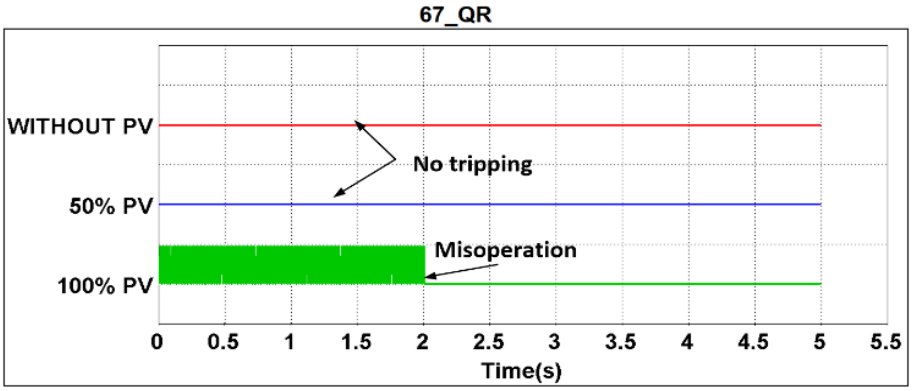


Fig.4.12. Response of 67QR connected at bus 8

## 4.4 Result and Discussion

To illustrate the malfunctioning of Relay response of negative sequence volage, negative sequence current and corresponding phase angle for nine bus system are plotted in the fig below respectively 4.13, 4.14, 4.15, 4.16 and 4.17. It can be observed that With PV and Without PV characteristics of negative sequence voltage, negative sequence current and corresponding phase angle are different. Negative sequence impedance phase angle is also been observed which used as input parameter to trip the relay which shows different characteristics without PV in the system and with integrating PV in the system. PV doesn't follow conventional characteristics which creates difficulty for protection scheme leading to mis operation of relays. Also, it has been observed from above case study in case of fault at remote location from PV bus impact of PV is lesser on the protectional relay. Furthermore, With the system dominating PV produces more complexity in protectional relaying. Negative sequence voltage produced during fault is inversely proportional to source behind the relay for forward fault. In case of stronger source lesser negative sequence impedance gets produced whereas more negative sequence impedance produced for weaker source.

It can be concluded from above results that impact on protection depends upon location of IBR and amount of generation by IBR.

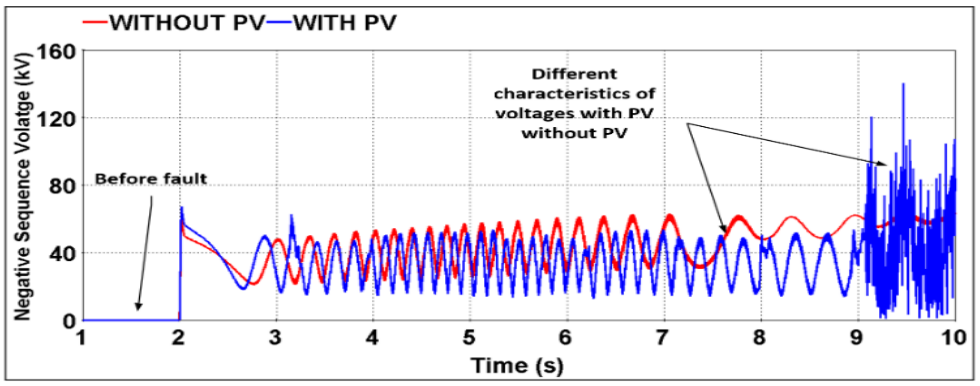


Fig.4.13. Response of Negative Sequence Voltage

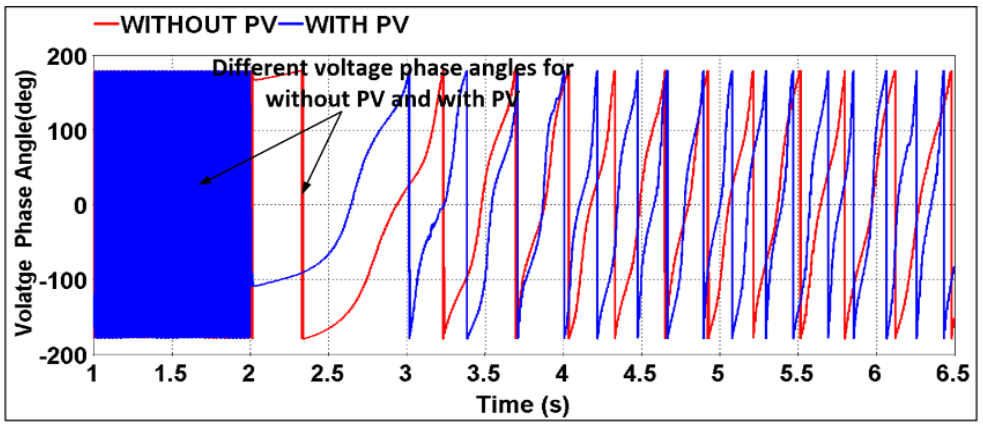


Fig.4.14. Response of Negative Sequence Voltage Phase Angle

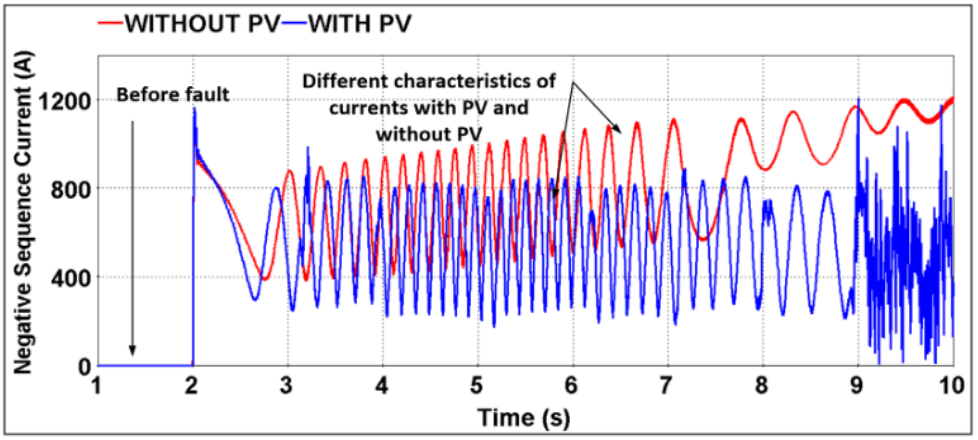


Fig.4.15. Response of Negative Sequence Current

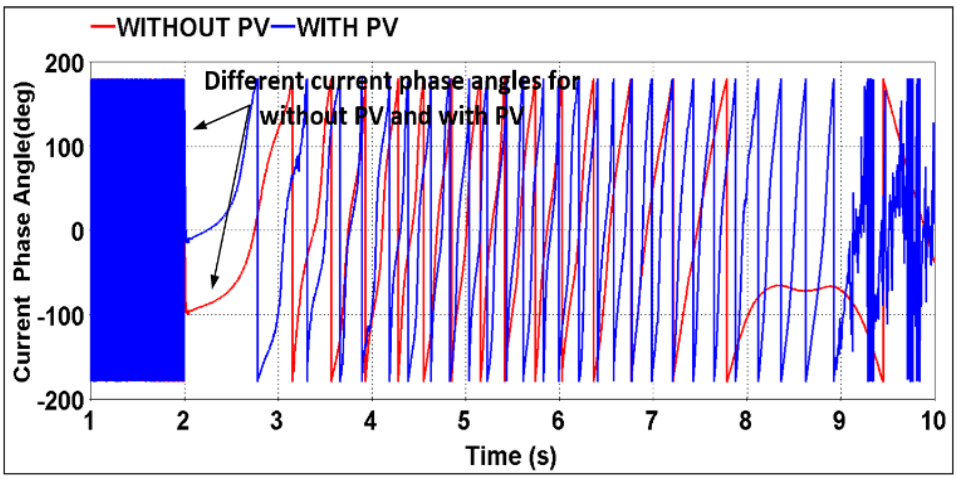


Fig. 4.16 Response of Negative Sequence Current Phase Angle

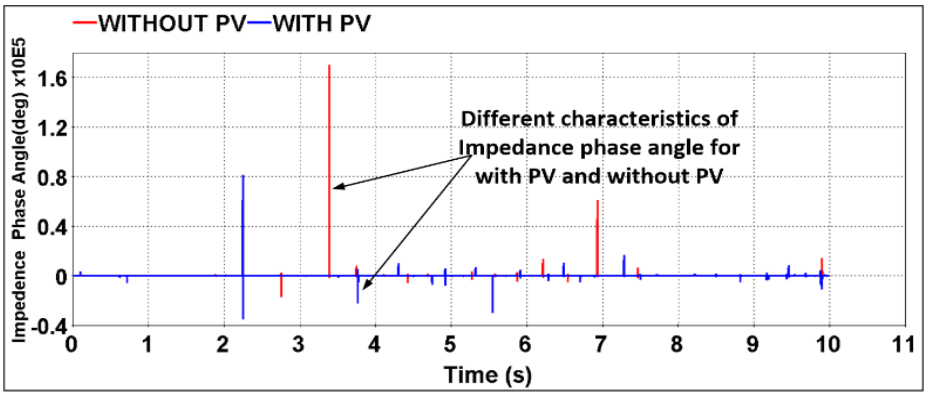


Fig.4.17. Response of Negative Sequence Impedance Phase Angle

## 4.5 Conclusion

Integration of IBR has affected the performance of protection equipment in power system. This paper investigates on negative sequence impedance based directional overcurrent relaying 67Q in the presence of IBR in the system. 67Q operates adequately on two benchmark model in the absence of IBR in the system, while with the integration of IBR in the system failures of relays have been detected. In case of fault at remote location from PV bus relays are not affected as much as it gets affected near PV bus. Also, it can be augmented that with the more generation by PV in the system negative sequence impedance based directional relay gets affected. Further in this study to understand response of 67_Q relay Negative sequence voltage, negative sequence phase angle, negative sequence current and negative sequence are analyzed which presents different characteristics for the system in absence of IBR and in presence of IBR in the system.

# CHAPTER 5

# IMPACT OF IBR ON DISTANCE PROTECTION

This chapter examines the application of distance protection in long transmission lines and evaluates its performance under high penetration of Inverter-Based Resources (IBRs). The presence of IBRs often leads to the maloperation of conventional mho relays, a phenomenon analyzed through detailed case studies. Additionally, the chapter discusses the blinder scheme developed to differentiate between actual faults and power swing conditions. A mathematical relationship between system inertia and the Rate of Change of Impedance (ROCI) is established, followed by a case study assessing the impact of IBR integration on the power swing blocking function of impedance relays.

## 5.1 Introduction

With the large-scale integration of inverter-based resources (IBRs), their widespread deployment introduces significant challenges to power system stability and protection. These deviations challenge the effective operation of conventional protection schemes that were designed under assumptions valid for synchronous machine-dominated systems. Among the most affected schemes are impedance-based distance relays and power swing blocking (PSB) functions, both of which play a crucial role in protecting transmission networks[72], [139], [140], [141]. Distance relays estimate the apparent impedance between relay location and fault point to detect and isolate faulty lines. However, with the integration of IBRs, fault current characteristics become non-sinusoidal, frequency-varying, and limited in magnitude, which can lead to distance relay maloperation such as under-reaching, over-reaching, or delayed operation. In particular, in the presence of doubly-fed induction generators (DFIGs) or photovoltaic (PV) systems, variations in rotor speed or inverter control actions may introduce frequency components that distort impedance measurement, undermining the relay's dependability and security.

Power swing blocking (PSB) function is equally important that prevents distance relays from maloperation during stable or unstable swings. Power swings are natural fluctuations in power transfer caused by disturbances such as line switching, faults, or generator disconnections, and are usually damped as the system returns to a new equilibrium. However, when swings resemble fault trajectories within the relay characteristic, incorrect tripping may occur, leading to unnecessary line outages or even cascading blackouts. Modern relays employ PSB functions, often using blinder

schemes or rate-of-change of impedance methods, to discriminate between genuine faults and power swings. With IBR integration, reduced inertia alters swing dynamics, accelerating the rate of change of impedance and potentially compromising PSB functionality. The joint impact of IBRs on distance protection and PSB functions thus raises new challenges in ensuring reliable transmission system protection. Traditional relay logic may fail to distinguish between faults and swings or may miscalculate impedance due to IBR-induced current characteristics. Motivated by these concerns, this research investigates the effect of IBR integration on both distance protection schemes and power swing blocking performance. Kundur's two-area test system and a 230 kV transmission benchmark system have been modelled in the OPAL-RT HYPERSIM real-time simulator, with photovoltaic (PV) units integrated to represent IBR penetration. Both fault and swing scenarios are considered to evaluate protection behavior under reduced inertia conditions [43]

### 5.1.1 Objectives

The specific objectives of this chapter are as follows:

- To analyze the impact of IBR integration on impedance-based distance relay operation, particularly under different fault conditions.
- To investigate the effect of reduced system inertia on power swing blocking (PSB) functionality in the presence of IBRs.
- To evaluate the rate of change of impedance ROCI under different swing and fault scenarios, with and without IBR penetration.
- To validate the combined performance of distance protection and PSB using real-time simulations on benchmark transmission system models.

### 5.1.2 Contributions

The main contributions of this chapter can be summarized as follows:

- A comprehensive investigation of the challenges posed by IBRs to impedance-based distance protection schemes and power swing blocking functions.
- Demonstration that distance relays may fail (under-reach, over-reach, or delay) due to altered fault current magnitude and frequency content introduced by IBRs.
- Analysis of how reduced inertia (Hsys) from IBR integration accelerates power swings and affects PSB discrimination, potentially leading to maloperation.
- Development and testing of a blinder-based PSB scheme under both swing and fault conditions, highlighting its sensitivity to IBR penetration levels.

## 5.2 Theoretical background

### 5.2.1 Distance Relay Working Operation

Distance relay measures the impedance of transmission line to detect the presence of fault. It works on the principle that if the measured impedance of the line is below its predefined value the fault lies within its specified reach. To specify the different reach of protected part of line different zones are defined. The zones of distance relay are selected as 70-80% of line length as zone 1 and 120-150% of line length as zone 2 in which 20-50% line included from adjacent line to provide back up protection with definite time delay for remote fault [72], [142]. Zones of distance relay is presented in the figure 5.1 below.

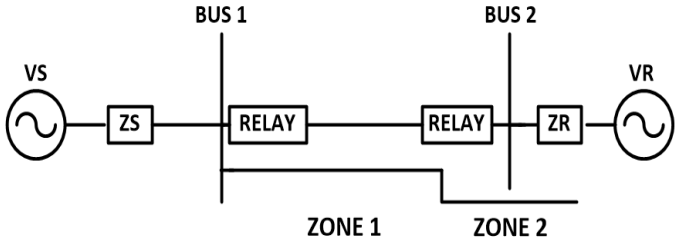


Fig. 5.1 Zones of Distance Relay

### 5.2.2 Mho Relay Setting

The well-known distance-based relay used to protect long transmission line is mho relay whose characteristics shown in the figure 5.2. The mho relay used for this study is set to be reach at 80% of transmission line to detect the fault in zone 1 while it is set to be reach at 120% of transmission line to detect fault in zone 2. The characteristics of mho relay is represented as circle passing through origin in RX plane which implies the directional element of relay.

Diameter of circle 1 is set to be 80% of total line impedance of transmission line length with time delay of 0.0083s and diameter of circle 2 is chosen as 120% of the transmission line length with definite time delay of 0.3333s.

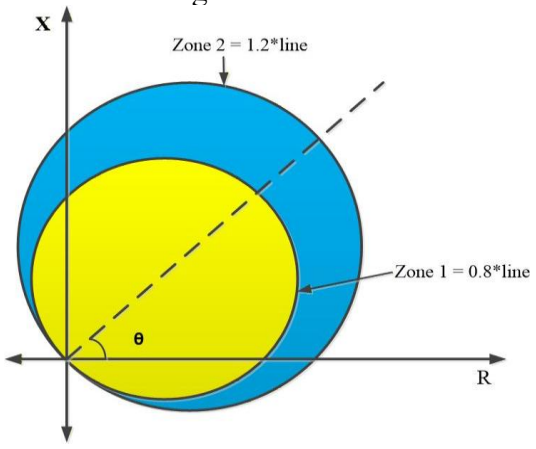


Fig 5.2. Characteristics of Mho relay

If impedance lies within circle 1 mho relay identifies the fault instantly while if impedance lies within circle 2 mho relay takes time to detect the fault. Relay then gives command to circuit breaker to trip the breaker and isolate the faulty section.

### 5.2.3 Blinder Schemes

The blinder scheme relies on the concept of measuring the duration required for an impedance vector to traverse a predefined delta impedance (Δz). The time measurement starts when the impedance vector intersects the outer blinder (ROB) and concludes upon crossing the inner blinder (RIB). A power swing condition is identified if the measured time (Δt) exceeds the delta time setting. Furthermore, while the impedance vector is inside this delta impedance region, the protective relay element may be restrained from tripping, since this condition might indicate either a substantial load or a stable power swing. Upon detection of an unstable swing, the mho element may either trip immediately or postpone tripping until the swing has passed, therefore reducing over-voltages across the opened breaker. Determining the appropriate settings for the blinds is sometimes complex and requires an advanced grid analysis. Blinder scheme adopted to analyze PSB is presented in figure 5.3.

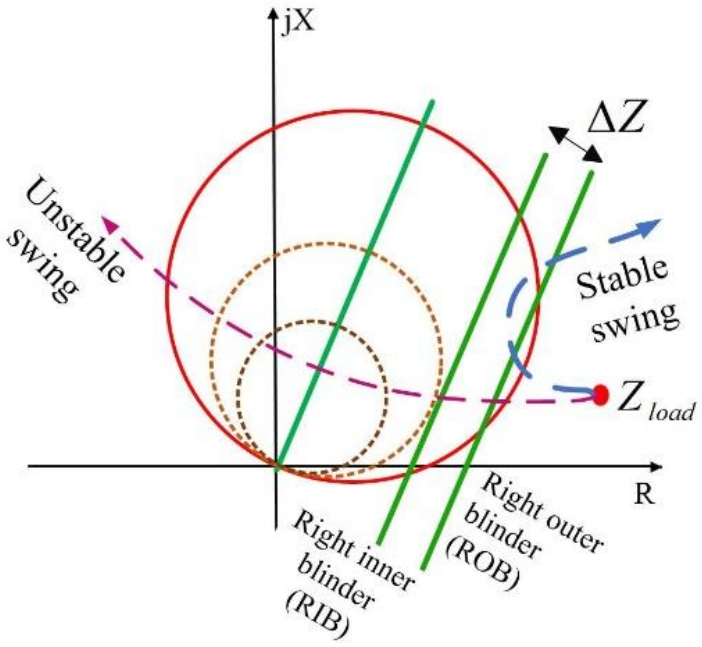


Fig 5.3. Blinder scheme adopted to analyze PSB

### 5.2.4 Mathematical Relationship Between Inertia and ROCI

The high penetration of Inverter-Based Resources (IBRs) displaces conventional synchronous generators, significantly reducing rotational inertia in modern power systems. During power swings, this lower inertia causes faster rotor angle excursions ($d\delta/dt$), which directly accelerates the Rate of Change of Impedance ROCI, or $dZ/dt$ observed by protective distance relays.

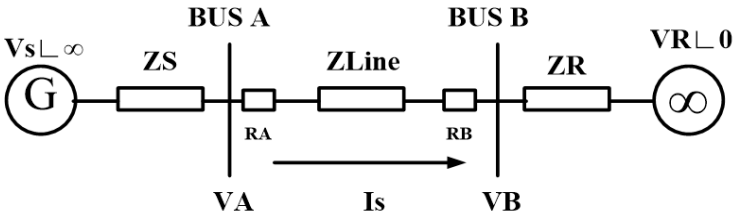

Fig. 5.4 Single machine infinite bus model

To quantify this relationship, consider a Single Machine Infinite Bus (SMIB) model shown in the figure 5.4. With total impedance $Z_{TOTAL}$ including $Z_s$, $Z_R$, $Z_{Line}$ and generator rotor angle $\delta$. Under balanced terminal voltages, the apparent impedance magnitude $|Z_A|$ seen by the relay at Bus A is expressed as:

$$|Z_A| = \frac{|Z_{TOTAL}|}{2\sin\left(\frac{\delta}{2}\right)} \tag{5.1}$$

Differentiating 5.1 with respect to time defines the trajectory speed of the apparent impedance observed at the relay terminal:

$$\left|\frac{d|Z_A|}{dt}\right| = \frac{|Z_{TOTAL}|}{4\sin^2\left(\frac{\delta}{2}\right)} \cdot \left|\frac{d\delta}{dt}\right| \tag{5.2}$$

Equation (5.2) demonstrates that ROCI is governed directly by the rate of change of the rotor angle $(d\delta/dt)$. To explicitly account for generator inertia $H$, system frequency $F$, and accelerating power $P_a$, the classical swing equation is integrated:

$$\frac{\mathrm{d}\delta}{\mathrm{dt}} = \sqrt{\frac{360\cdot \mathrm{F}}{\mathrm{H}} \int_{\delta_0}^{\delta} \mathrm{P_a}\ \mathrm{d}\delta} \tag{5.3}$$

Extending equation 5.3 to a two-machine system with individual inertias $H_1$ and $H_2$ yields the general multi-machine dynamic ROCI formulation:

$$\left|\frac{d|Z|}{dt}\right| = \frac{|Z_{TOTAL}|}{4\sin^2\left(\frac{\delta_1-\delta_2}{2}\right)} \cdot \left|\sqrt{\frac{360\cdot F}{H_1}\int_{\delta_{01}}^{\delta_1} P_{a1}\ d\delta_1} - \sqrt{\frac{360\cdot F}{H_2}\int_{\delta_{02}}^{\delta_2} P_{a2}\ d\delta_2}\right| \tag{5.4}$$

Equation 5.4 confirms that ROCI ($\left|\frac{d|Z|}{dt}\right|$) is inversely proportional to machine inertia ($\sqrt{H}$). In low-inertia grids, the resulting rapid impedance trajectories can traverse dual-blinder Power Swing Blocking (PSB) zones faster than standard delay timers ($\Delta t$), leading to potential relay maloperations or unnecessary line trips.[103].

## 5.3 Case Study

Two case study have been performed to investigate impact of IBR on distance relay and Power Swing Blocking function of distance relay.

### 5.3.1 Case Study I

The IEEE standard Nine bus benchmark system has been simulated in OPAL RT HYPERSIM real time simulator for different types of fault scenarios. Nine bus system consists of three synchronous generators are of rating 512 MVA, 270MVA, 125 MVA respectively. Three loads A, B, C consumes total power of 115 MW. In this study to incorporate PV farm in the system synchronous generator G2 has been splitted into five small synchronous generators $G_{21}$, $G_{22}$, $G_{23}$, $G_{24}$ and $G_{25}$. Mho relays are connected at each end of line to detect the fault and command trip signal to circuit breaker. Different types of faults have been applied at different locations in line 7-8 and 8-9 to verify the performance of the mho relay. Figure of nine bus system is shown in the figure below 5.5. [15].

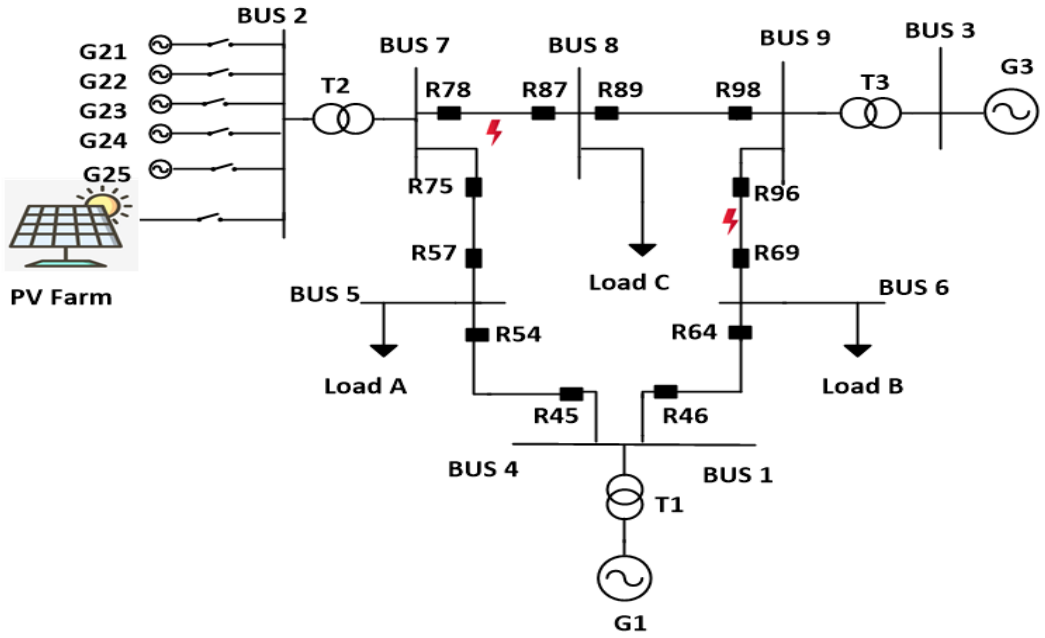


Fig. 5.5 Nine bus system

Following five fault scenarios have been tested on the system.

- Fault Scenario I: LLL fault is created at 25km from bus 7
- Fault Scenario II: LLL fault is created at 50 km from bus 7
- Fault Scenario III: LG fault is created at 50 km from bus 7
- Fault Scenario IV: LLL fault is created at 90 km from bus 8
- Fault Scenario V: LG fault is created at 30 km from bus 8

### 5.3.1.1 Scenario I: LLL fault at 25km from bus 7

Three phase fault LLL is applied at 2 seconds on the system at line 7-8 line length of which is 76km. Fault is applied at a distance of 25 km from bus 7 mho relay placed at bus 7 detects the fault in zone 1 and give command to circuit breaker instantly shown in the figure 5.6. Circuit breaker trips the line 7-8 from remaining system as the current drops to zero shown in the figure below 5.7 and 5.8 impedance trajectory is plotted in the figure 5.9. To analyze impact of IBR in the system G21 has been tripped off and PV farm of equivalent rating has been integrated in the system mho relay operation and command to circuit breaker has been indicated with the blue color in the figure 5.6 and 5.7 below. Also, the current response has been marked in the figure 5.8.

Similarly, PV share has been increased till 60% of synchronous generation to study its response on relay and other parameters. From the figures it can be analyzed that with the increasing share of PV into the system mho relay takes more time to detect the fault also during fault the peak of short circuit current reduces with increasing share of PV.

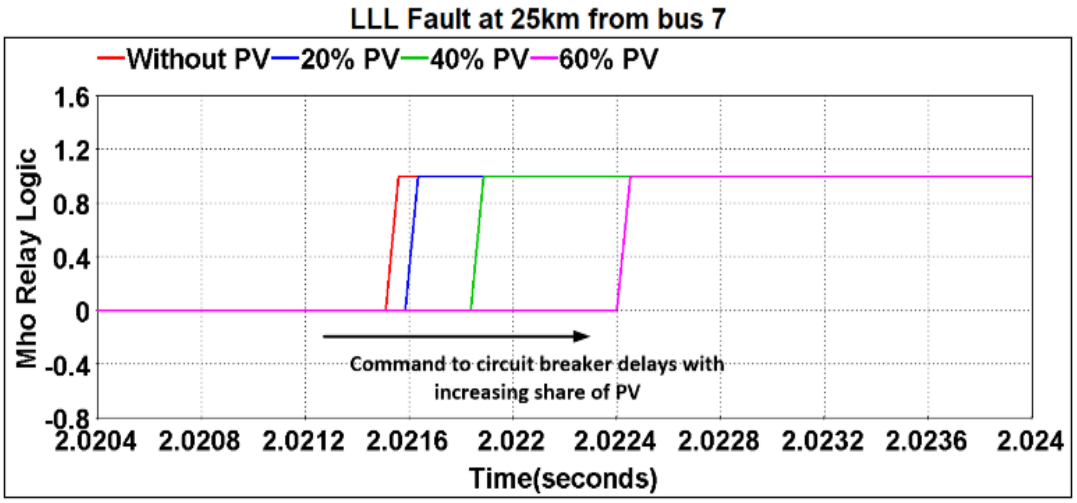


Fig.5.6. Mho relay operation during LLL fault at 25km

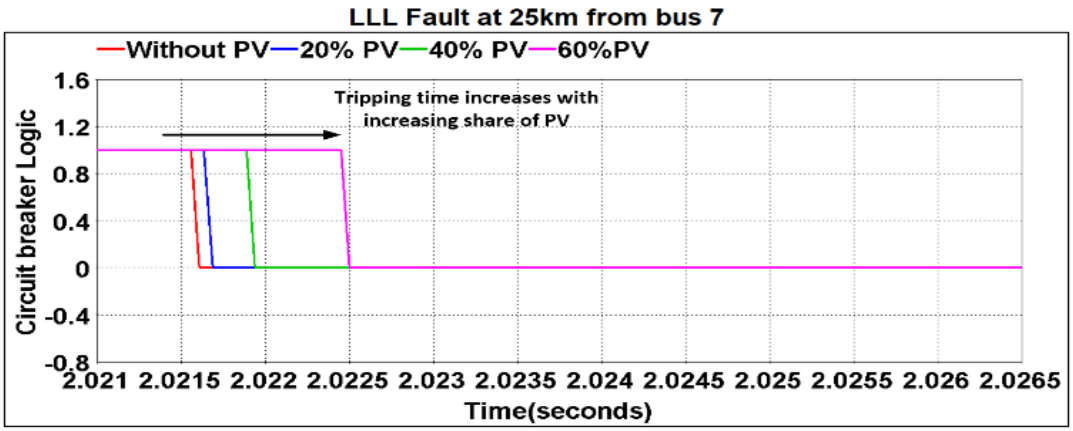


Fig.5.7 Response of circuit breaker post action from relay

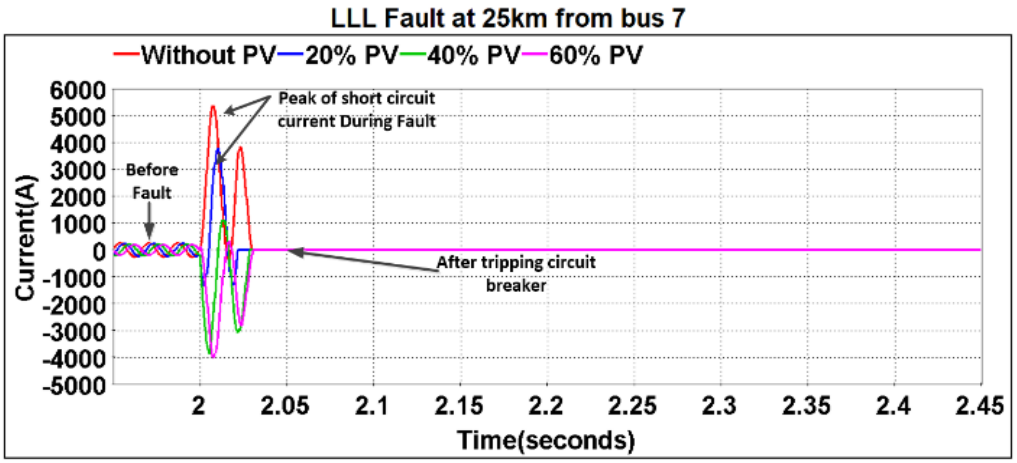


Fig.5.8 Response of current during LLL fault

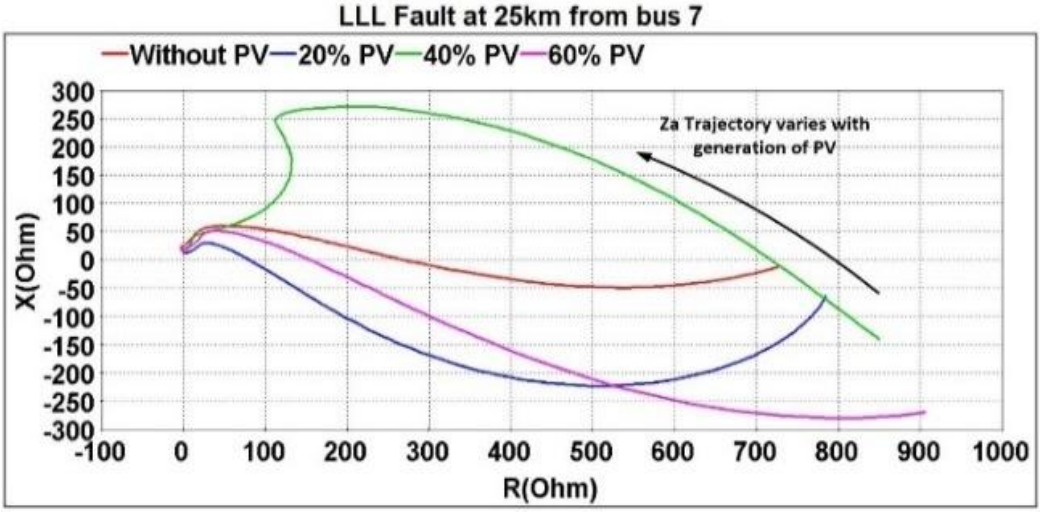


Fig.5.9. Impedance locus observed by Relay R78 during LLL fault at 25km

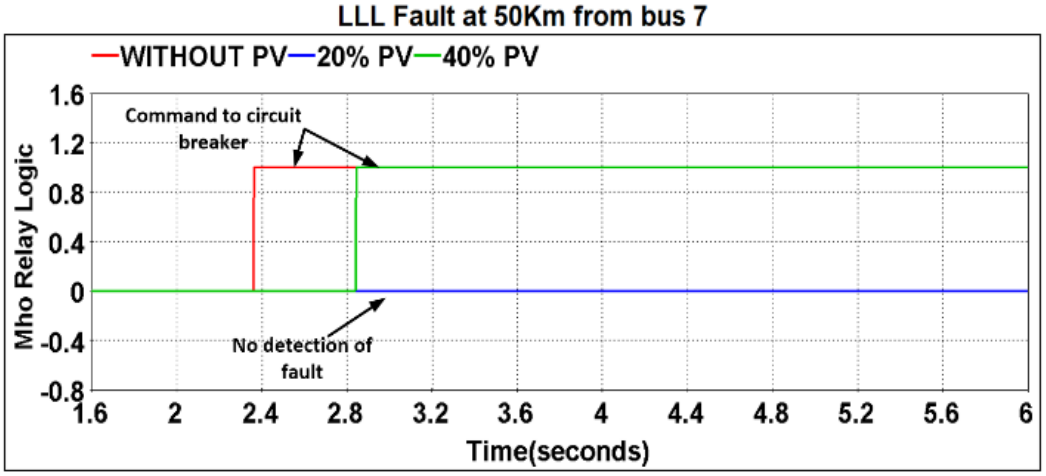


Fig.5.10. Mho relay operation during LLL fault at 50km

### 5.3.1.2 LLL Fault at 50km From Bus 7

In this scenario LLL fault is applied in zone 2 of line 7-8. Fault has been applied at 50 km from bus 7. Without PV in the system mho relay operates accurately giving command to circuit breaker which makes current to zero shown in the figure 5.10,5.11 and 5.12 respectively. Impedance trajectory is plotted to observe its locus on the plane as shown in figure 5.13

To integrate PV in the system G21 has been tripped off and replaced by PV in the system. Same fault has been applied on line 7-8 at same time but mho relay shows unpredictable behavior fails to respond to fault due to which short circuit current continues to flow in the system. When PV share has been increased further till 40% of G2 with tripping off of G21 and G22. Mho relay takes time to sense the fault and gives command to circuit breaker which than breaks line 7-8. Observations have been tabulated in table

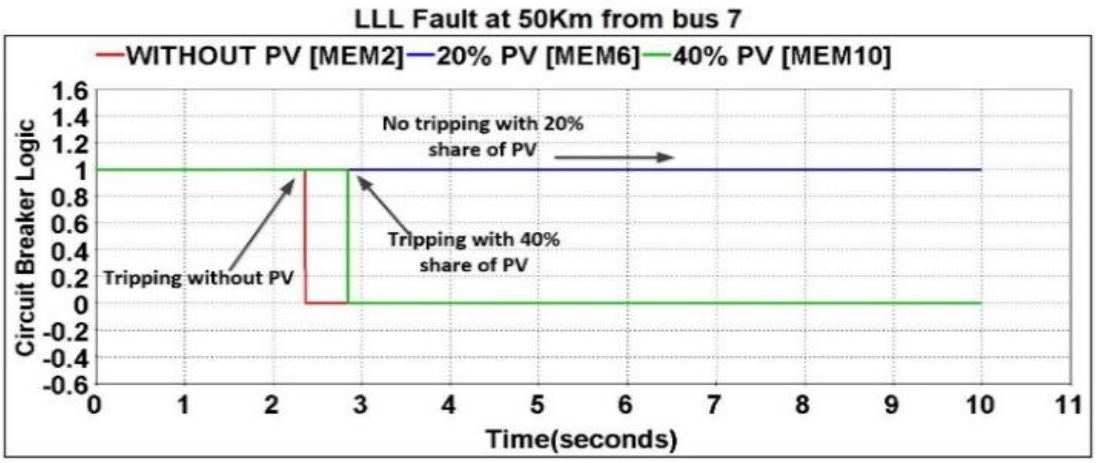


Fig.5.11. Response of circuit breaker post action from relay

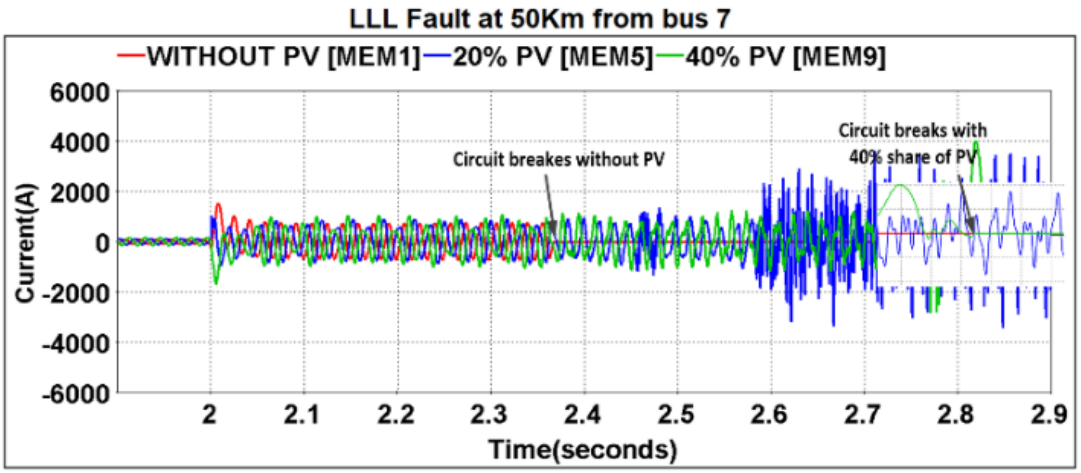


Fig.5.12. Response of current during LLL fault

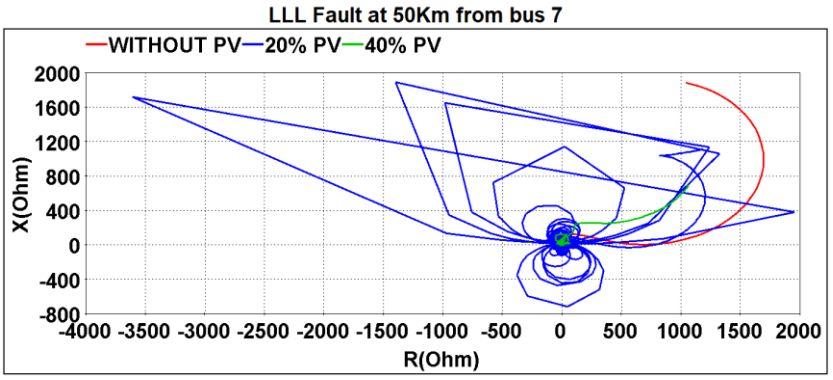


Fig. 5.13. Impedance locus observed by Relay R78 during LLL fault at 50km

### 5.3.1.3 Scenario III: LG Fault at 50km From bus 7

In this scenario LG fault has been applied at 2 seconds at a distance of 50km from bus 7. Mho relay detects the fault instantly and commands the signal to circuit breaker which in turn makes current zero to line 7-8 shown in the figure 5.14, 5.15 and 5.16. Impedance locus has been plotted in figure 5.17. To implement PV in the system G21 has been tripped off and replaced by PV in the system mho relay fails to detect the fault in the system. Then after G21 and G22 have been tripped off to replace 40% of PV in the system and tested the system again for same fault mho relay fails to respond as indicated in the figure below 5.14, 5.15 and 5.16.

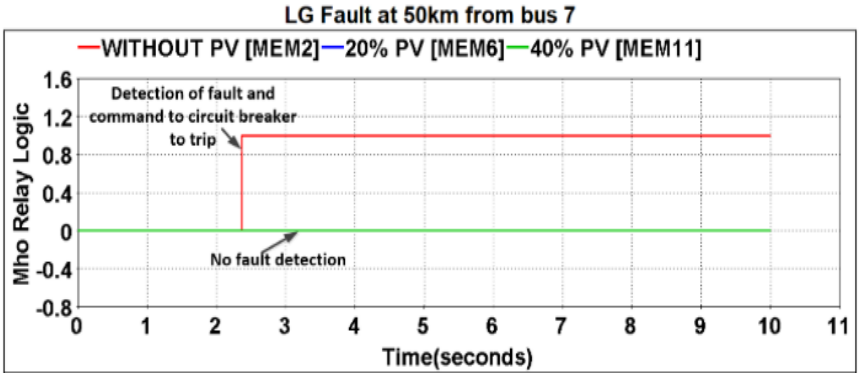


Fig.5.14. Mho relay operation during LG fault at 50km

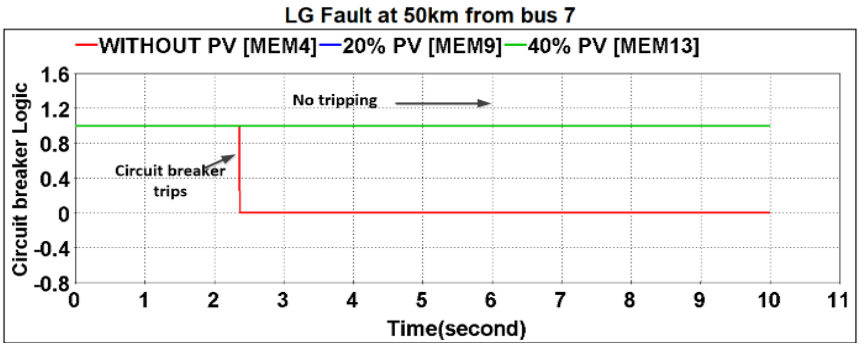


Fig.5.15. Response of circuit breaker post action from relay

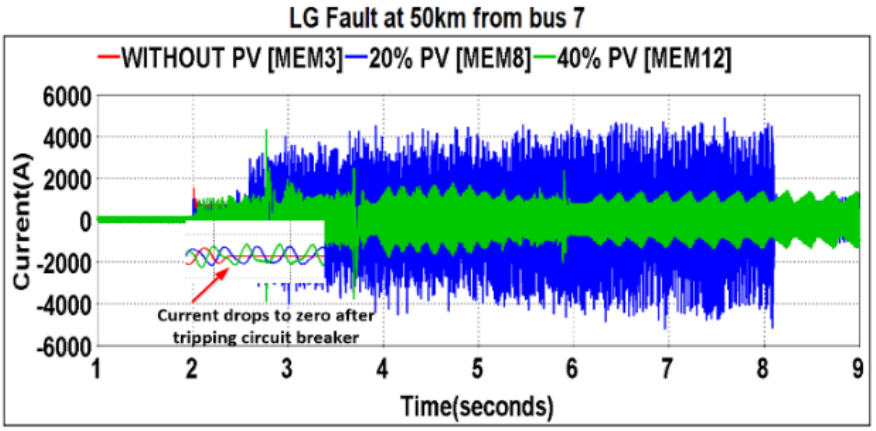


Fig.5.16. Response of current during LG fault

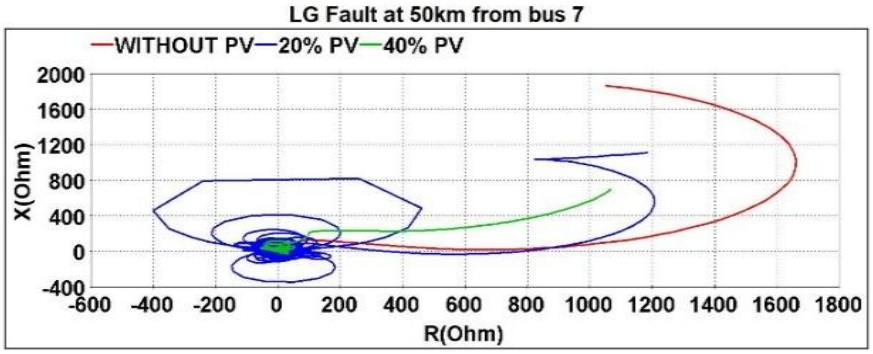


Fig.5.17. Impedance locus observed by Relay R78 during LLL fault at 25km

### 5.3.1.4 Scenario IV LLL Fault at 90km from bus 8

In this scenario LLL fault has been applied at 2 seconds at line 8-9 length of which is 106.646km. Bus 8 is far from IBR bus fault is applied at 90km from this bus. Although fault is in the zone 2 for line 8-9 mho relay detects the fault and passes signal to circuit breaker. Circuit breaker trips the line 8-9 from remaining system making current zero. While with integration of PV farm in the system mho relay detects the fault and trips the circuit but takes longer time. PV farm share has been increased till 60% of total generation of G2 mho relay operation delays with the increasing share of PV in the system as shown in the figure below 5.18, 5.19 and 5.20 respectively.

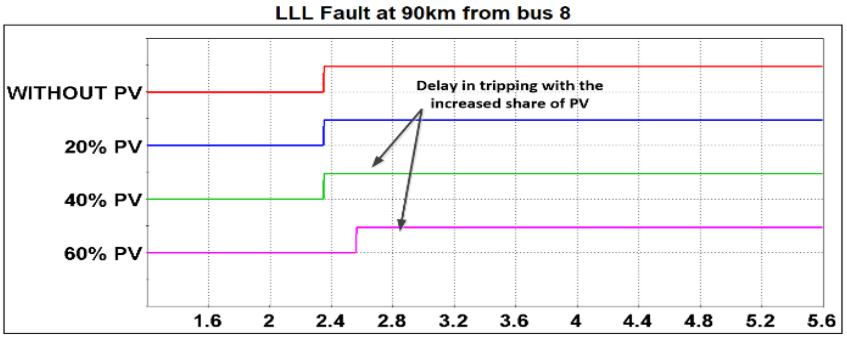


Fig.5.18. Mho relay operation during LLL fault at 90km from bus 8

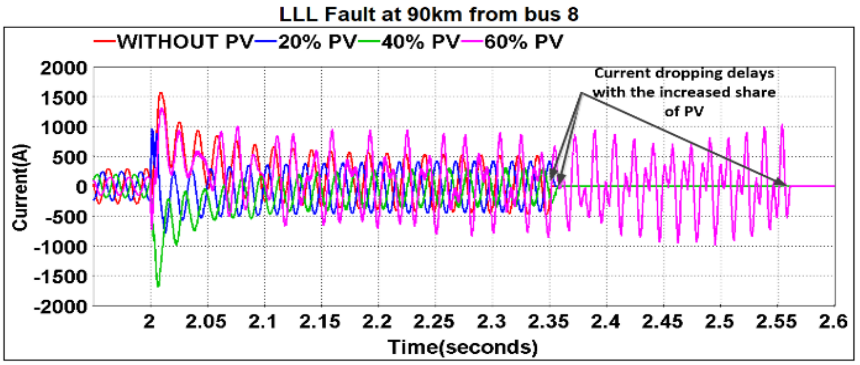


Fig.5.19 Response of current during LLL fault

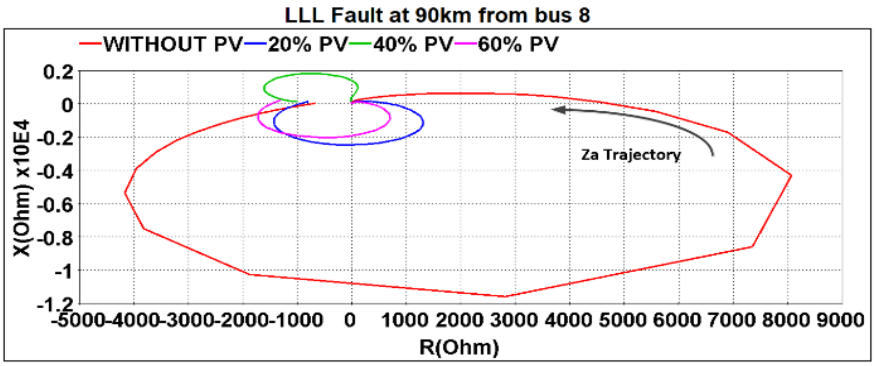


Fig.5.20 Impedance locus observed by Relay R89 during LLL fault at 90km

### 5.3.1.5 Scenario V LG Fault at 30km from bus 8

LG fault has been applied at 2 seconds at line far from IBR bus at location of 30 km from bus 8. Mho relay detects the fault passing signal to circuit breaker which breaks current in the line shown in the figure 5.21, 5.22 and 5.23 respectively. Corresponding impedance has been plotted in figure 5.24. Then after 20% share of PV has been incorporated in the system and same fault has been applied in the system mho relays delays in detecting the fault while with integrating more PV in the system it takes lesser time to detect the fault than with synchronous generator. Results showing graph is the figure below.

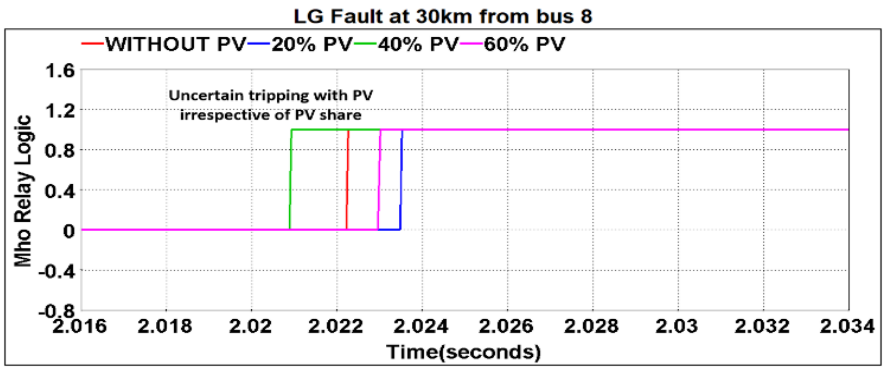


Fig.5.21 Mho relay operation during LG fault at 30km from bus 8

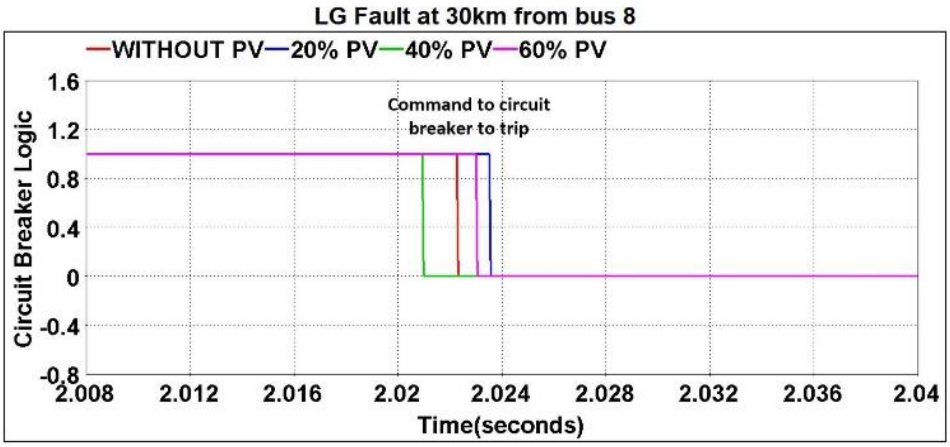


Fig.5.22 Response of circuit breaker post action from relay

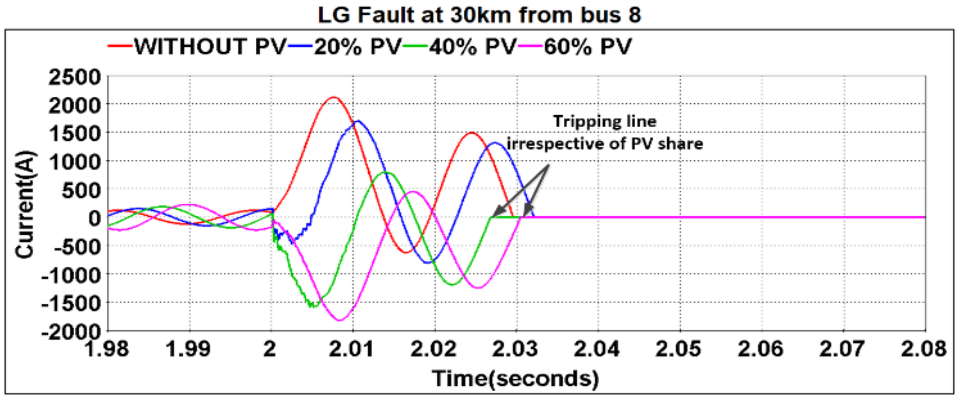


Fig.5.23 Response of current during LG fault

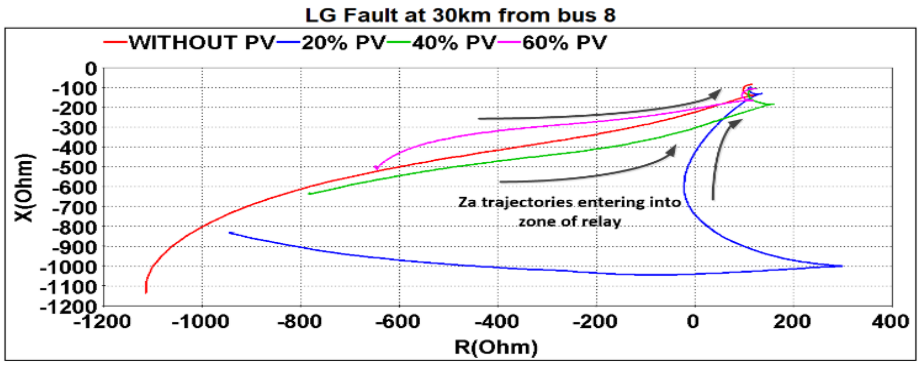


Fig.5.24 Impedance locus observed by Relay R89 during LG fault at 30km

As presented in the table 5.1 for the LLL fault in zone 1 of line connected to PV bus mho relay operates adequately but delays in detection with the increased share of PV farm in the system. While LLL fault in zone 2 of the same line with the implementing of PV farm in the system mho relay fails to detect the fault furthermore addition of PV makes relay to identify the fault but takes too long time. In case of LG fault in zone 2 relay does not detect the fault when PV implemented in the power system.

Table 5.1 Summary of all performed scenarios

| Type and location of fault | mplementation of PV farm | Tripping action |
|---|---|---|
| LLL fault at 25km from bus 7 | Without PV | 2.02156 |
| | 20% PV | 2.02164 |
| | 40% PV | 2.02189 |
| | 60% PV | 2.02245 |
| LLL fault at 50km from bus 7 | Without PV | 2.3598 |
| | 20% PV | No tripping |
| | 40% PV | 2.84283 |
| LG fault at 50km from bus 7 | Without PV | 2.3562 |
| | 20% PV | No tripping |
| | 40% PV | No tripping |
| LLL fault at 90km from bus 8 | Without PV | 2.34942 |
| | 20% PV | 2.34943 |
| | 40% PV | 2.34950 |
| | 60%PV | 2.56413 |
| LG fault at 30km from bus 8 | Without PV | 2.0222 |
| | 20% PV | 2.02348 |
| | 40% P V | 2.02088 |
| | 60% PV | 2.0230 |

In another scenario IV fault is in zone 2 of line 89 which is at remote location from IBR bus the relay operates but takes more time to detect the fault. When LG fault is applied at 30km from bus 8 with 20% integration of PV farm in the system relay takes more time to detect the fault but furthermore addition of PV in the system makes mho relay to detect the fault even prior with synchronous generator.

This can be concluded from this study that with the integration of IBR in the power system mho relay shows unpredictable nature. In some fault cases relay does not respond while in some fault cases it takes more time to detect fault. Fault for longer duration may cause instability of power system also detecting the fault prior may create unnecessary tripping of system.

## 5.4.2 Case Study II

This section examines the impact of IBR on the power swing blocking function of an impedance-based relay, using Kundur's two-area model. Two-area system has two areas consisting of four synchronous generators, each rated at 900MVA plotted in the figure 5.25. The tie line connects two areas, transmitting 413 MW from area 1 to area 2. The Mho relay is installed at bus 7 to protect the tie line connected between bus 7 and bus 9. The Mho relay settings are as follows: Zone 1

protects 80%, Zone 2 protects 120%, and Zone 3 protects 210% of the transmission line. Blinder has been set at 105 - 110 ohm. The purpose of this relay is to analyze the behavior of power swings during system disturbances. PMU has been placed at bus 7 and bus 9 to observe the voltage angle difference between two buses.

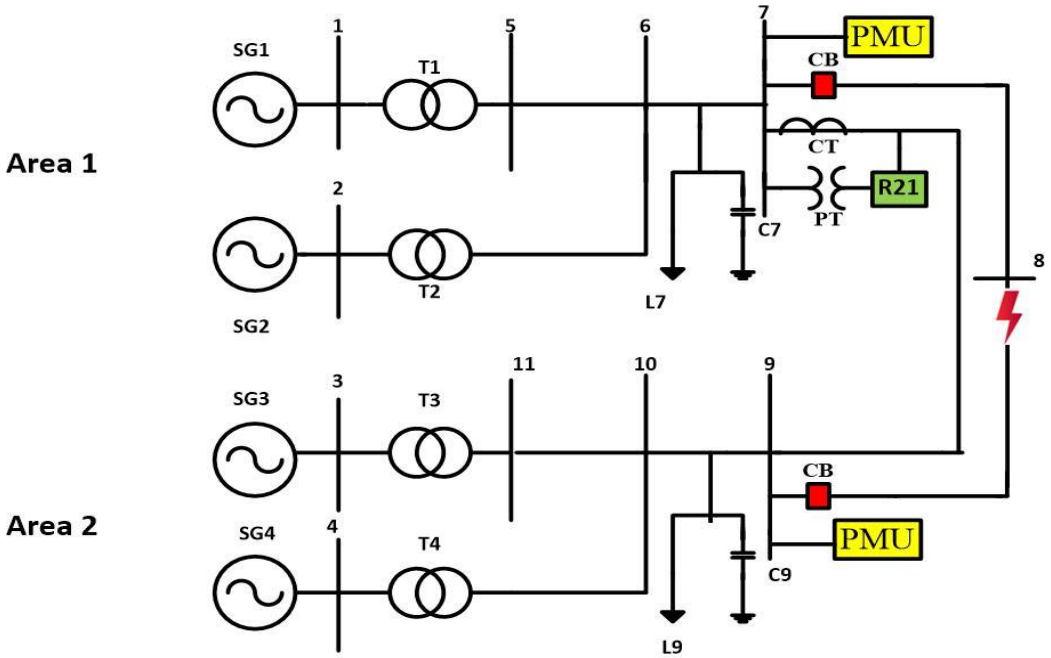


Fig. 5.25 Kundur's Two area model

PV farm has been incorporated in the system which decreases inertia of the system $H_{sys}$. Henceforth response of PV on PSB has been investigated. Without integrating PV in the system $H_{sys}$ is assumed to be 6.3375s calculated using equation 1. Furthermore, PV farm has been integrated at bus 10 and SG4 has been replaced with small generators, upto 60% of SG4 has been replaced with PV for which $H_{sys}$ can be calculated using equation 3.2 and presented in the table no. 5.2.

$$H_{system} = \frac{MVA_1H_1 + MVA_2H_2 + MVA_3H_3 + MVA_4H_4}{MVA_1 + MVA_2 + MVA_3 + MVA_4}$$

$$H_{system} = \frac{MVA_1H_1 + MVA_2H_2 + MVA_3H_3 + MVA_4H_4}{MVA_{system}}$$

Two different fault scenarios have been performed on the system.

1) Clearance of fault without removing line.

2) Removal of line 7-8-9

Table 5.2 $H_{sys}$ for the different generation share of PV

| **Sr. No.** | **SG1 (MVA)** | **$H_1$ (s)** | **SG2 (MVA)** | **$H_2$ (s)** | **SG3 (MVA)** | **$H_3$ (s)** | **SG4 (MVA)** | **$H_4$ (s)** | **PV Farm Share (MVA)** | **$H_{sys}$ (s)** |
|---|---|---|---|---|---|---|---|---|---|---|
| 1 | 900 | 6.5 | 900 | 6.5 | 900 | 6.175 | 900 | 6.175 | 0 | 6.3375 |
| 2 | 900 | 6.5 | 900 | 6.5 | 900 | 6.175 | 720 | 6.175 | 180 | 6.0287 |
| 3 | 900 | 6.5 | 900 | 6.5 | 900 | 6.175 | 540 | 6.175 | 360 | 5.72 |
| 4 | 900 | 6.5 | 900 | 6.5 | 900 | 6.175 | 360 | 6.175 | 540 | 5.4113 |

78

### 5.4.2.1 Scenario 1 Clearance of Fault without Removing Line

In this scenario, three phase to ground fault at bus 8 has been applied at 1 second and cleared at 1.1 second. Response of impedance viewed by relay during the fault and post fault at bus 7 has been plotted for the different $H_{sys}$. During the fault impedance drops down close to 0 and after clearing the fault at 1.1second impedance jumps to 320 ohms continues to oscillate to settle down. With incorporating PV thereby reducing $H_{sys}$ till 5.4133second impedance oscillates as same as with inertia 6.3375. However, after the clearance of fault with the reduction in inertia impedance height of jump increases also it takes time to gets settle down. Frequency of oscillation increases with the reduction in inertia. When impedance trajectories plotted on RX plane rate at which impedance enters and leaves blinder for different values of inertia is tabulated in table below: From table no 5.3 it can be observed time at which impedance trajectory entering and leaving blinder is different also time to cross the blinder decreases with reduction in $H_{sys}$ hence rate of change of impedance at blinder increases with reduction in inertia.

Table 5.3 Variation in the response of impedance for different $H_{sys}$

| Hsystem (s) | Time at which blinder enters (s) | Time at which blinder leaves (s) | Time to cross the blinder (s) | Δz/Δt (ohms/sec) |
|---|---|---|---|---|
| 6.3375 | 1.00855 | 1.00905 | 0.0005 | 10000 |
| 6.0287 | 1.0086 | 1.009 | 0.0004 | 12500 |
| 5.72 | 1.00865 | 1.00895 | 0.0003 | 16666.6 |
| 5.4133 | 1.0087 | 1.00885 | 0.00015 | 33333.3 |

In addition, Rate of change of impedance (ROCI) is plotted for different values of inertia. Immediate after removal of fault ROCI increases with lowering inertia till $H_{sys}$ is 5.72s further reduction it starts decreasing when $H_{sys}$ 5.4113s.

### 5.4.2.2 Scenario 2 Removal of line connected between bus 7-8-9

After performing load flow one of the tie line connected between bus 7-8-9 has been tripped off by opening breaker at 1second. Response of impedance viewed by relay bus 7 has been plotted for the different $H_{sys}$ in figure 5.26. Initial impedance observed by the relay is around 245ohms with the removal of line impedance drops to 85ohms and oscillates continuously to settle down however with incorporating PV into the system as the PV share increases $H_{sys}$ decreases impedance doesn't reach to 85ohms and oscillates to settle down. Frequency of oscillation increases with the reduction in inertia. When impedance trajectories plotted on RX plane as in figure 5.27. ROCI and voltage angle difference have been plotted in the figure 5.28 and 5.29

respectively.  ate at which impedance enters and leaves blinder for different values of inertia is tabulated in table below 5.4

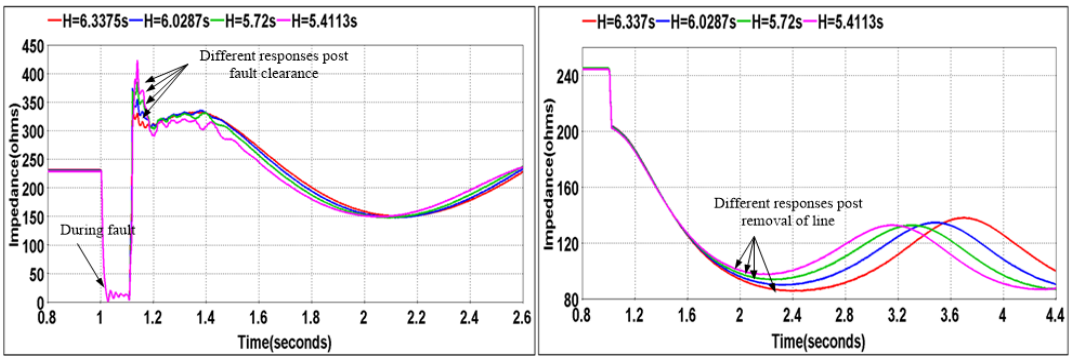


Fig.5.26 Impedance viewed by Relay at bus 7

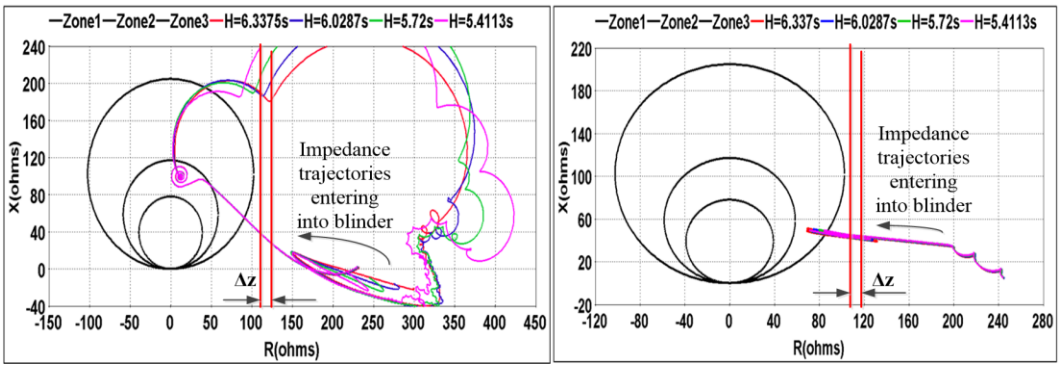


Fig. 5.27 Impedance trajectories on RX plane

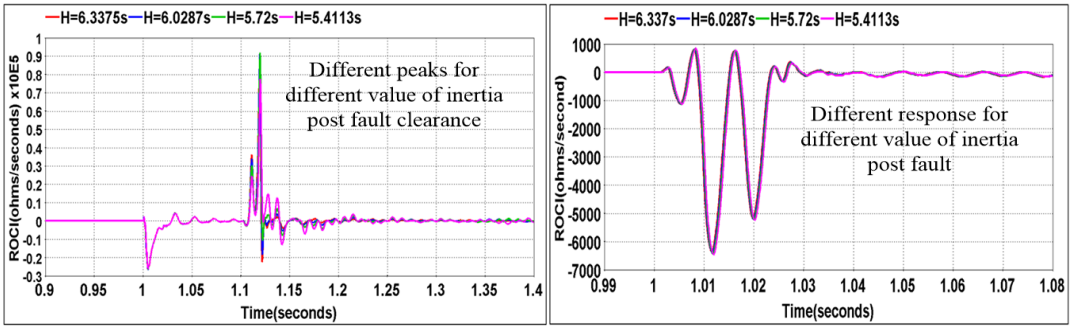


Fig.5.28 Rate of change of Impedance (ROCI) viewed by relay at bus 7

From table 5.4 it can be observed time at which impedance trajectory entering and leaving blinder is different. Also, time to cross the blinder decreases with reduction in $H_{sys}$ hence rate of change of impedance for crossing the blinder increases with reduction in inertia. In addition, Rate of change of impedance (ROCI) is plotted for different values of inertia. ROCI increases with lowering inertia.

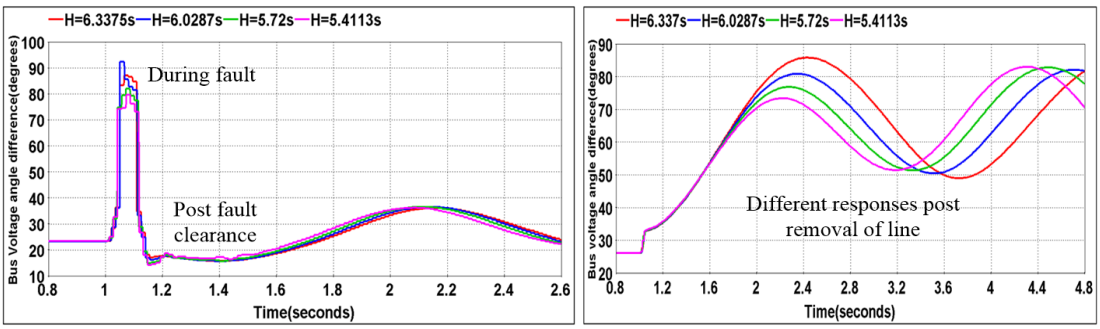


Fig. 5.29 Voltage angle difference between the buses 7 and 9

Table 5.4 Variation in the response of impedance for different $H_{sys}$

| **Hsystem (s)** | **Time at which blinder enters (s)** | **Time at which blinder leaves (s)** | **Time to cross the blinder (s)** | **Δz/Δt (ohms/sec)** |
|---|---|---|---|---|
| 6.3375 | 1.6791 | 1.7296 | 0.0505 | 99.0099 |
| 6.0287 | 1.671 | 1.7201 | 0.0491 | 101.8329 |
| 5.72 | 1.66345 | 1.7112 | 0.0477 | 104.7120 |
| 5.4133 | 1.6607 | 1.7029 | 0.0422 | 118.4834 |

## 5.5 Conclusion

Mho relay is effective in long transmission line to detect the fault and isolating the faulty section preventing the power system from blackout. With the integration of IBR in the system protection of transmission line fails. This research investigates the operation of mho relay on IEEE standard benchmark nine bus system and integrates IBR into the system. With synchronous generators in the system mho relays works abruptly while with the integration of IBR in the system mho relay either fails to operate or takes time to trip. It may lead to instability of power system. Different responses of fault current have been observed during different scenarios. Unpredictable and different behavior of mho relay for different fault scenario makes power system protection challenging.

In addition, this research presents comprehensive analysis on impact of IBR on PSB. With the integration of IBR inertia of the system is reduced which affects PSB function of impedance relays. Simulation study has been conducted on Kundur's two area system for two fault scenarios using HYPERSIM real time simulator. Integration of IBR reduces overall $H_{system}$ which causes change in ROCI. Response of impedance plot, impedance trajectories, ROCI and voltage angle difference between buses for different values of $H_{system}$ has been analyzed. With the different responses for different $H_{system}$ due to integration of IBR leads to maloperation of relays.

# CHAPTER 6

# ONLINE INERTIA ESTIMATION USING PMU

This chapter highlights the significance of online inertia estimation in modern power systems and introduces a novel algorithm designed for accurate inertia assessment. The proposed method utilizes a signal derived from phasor measurement units (PMUs) in combination with a fuzzy logic-based approach to enhance estimation precision. Its performance has been verified and validated using standard IEEE benchmark models, demonstrating high accuracy and robustness across diverse operating conditions.

## 6.1 Introduction

With the continuous increase in the electric power demand, the integration of Renewable energy sources (RES) in the power system has grown exponentially in the last few decades. Integration of RES into existing power systems has been executed by interfacing power electronic converters. The presence of power electronic converter has brought major challenges to the stability and reliability of the power system due to the absence of inertia in the system[1], [11]. Inertia is a vital parameter of the power system, which reduces the frequency deviation, causing a reduction in the rate of change of frequency (ROCOF) during any perturbation in the system[143], [144], [145]. Reduction in system inertia due to RES increases the frequency deviation during the disturbance in the system. Therefore, it is essential to monitor continuously to alert the system operator to take any primitive actions to avoid any power failure[21]. However, inertia measurement in power system is challenging for power engineers as it is not a directly measurable quantity.

Inertia estimation methods present in the literature can be broadly categorized based on:

1) Time frame of estimation:
- Offline estimation using simulation models and historical data.
- Online or real-time estimation using real-time system measurements.
- Forecast-based methods predicting future inertia levels based on expected generator dispatch and IBR operation.

2) Target level of estimation:
- System-wide inertia for overall grid stability assessment.

- Regional inertia in partitioned areas of a large interconnected grid.
- Individual generator or IBR inertia, including both synchronous and converter-based sources.
- Demand-side inertia, considering the contribution of responsive loads.

Among these, real-time system-level inertia estimation has gained significant traction due to its relevance for wide-area monitoring systems (WAMS), adaptive protection, and emergency control actions. Advances in high-speed measurement technology, particularly Phasor Measurement Units (PMUs), have enabled the development of measurement-based estimation techniques. PMUs provide synchronized, high-resolution data on voltage phase angles, frequencies, and other dynamic parameters, which can be used to infer inertia by analyzing the system's response to disturbances.

In this research novel parameter bus voltage angles have been measured with PMUs for estimating power system inertia. The main idea in this research work stems from the close relation between the rotor angle oscillations of the generator to the bus voltage phase angle oscillations. In particular, the derivative of phase angle has been explored with artificial intelligence techniques like fuzzy logic to estimate system inertia $H_{system}$. The Proposed approach has been validated on standard benchmark systems and simulation has been performed in OPAL RT real time simulator with HYPERSIM environment.

This chapter present and validate a novel methodology for online estimation of power system inertia in modern grids with high penetration of renewable energy sources.

### 6.1.1 Specific Objectives

Objectives of the chapter are as follows:

- Establish the relationship between the bus voltage phase angle derivative and system inertia to develop a robust theoretical basis.

- Explore and utilize a new signal derived from Phasor Measurement Unit (PMU) measurements for accurate and real-time inertia estimation.

- Develop an AI-based fuzzy logic estimator capable of estimating system inertia under varying operating conditions and disturbance scenarios.

- Demonstrate that the proposed algorithm can accurately estimate system inertia irrespective of the share of inverter-based resources or the type of disturbance.

- Validate the effectiveness and reliability of the proposed method through simulation and performance evaluation under diverse operating conditions.

### 6.1.2 Contributions

Contribution in this chapter are as follows:

- A novel approach for online system inertia estimation has been proposed.
- Unique response of bus voltage phase angle derivative, with a given system inertia has been established.
- A new signal, based on bus voltage phase angle measured by the PMU has been explored for inertia estimation purpose.
- AI based fuzzy logic inertia estimator has been developed for online estimation of system inertia.
- The Proposed algorithm can estimate system inertia accurately in presence of renewable energy sources and does not get influenced by generation shared by RES.
- Proposed algorithm estimates system inertia with high accuracy irrespective of type of disturbance.

## 6.2 Voltage phase angle for estimation of system inertia

In this section, mathematical background of relation between the proposed bus voltage phase angle from PMU and the system inertia has been developed along with the Relation between phase angle and inertia.

### 6.2.1 Mathematical background of proposed concept for Inertia Estimation

Voltage Phase angle of buses is constant under stable operating condition and it oscillates during contingency in the system, which is influenced by inertia of the system. The relation between inertia of the system and voltage phase angle oscillations can be established in the following expressions.

In a linear system, stability can be assessed by examining characteristic equation 6.1 [134],

$$s^2 + 2\,\zeta\,\omega_n\ s + \omega_n^2 = 0 \tag{6.1}$$

Where $\omega_n$ is natural frequency of oscillation. Roots of this characteristic equation can be expressed as,

$$s_1, s_2 = -\zeta\omega_n \pm j\omega_n\sqrt{1-\zeta^2} = -\zeta\omega_n \pm j\omega_d$$

Where $\omega_d$ $is$ damped frequency of oscillation and ζ is damping ratio, with $\omega_d$ as in equation6.2,

$$\omega_d = \omega_n \sqrt{(1-\zeta^2)} \tag{6.2}$$

Equation 6.1 can be represented in terms of generator parameters as,

$$\frac{d^2\Delta\delta}{dt^2} + \frac{\pi f_0}{H} \mathrm{D} \frac{d\Delta\delta}{dt} + \frac{\pi f_0}{H} P_S\Delta\delta = 0 \tag{6.3}$$

Where δ is rotor angle position, H is inertia constant of rotor, $f_0$ is system frequency and $P_S$ is synchronizing power. Solving above equation 6.3 in state space form (derived in Appendix II), we get,

$$\delta = \delta_0 + \frac{\Delta\delta_0}{\sqrt{(1-\zeta^2)}} e^{-\zeta\omega_n t} \sin(\omega_d t + \theta)$$

Taking its derivative, we get

$$\frac{d\delta}{dt} = -\zeta\omega_n^2 \Delta\delta_0 e^{-\zeta\omega_n t} \cos(\omega_d t + \theta) \tag{6.4}$$

It can be observed that the derivative of rotor angle oscillation is independent of initial condition and oscillates at a frequency of $\omega_d$ . The generator bus voltage phase angle is approximately same as rotor angle as the generators reactance are negligible [25]. Therefore equation (6.4) can be considered as bus voltage phase angle whose natural frequency of oscillation $\omega_n$ can be expressed in terms of generator parameters as,

$$\omega_n = \sqrt{\frac{\pi f_0 P_S}{H}} \quad \text{or} \quad H = \frac{\pi f_0 P_S}{\omega_n^2} \tag{6.5}$$

From the equation 6.5 inertia constant H can be evaluated if $\omega_n$ is measured with other parameters being constant. However, it can be observed from equation 6.4, only $\omega_d$ is measurable directly from the response of the system and $\omega_n$ is dependent upon ζ as per equation 6.2. In real power system the variation of ζ is small and can be taken into account with artificial intelligence technique to map $\omega_d$ with inertia H instead of $\omega_n$. Thus, by measuring the oscillation $\omega_d$ of the system with only conventional generators, inertia estimation can be trained in fuzzy logic to determine the inertia in the presence of renewable energy sources.

### 6.2.2 Relation between phase angle and inertia constant H

To further explain, a plot for derivative of bus voltage phase angle ($\dot{\delta}$) for low, medium and high values of system inertia from synchronous generators is shown in the figure 6.1 for a sudden increment of load in the system. Figure 6.2 is the response of the system for different magnitudes of load with same system inertia.

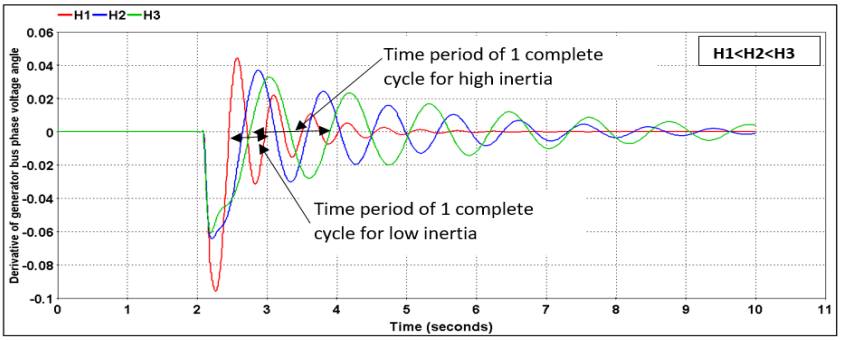


Fig.6.1. Derivative of generator bus voltage phase angle $\dot{\delta}$ for different inertia constant

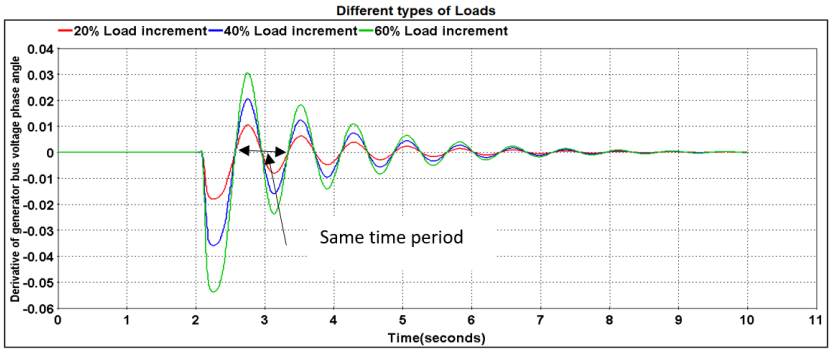


Fig.6.2. Derivative of generator bus voltage phase angle $\dot{\delta}$ for different types of loads

It can be observed from the figures 6.1 and 6.2 that the derivative $\dot{\delta}$ shows unique nature of response for various values of system inertia constant and does not get affected by type of load. The time period (or frequency) of oscillation of derivative $\dot{\delta}$ provides an opportunity to explore this signal for estimating inertia. The time period between two consecutive zero crossings after its first lower or higher peak can be considered for calculating the frequency of oscillation of $\dot{\delta}$.

## 6.3 Proposed Procedure for System Inertia Estimation

### 6 3.1 Design of Fuzzy Logic Estimator

Fuzzy logic is one of the artificial intelligences (AI) technique which takes decision intelligently on the basis of previous numerical data, pictures etc. [146]. In

this research Double input single output Mamdani fuzzy logic has been explored as a tool for estimation of inertia. Step involved for designing the fuzzy logic estimator are explained below.

### 6.3.1.1 Fuzzification

For designing fuzzy logic estimator, oscillating frequency of $\dot{\delta}$ at generator buses 1,2,3,4….n-1 are chosen as input for fuzzy logic estimator. Generator bus number n is considered as swing bus, as shown in figure 6.3.

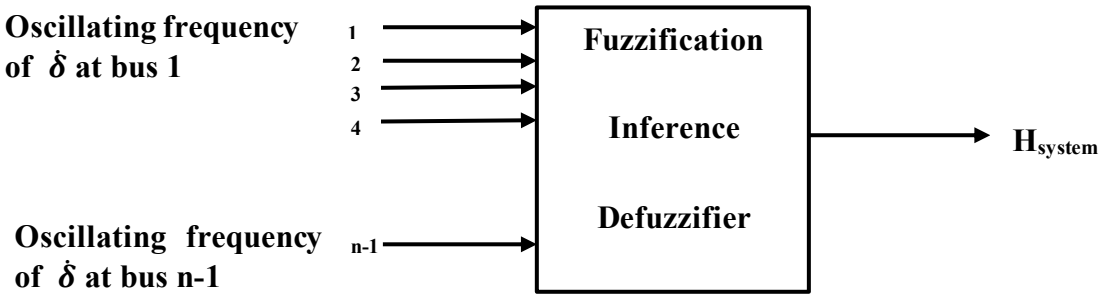


Fig.6.3 Block diagram representation of Fuzzy logic

Triangular shaped 11 membership function for input as well as for output has been designed as shown in figure 5. 11 linguistic variables are selected as Extreme low (EL), Very low (VL), Low(L), Medium low(ML), Normal low (NL), Normal(N), Normal High(NH), Medium High(MH), High(H), Very High(VH), Extreme High(EH) for both input and output.

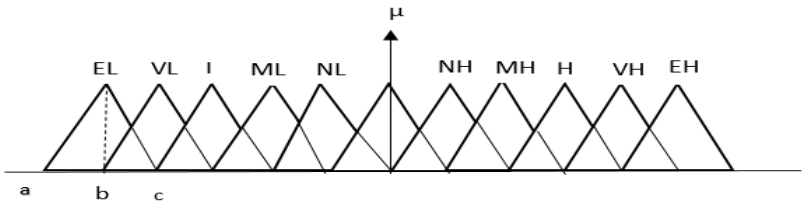


Fig.6.4 Membership function developed for fuzzy logic toolbox

$$\mu_{triangular}(x; a, b, c) = 0 \quad x \le a;$$
$$= \frac{x-a}{b-a} \quad a \le x \le b$$
$$= \frac{c-x}{c-b} \quad b \le x \le c$$
$$= 0 \quad x \ge c$$
$$= \max(\min(\frac{x-a}{b-a}, \frac{c-x}{c-b}), 0)$$

Values of a,b,c are determined from response of the system with synchronous generators.

### 6.3.1.2 Fuzzy Rule Base

By considering 11 linguistic variable truth table developed for fuzzy logic estimator of nine bus system is as shown below table no 6.1. By increasing number of input N, $Rule^N$ can be formed to increase accuracy of the output.

Table 6.1 Truth table for fuzzy logic development

| Rule | Oscillating frequency of $\dot{\delta}$ | $H_{sys}$ |
|---|---|---|
| 1 | EL | EH |
| 2 | VL | VH |
| 3 | L | H |
| 4 | ML | MH |
| 5 | NL | NH |
| 6 | N | N |
| 7 | NH | NL |
| 8 | MH | ML |
| 9 | H | L |
| 10 | VH | VL |
| 11 | EH | EL |

### 6.3.1.3 Defuzzification

For converting output into crisp value centre of gravity method has been utilized formula which represented in equation 6.

$$Crisp\ output = \frac{\sum_{i=1}^{11} bi \int \mu\,(i)}{\sum_{i=1}^{11} \int \mu\,(i)} \tag{6.5}$$

Where μ(i) is the membership function of output i, bi is the center of membership function.

## 6.3.2 Proposed Algorithm

Proposed algorithm for estimation of inertia from the derivate of generator bus voltage phase angle and trained fuzzy logic estimator is shown in figure 6.5. Bus voltage phase angle V∠ δ are measured by PMUs from all the generator buses in the system. Derivative of phase angle $\dot{\delta}$ is computed by taking difference between two consecutive data of voltage phase angle with respect to time. Calculated derivative of generator bus voltage phase angle $\dot{\delta}$ are passed to trained fuzzy logic as input for estimating inertia.

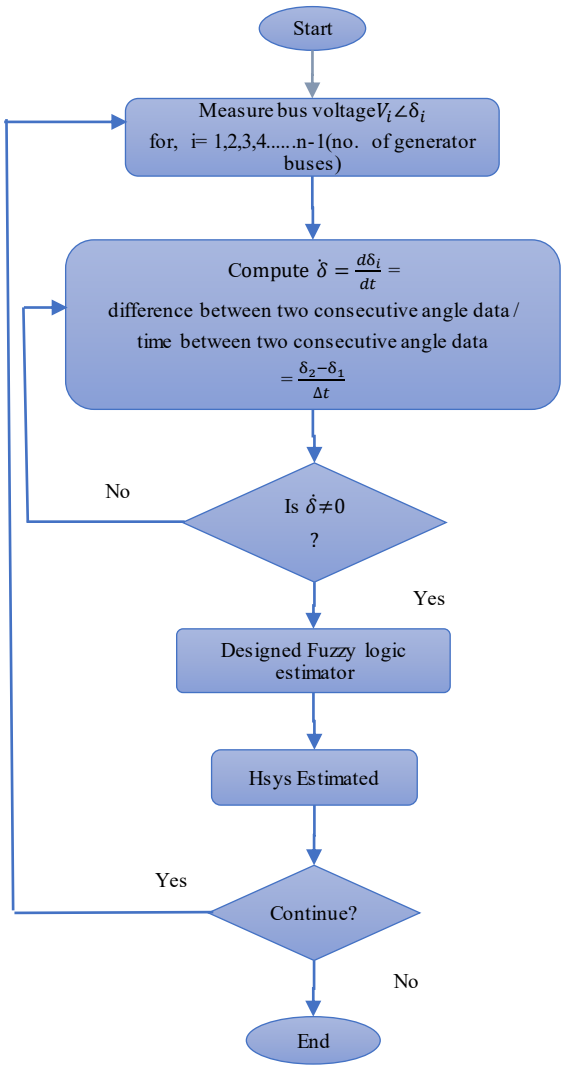


Fig.6.5 Proposed algorithm for inertia estimation

## 6.4 Case Study

Simulation studies have been carried out in OPAL RT real time simulator in HYPERSIM environment on two benchmark power systems: Nine bus system and Two area system.

### 6.4.1 Case –I Nine bus system

A Nine bus system [15]consisting of three generators G1, G2, G3 with 512 MVA, 270 MVA and 125MVA respectively has been considered as shown in figure 6.6 for this study. G1 is considered as swing machine with inertia constant at 6s. Three loads A, B, C of 125MW, 90MWand 100MW are connected at bus 5, 6 and 8 respectively. Initial load flow has been executed by Newton Raphson load flow method according to which power supplied by generators are 71MW, 163MW and 85 MW respectively. All the generator buses are connected with PMUs to obtain voltage

phase angle. The time period T between zero crossings from the voltage phase angle has been measured, inverse of this time period is the frequency of oscillation $f_d$ of $\dot{\delta}$ which is considered to be the input parameter for fuzzy logic system inertia estimator.

The proposed algorithm for estimation of inertia has been carried out in two stages (i) Design of fuzzy logic estimator and (ii) $H_{sys}$ estimation in presence of Photovoltaic farm.

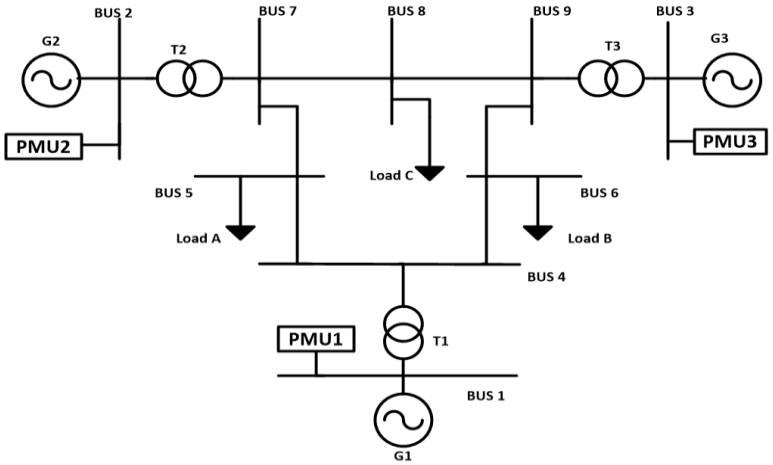


Fig. 6.6. Nine bus system

### 6.4.1.1 Stage I: Design of fuzzy logic estimator to estimate Hsys

To design the fuzzy logic estimator, inertia of generator $G_1$ is kept to be constant at 6s. Whereas inertia of $G_2$ and $G_3$ have been varied in the range of 2-6s in steps of 0.5s to obtain the response for a disturbance of additional 50MW load with load C at 2 seconds. Sample responses of derivative $\dot{\delta}$ at generator bus 2 is shown in figure 6.7. It can be observed from the figure 6.7 that with the increase in inertia the time period increases which implies to reduction in frequency of oscillation $f_d$ of $\dot{\delta}$.

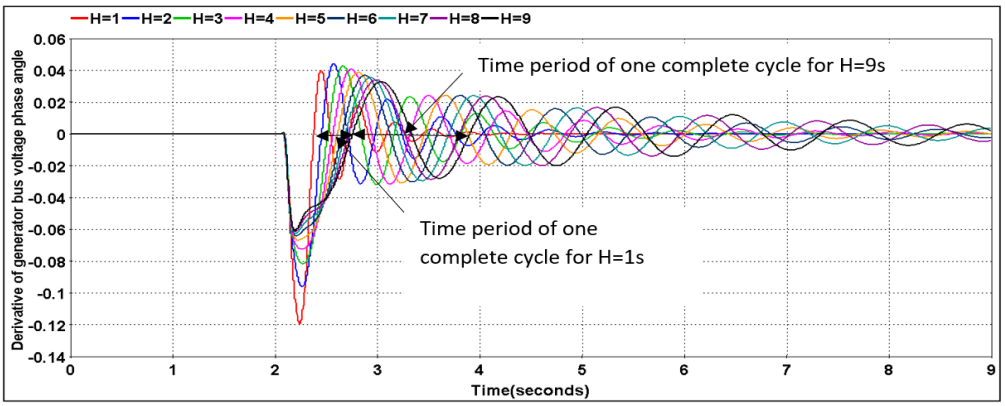


Fig.6.7. Response of derivative of generator bus voltage phase angle $\dot{\delta}$ at bus 2

For each variation of generator inertia in the system, System inertia can be calculated by using the following equations 3.2 [8]

In this case, eighty-one values of $H_{sys}$ has been calculated by using equation 3.2. Eighty one unique responses of $\dot{\delta}$ at generator buses 2 and 3 as well as $H_{sys}$ are utilized to design the membership function value of the fuzzy logic estimator. Twenty five sample data of $f_d$ of derivative $\dot{\delta}$ for bus 2 and 3 as well as $H_{sys}$ are represented in table no 6.2. Where, G1, G2 and G3 are MVA rating of the generators 1,2 and 3 also $H_1$, $H_2$ and $H_3$ represents inertia of the generators 1, 2 and 3 in seconds respectively which are used to calculate the actual $H_{sys}$. One sample calculation to find $H_{sys}$ for the values of 1st row of table no. 6.2 is expressed below.

$$H_{sys} = \frac{(MVA1 \times H1) + (MVA2 \times H2) + (MVA3 \times H3)}{G1+G2+G3} \quad [s]$$

$$H_{sys} = \frac{(512 \times 6) + (270 \times 2) + (125 \times 2)}{512 + 270 + 125}$$

$$H_{sys} = 4.54024 \quad [s]$$

Table 6.2 Input data for fuzzy logic design

| Sr. No. | G1 (MVA) | G2 (MVA) | G3 (MVA) | $H_1$ (s) | $H_2$ (s) | $H_3$ (s) | Calculated Hsys (s) | $f_d$ of $\dot{\delta}$ at bus 2 | $f_d$ of $\dot{\delta}$ at bus 3 |
|---|---|---|---|---|---|---|---|---|---|
| 1 | 512 | 270 | 125 | 6 | 2 | 2 | 4.54024 | 1.1964 | 1.1809 |
| 2 | 512 | 270 | 125 | 6 | 2 | 3 | 4.678059 | 1.1504 | 1.1487 |
| 3 | 512 | 270 | 125 | 6 | 2 | 4 | 4.815876 | 1.0593 | 1.0745 |
| 4 | 512 | 270 | 125 | 6 | 2 | 5 | 4.953693 | 0.9895 | 0.9929 |
| 5 | 512 | 270 | 125 | 6 | 2 | 6 | 5.09151 | 0.9999 | 0.9934 |
| 6 | 512 | 270 | 125 | 6 | 3 | 2 | 4.837927 | 1.0571 | 0.9998 |
| 7 | 512 | 270 | 125 | 6 | 3 | 3 | 4.975744 | 1.0417 | 0.9928 |
| 8 | 512 | 270 | 125 | 6 | 3 | 4 | 5.113561 | 1.0101 | 1.0119 |
| 9 | 512 | 270 | 125 | 6 | 3 | 5 | 5.251378 | 0.9788 | 0.9648 |
| 10 | 512 | 270 | 125 | 6 | 3 | 6 | 5.389195 | 0.9666 | 0.9261 |
| 11 | 512 | 270 | 125 | 6 | 4 | 2 | 5.135611 | 0.9713 | 0.9773 |
| 12 | 512 | 270 | 125 | 6 | 4 | 3 | 5.273428 | 0.9524 | 0.9887 |
| 13 | 512 | 270 | 125 | 6 | 4 | 4 | 5.411245 | 0.9383 | 0.9256 |
| 14 | 512 | 270 | 125 | 6 | 4 | 5 | 5.549062 | 0.9264 | 0.926 |
| 15 | 512 | 270 | 125 | 6 | 4 | 6 | 5.686879 | 0.9252 | 0.9009 |
| 16 | 512 | 270 | 125 | 6 | 5 | 2 | 5.433296 | 0.9386 | 0.8951 |
| 17 | 512 | 270 | 125 | 6 | 5 | 3 | 5.571113 | 0.9042 | 0.8992 |

continued on page no. 92

Table 6.2 (continued)

| | | | | | | | | | |
|---|---|---|---|---|---|---|---|---|---|
| 18 | 512 | 270 | 125 | 6 | 5 | 4 | 5.70893 | 0.8875 | 0.8434 |
| 19 | 512 | 270 | 125 | 6 | 5 | 5 | 5.846747 | 0.8666 | 0.8264 |
| 20 | 512 | 270 | 125 | 6 | 5 | 6 | 5.984564 | 0.8766 | 0.8389 |
| 21 | 512 | 270 | 125 | 6 | 5 | 2 | 5.730981 | 0.8721 | 0.8986 |
| 22 | 512 | 270 | 125 | 6 | 6 | 3 | 5.868798 | 0.8421 | 0.7826 |
| 23 | 512 | 270 | 125 | 6 | 6 | 4 | 6.006615 | 0.8432 | 0.8196 |
| 24 | 512 | 270 | 125 | 6 | 6 | 5 | 6.144432 | 0.8484 | 0.7449 |
| 25 | 512 | 270 | 125 | 6 | 6 | 6 | 6.282249 | 0.7843 | 0.7168 |

By using above input data eleven triangular membership function are formed for two crisp input which are $f_d$ of $\dot{\delta}$ at bus 2 and bus 3 and crisp output is $H_{sys}$. For each membership function values of a, b and c are represented in table no 6.3.

Table 6.3 Membership function data for fuzzy logic

| | **Triangular membership function values** | | | | | | | | |
|---|---|---|---|---|---|---|---|---|---|
| | ***Crisp Input1*** $f_d$ ***at bus 2*** | | | ***Crisp Input2*** $f_d$ ***at bus 3*** | | | ***Crisp Output*** $H_{sys}$ | | |
| | ***a*** | ***b*** | ***c*** | ***a*** | ***b*** | ***c*** | ***a*** | ***b*** | ***c*** |
| **MF1** | 0.6402 | 0.7843 | 0.8442 | 0.7158 | 0.7168 | 0.7635 | 4.3402 | 4.5402 | 4.689 |
| **MF2** | 0.7843 | 0.8442 | 0.8766 | 0.7168 | 0.7635 | 0.8389 | 4.5402 | 4.689 | 4.8379 |
| **MF3** | 0.8421 | 0.8649 | 0.8878 | 0.7652 | 0.8264 | 0.8775 | 4.8848 | 4.9537 | 5.0336 |
| **MF4** | 0.8668 | 0.9013 | 0.9256 | 0.8108 | 0.8652 | 0.9013 | 5.045 | 5.1246 | 5.1825 |
| **MF5** | 0.9042 | 0.9225 | 0.9442 | 0.8669 | 0.8992 | 0.9164 | 5.1935 | 5.2734 | 5.3313 |
| **MF6** | 0.9260 | 0.9495 | 0.9666 | 0.8939 | 0.9228 | 0.9512 | 5.3423 | 5.4222 | 5.4801 |
| **MF7** | 0.9476 | 0.9809 | 1.0091 | 0.9371 | 0.9648 | 0.9771 | 5.4911 | 5.5711 | 5.6289 |
| **MF8** | 0.9713 | 0.9999 | 1.0268 | 0.9511 | 0.9934 | 1.012 | 5.6400 | 5.7089 | 5.7778 |
| **MF9** | 0.9895 | 1.0012 | 1.0751 | 0.9928 | 1.022 | 1.074 | 5.7888 | 5.8577 | 5.9377 |
| **MF10** | 1.0571 | 1.13 | 1.1964 | 0.999 | 1.088 | 1.181 | 5.9845 | 6.0755 | 6.2822 |
| **MF11** | 1.13 | 1.1964 | 1.2044 | 1.087 | 1.181 | 1.229 | 6.0755 | 6.2822 | 6.3822 |

The fuzzy logic estimator was developed using offline simulation data obtained for different system inertia conditions and operating scenarios. The derivative of the generator-bus voltage phase angle, $\dot{\delta}$, obtained from PMU measurements was used as the input, while the corresponding known system inertia, $H_{sys}$, from each simulation was used as the target output. Based on these input-output data, the fuzzy membership functions and rules were established to represent the relationship between $\dot{\delta}$ and $H_{sys}$.

The parameters $a$, $b$, and $c$ define the lower limit, peak, and upper limit of the triangular membership functions, respectively. They were selected according to the

range and distribution of the available simulation data so that the complete input and output ranges were adequately covered with suitable overlap between adjacent membership functions. The selected values of $a$, $b$, and $c$are fixed after the offline fuzzy estimator design stage and are not changed during online inertia estimation. Therefore, these parameters are dependent on the data and operating range used to develop the estimator, but remain constant for all subsequent online test cases.

During online operation, the PMU-measured $\dot{\delta}$values at generator buses 2 and 3 are supplied to the fuzzy estimator, and the corresponding $H_{sys}$is estimated using the fixed membership functions and fuzzy rules. If the system configuration or operating range changes significantly beyond the range represented in the offline simulation data, the membership functions and fuzzy rule base would need to be redesigned or updated using new simulation data.

Eleven fuzzy rules are formed using crisp input and output values are as follows.

Rule no 1- If MF1 and MF1 then MF11.

Rule no 2- If MF2 and MF2 then MF10.

Rule no 3- If MF3 and MF3 then MF9.

Rule no 4- If MF4 and MF4 then MF8.

Rule no 5- If MF5 and MF5 then MF7.

Rule no 6- If MF6 and MF6 then MF6.

Rule no 7- If MF7 and MF7 then MF5.

Rule no 8- If MF8 and MF8 then MF4.

Rule no 9- If MF9 and MF9 then MF3.

Rule no 10- If MF10 and MF10 then MF2.

Rule no 11- If MF11 and MF11 then MF1.

The first and second membership functions in each rule correspond to the inputs at generator buses 2 and 3, respectively, while the membership function following "then" represents the fuzzy output corresponding to $H_{sys}$.

The fuzzy logic estimator uses the derivatives of the generator-bus voltage phase angles as inputs and the system inertia $H_{sys}$as the output. The membership functions are triangular, and the parameters $a$, $b$, and $c$ define the shape and range of each membership function. The values of $a$, $b$, and $c$ are obtained from the input-output data used for developing the fuzzy estimator. Therefore, these parameters are case-dependent during the development of the estimator. Once the membership functions and rule base are established for a particular system, their parameters remain constant during online estimation.

The fuzzy rules define the relationship between the input membership functions and the output membership functions. For example, a rule such as "If Input 1 is MF1 and Input 2 is MF1, then Output is MF11" means that this particular combination of input membership functions produces MF11 as the output membership function. The complete rule base is formed according to the combinations represented in the training data. If an input lies in an overlapping region, it executes multiple membership functions with corresponding partial membership grades. The fuzzy

estimator evaluates all active rules using the AND logic operator, combines their output regions using the OR logic operator, and calculates the final crisp value of system inertia ($H_{\text{sys}}$) using centre of gravity defuzzification.

The above designed fuzzy logic estimator has been utilized to estimate inertia when PV is incorporated in nine bus system.

### 6.4.1.2 Stage II: Hsys estimation with Photovoltaic farm

The same nine bus system above, is now modified with addition of photovoltaic farm at bus 2 and bus 3 is shown in the figure 6.8. The schematic representation of the PV farm integrated to the grid and details of PV farm has been attached in Appendix III. Developed fuzzy logic inertia estimator has been utilized with actual implementation of PV farm in nine bus system. Initially G2 has been replaced with four small generators as shown in the figure 6.8 each of them represents 25% power rating of G2, one generator has been tripped off at a time to decrease generation by 25% of synchronous generator and to incorporate PV of equivalent rating in the system in order to maintain the same power flow of system. Inertia of G1 is remained to be constant at 6s and that of G2 and G3 are kept to be constant at 4s. With the reduction in synchronous generation in the system $H_{\text{sys}}$ gets change and its corresponding response on $\dot{\delta}$ has been plotted in figure 6.9 and 6.10.

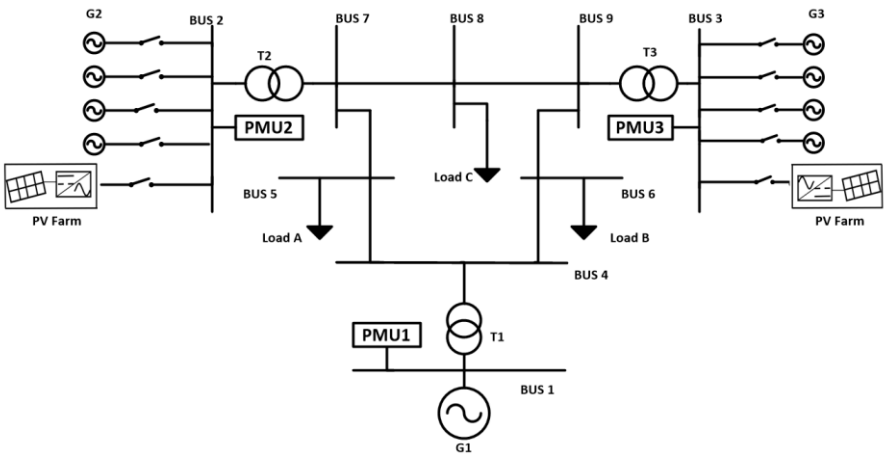


Fig. 6.8. Nine bus system with implementation of PV farm

The response of $\dot{\delta}$ at bus 2 and 3 for various values of generation by PV with G2 are plotted in figure 6.9 and 6.10 respectively. It can be observed from the figures with increase in PV generation, oscillating frequency $f_d$ increases as time period decreases.

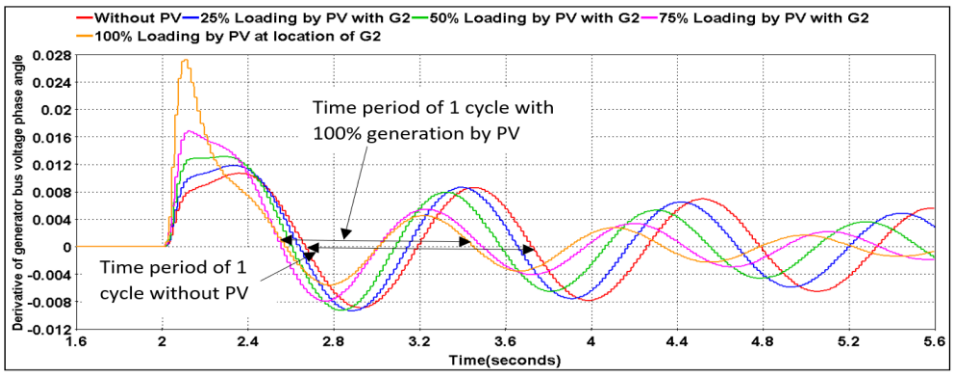


Fig.6.9. Response of derivative of generator bus voltage phase angle $\dot{\delta}$ at bus 2

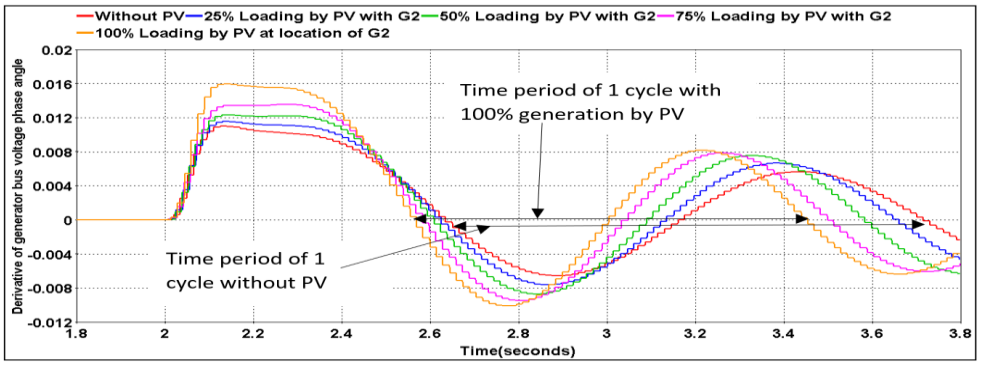


Fig. 6.10. Response of derivative of generator bus voltage phase angle $\dot{\delta}$ at bus 3

Table 6.4 below represents the PV incorporation and MVA rating of generators for which actual $H_{sys}$ has been calculated using equation 6.6. Also, by taking its response on $f_d$ of $\dot{\delta}$ at generator bus 2 and 3 $H_{sys}$ estimated using designed fuzzy logic estimator.

In a similar manner G3 has been replaced with four small generators and incorporation of PV has been implemented by tripping off small synchronous generators. Then after, same procedure has been followed to estimate $H_{sys}$ as performed for G2. All the responses collected for both the generators and summarized in table no 6.4.

Percentage error has been calculated for actual calculated inertia and estimated inertia by designed fuzzy logic estimator using formula expressed in equation 6.7 and tabulated in last column of table no 6.4. Error found in the range from 0.023% to 3.803%.

$$\%\ error = \frac{Theoretical\ H_{system} - Estimated H_{system}}{Theoretical\ H_{system}} \times 100 \qquad (6.7)$$

Graphical representation of theoretical calculated inertia and estimated inertia is plotted in figure 6.11.

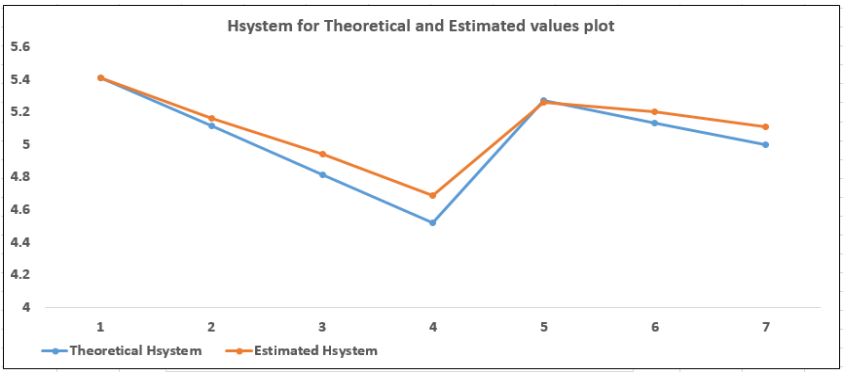


Fig. 6.11. Graphical representation of Theoretical Inertia and Inertia estimated

Table no. 6.4 PV implementation to 9 bus system

| Sr. No. | % Share of PV | PV Share MVA | G1 (MVA) | G2 (MVA) | G3 (MVA) | Calculated Hsys (s) | $f_d$ of $\dot{\delta}$ at bus 2 cycles/s | $f_d$ of $\dot{\delta}$ at bus 3 cycles/s | Estimated Hsys (s) | % Error |
|---|---|---|---|---|---|---|---|---|---|---|
| 1 | No PV | 0 | 512 | 270 | 125 | 5.4112 | 0.9493 | 0.9259 | 5.41 | 0.023 |
| 2 | 25% PV with G2 | 67.5 | 512 | 202.5 | 125 | 5.1135 | 0.9806 | 0.9632 | 5.16 | -0.908 |
| 3 | 50% PV with G2 | 135 | 512 | 135 | 125 | 4.8158 | 1.0273 | 1.0256 | 4.94 | -2.577 |
| 4 | 75% PV with G2 | 202.5 | 512 | 67.5 | 125 | 4.5181 | 1.0787 | 1.0768 | 4.69 | -3.803 |
| 5 | 25% PV with G3 | 31.25 | 512 | 270 | 93.75 | 5.2734 | 0.9601 | 0.9332 | 5.26 | 0.254 |
| 6 | 50% PV with G3 | 62.5 | 512 | 270 | 62.5 | 5.1334 | 0.9829 | 0.9747 | 5.2 | -1.29 |
| 7 | 75% PV with G3 | 93.75 | 512 | 270 | 31.25 | 4.9988 | 0.9936 | 0.9885 | 5.11 | -2.22 |

### 6.4.2 Case –II Two area system

In this case Kundur's benchmark two area system as shown in the figure 6.12 has been considered, in which two areas are separated by tie line of 220 km. All the four generators have similar rating of 900MVA supplying 700MW. G3 has been considered as swing machine with inertia constant at 6.5s, while other generator's inertia are varied in the range of 2-6s during the study. PMUs are considered to be connected at each of the generator bus in order to obtain bus voltage phase angle. A single line to ground fault has been applied at 1 seconds on one of the tie line between bus 7 and 8 and cleared at 1.0176 seconds to study the response of $\dot{\delta}$ . $f_d$ of $\dot{\delta}$ has been used to design the fuzzy logic base estimator for estimation of inertia. The study system has been initialized with load flow before the application of disturbance. The proposed method for estimation of inertia has been carried out in two stages (i) Design of fuzzy logic estimator and (ii) $H_{sys}$ estimation in presence of Photovoltaic farm.

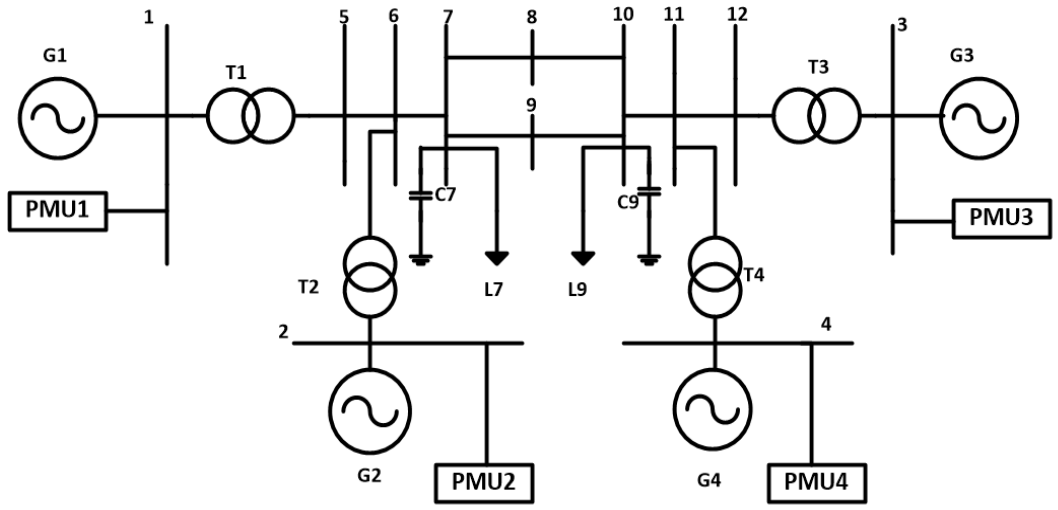


Fig .6.12. Two area system

### 6.4.2.1 Stage I- Design of fuzzy logic to estimate inertia ($H_{sys}$)

To design the fuzzy logic estimator for two area system MVA rating of all generators is considered to be 900MVA and inertia of one of the generators among G1, G2 and G4 is varied in the range of 2-6seconds in order to get different response of $\dot{\delta}$ for various values of $H_{sys}$. System inertia has been calculated by using equation (6.6) and its response $f_d$ has been obtained from $\dot{\delta}$ at generator bus 1, 2 and 4 and presented in table no 6.5.

By using above input data thirteen triangular membership function are formed for three crisp input which are $f_d$ of $\dot{\delta}$ at bus 1, 2 and 4 and one crisp output is $H_{sys}$. For each membership function values of a, b and c are represented in table no 6.6.

Table 6.5 Input data to design fuzzy logic for two area system

| Sr. No. | $H_1$ (s) | $H_2$ (s) | $H_3$ (s) | $H_4$ (s) | Calculated Hsys(s) | $f_d$ of $\dot{\delta}$ at bus 1 Cycles/s | $f_d$ of $\dot{\delta}$ at bus 2 Cycles/s | $f_d$ of $\dot{\delta}$ at bus 4 Cycles/s |
|---|---|---|---|---|---|---|---|---|
| | 2 | 2 | 6.5 | 2 | 3.125 | 0.670355 | 0.675898 | 1.98956 |
| 2 | 2 | 2 | 6.5 | 3 | 3.375 | 0.669882 | 0.673401 | 1.97417 |
| 3 | 2 | 2 | 6.5 | 4 | 3.625 | 0.6666 | 0.66701 | 1.96213 |
| 4 | 2 | 2 | 6.5 | 5 | 3.875 | 0.66335 | 0.6637 | 1.9478 |
| 5 | 2 | 2 | 6.5 | 6 | 4.125 | 0.66 | 0.66009 | 1.86471 |
| 6 | 3 | 2 | 6.5 | 6 | 4.375 | 0.65462 | 0.653189 | 1.84706 |
| 7 | 5 | 2 | 6.5 | 6 | 4.875 | 0.63315 | 0.62989 | 1.75134 |
| 8 | 6 | 2 | 6.5 | 6 | 5.125 | 0.61139 | 0.612632 | 1.68862 |

Table 6.6 Membership function data for fuzzy logic

| | **Triangular membership function values** | | | | | | | | | | | |
|---|---|---|---|---|---|---|---|---|---|---|---|---|
| | ***Crisp Input1*** $f_d$ ***at bus 1*** | | | ***Crisp Input2*** $f_d$ ***at bus 2*** | | | ***Crisp Input3*** $f_d$ ***at bus 4*** | | | ***Crisp Output*** $H_{sys}$ | | |
| | ***a*** | ***b*** | ***c*** | ***a*** | ***b*** | ***c*** | ***a*** | ***b*** | ***c*** | ***a*** | ***b*** | ***c*** |
| **MF1** | 0.6645 | 0.6703 | 0.6698 | 0.6658 | 0.6758 | 0.6734 | 1.9999 | 1.9895 | 1.9741 | 2.850 | 3.125 | 3.375 |
| **MF2** | 0.6703 | 0.6698 | 0.6666 | 0.6758 | 0.6734 | 0.6670 | 1.9895 | 1.9741 | 1.9621 | 3.125 | 3.375 | 3.625 |
| **MF3** | 0.6698 | 0.6666 | 0.6633 | 0.6734 | 0.6670 | 0.6637 | 1.9741 | 1.9621 | 1.9478 | 3.375 | 3.625 | 3.875 |
| **MF4** | 0.6666 | 0.6635 | 0.66 | 0.6670 | 0.6637 | 0.6600 | 1.9621 | 1.9478 | 1.8647 | 3.625 | 3.875 | 4.125 |
| **MF5** | 0.6635 | 0.66 | 0.6546 | 0.6637 | 0.6600 | 0.6531 | 1.9478 | 1.8647 | 1.8470 | 3.875 | 4.125 | 4.375 |
| **MF6** | 0.66 | 0.6546 | 0.6331 | 0.6600 | 0.6531 | 0.6298 | 1.8647 | 1.8470 | 1.7513 | 4.125 | 4.375 | 4.875 |
| **MF7** | 0.6546 | 0.6331 | 0.6113 | 0.6531 | 0.6298 | 0.6126 | 1.8470 | 1.7513 | 1.6886 | 4.375 | 4.875 | 5.125 |
| **MF8** | 0.6331 | 0.6113 | 0.6019 | 0.6298 | 0.6126 | 0.6027 | 1.7513 | 1.6886 | 1.6667 | 4.875 | 5.125 | 5.375 |
| **MF9** | 0.6113 | 0.6019 | 0.5992 | 0.6126 | 0.6027 | 0.6006 | 1.6886 | 1.6667 | 1.6663 | 5.125 | 5.375 | 5.625 |
| **MF10** | 0.6019 | 0.5992 | 0.5808 | 0.6027 | 0.6006 | 0.5884 | 1.6667 | 1.6663 | 1.6260 | 5.375 | 5.625 | 5.875 |
| **MF11** | 0.5992 | 0.5808 | 0.5427 | 0.6006 | 0.5884 | 0.5473 | 1.6663 | 1.6260 | 1.5874 | 5.625 | 5.875 | 6.125 |
| **MF12** | 0.5808 | 0.5427 | 0.5133 | 0.5884 | 0.5473 | 0.5195 | 1.6260 | 1.5874 | 1.5145 | 5.875 | 6.125 | 6.325 |
| **MF13** | 0.5427 | 0.5133 | 0.5033 | 0.5473 | 0.5195 | 0.5095 | 1.5874 | 1.5145 | 1.5023 | 6.125 | 6.325 | 6.525 |

Thirteen fuzzy rules are formed using crisp input and output values two of which shown below.

Rule no 1- If MF1 and MF1 then MF13.

Rule no 2- If MF2 and MF2 then MF12.

The developed fuzzy logic estimator has been considered for estimation of inertia of two area system in the presence of Photovoltaic farms.

### 6.4.2.2 Stage II- $H_{sys}$ estimation with Photovoltaic farm

Now, the two-area system has been modified with PV farm incorporated in area 2 at bus 4 to study its impact on $H_{sys}$. Additional power in the range of 5-50% of total generation of area 2 has been added in steps with PV farms. Inertia of the synchronous generators G1, G2, G3, G4 kept to be constant at 6s, 6s, 6.5s and 6s respectively. After the application of disturbance for each step of power addition by PV farms at bus 4 the PMU response of $\dot{\delta}$ at bus 1, 2 and 4 are measured and recorded. The $f_d$ of $\dot{\delta}$ at bus 1, 2 and 4 are used as input quantities to estimate $H_{sys}$. Calculated $H_{sys}$, estimated $H_{sys}$ along with percentage error are tabulated in table no. 6.7. Percentage error has been calculated for each step by using equation expressed in 6.7. Percentage error lies in the range of 0.629% to 3.869%. Theoretical Inertia and Estimated Inertia of two area system has been plotted in figure 6.13.

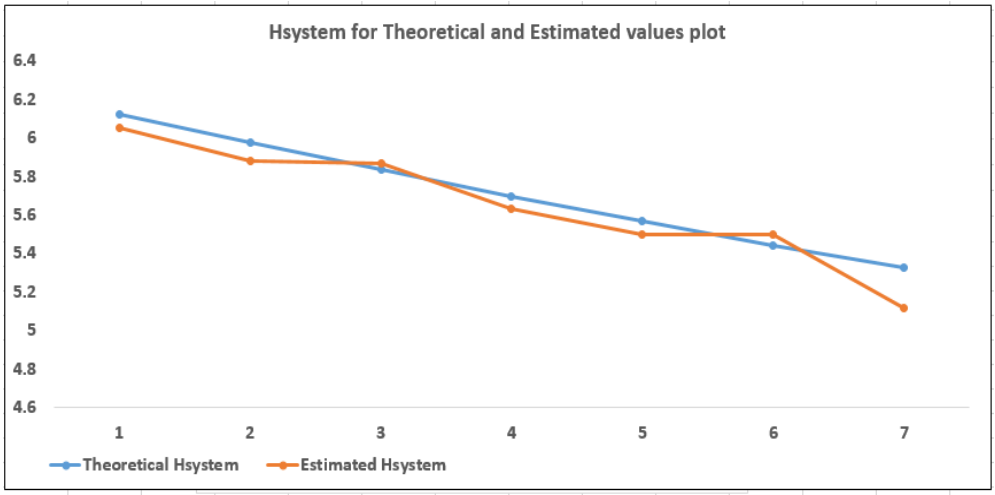


Fig. 6.13 Graphical representation of Theoretical Inertia and Estimated Inertia of Two Area System

The following section presents the drawback of conventional techniques of estimation of inertia.

Table no. 6.7 PV Farm addition to Two Area System

| Sr. No. | Rating of PV MVA | Power of PV MW | $f_d$ of $\dot{\delta}$ at bus 1 Cycles/s | $f_d$ of $\dot{\delta}$ at bus 2 Cycles/s | $f_d$ of $\dot{\delta}$ at bus 4 Cycles/s | Calculated $H_{sys}$ (s) | Estimated $H_{sys}$ (s) | % Error |
|---|---|---|---|---|---|---|---|---|
| 1 | 90 | 70 | 0.505043 | 0.510318 | 1.5238 | 6.15 | 6.05 | 1.224 |
| 2 | 180 | 140 | 0.540276 | 0.54619 | 1.53251 | 5.97560 | 5.88 | 1.6 |
| 3 | 270 | 210 | 0.56042 | 0.5611135 | 1.5667 | 5.83333 | 5.87 | -0.629 |
| 4 | 360 | 280 | 0.586295 | 0.588028 | 1.59043 | 5.69767 | 5.63 | 1.188 |
| 5 | 450 | 350 | 0.602142 | 0.603189 | 1.60214 | 5.56818 | 5.5 | 1.224 |
| 6 | 560 | 420 | 0.619307 | 0.619763 | 1.62018 | 5.44444 | 5.5 | -1.02 |
| 7 | 630 | 490 | 0.624176 | 0.625122 | 1.63213 | 5.32608 | 5.12 | 3.869 |
| 8 | 720 | 560 | 0.6304 | 0.635607 | 1.71759 | 5.21276 | 5.09 | 2.355 |
| 9 | 810 | 630 | 0.640639 | 0.641952 | 1.72826 | 5.10416 | 4.97 | 2.629 |
| 10 | 900 | 700 | 0.641622 | 0.64722 | 1.73476 | 5 | 4.95 | 1 |

## 6.5 Limitation of traditional methods of estimation of system inertia based on frequency response

Traditional inertia estimations were based on the frequency response of the system governed by the swing equation expressed in 6.8 [25],

$$\frac{2H}{\omega}\frac{d\omega}{dt} = P_m - P_e \tag{6.8}$$

On simplifying,

$$\mathrm{H} = \Delta\mathrm{P}\ \frac{f_0}{\frac{\mathrm{df}}{\mathrm{dt}}} \tag{6.9}$$

Where inertia constant H can be estimated from measurement of rate of change of frequency (ROCOF) and power change ($\Delta\mathbf{P}$) at the instance of disturbance given in equation 6.9. This method of estimation suffers from the following drawback:

- Calculating accurate size of disturbance is challenging.
- ROCOF cannot be directly measured has to be estimated from frequency response.
- Frequency deviates not only with the inertia but also with the changes in the load on the system.

To further explain frequency response in a single machine infinite bus system with same generator inertia for various magnitudes of disturbance has been plotted in figure 6.14 and with same disturbance various generator inertia is plotted in figure 6.15. From these responses it can be observed that the change in nadir frequency is not unique to disturbance or system inertia.

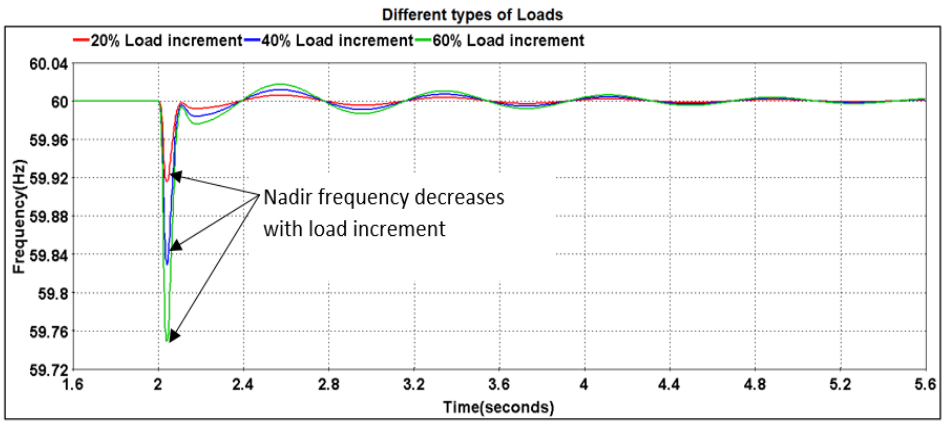


Fig.6.14 Frequency response during addition of different types of loads in the system for constant inertia

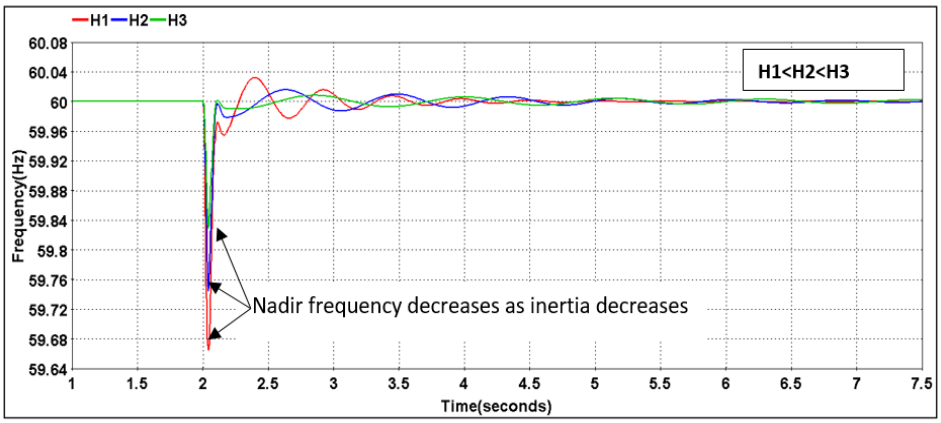


Fig.6.15 Frequency response during addition of load in the system for various values of inertia

However, proposed methodology overcomes the limitations with the following advantages.

- Proposed method shows unique approach to estimate system inertia $H_{sys}$ as in figure no 6.2.
- Voltage phase angle has been utilized which is directly obtained from PMU.
- The proposed algorithm can estimate system inertia in presence of RES with minimal error.

## 6.6 Conclusion

With increasing integration of RES into power system, the system inertia deviates continuously. The system inertia has to be calculated by measurement of observable electrical quantities. In this paper, a novel estimation of power system inertia with measurements from PMUs has been proposed. To be specific, proposed method utilizes all the bus voltage angle measured from PMUs to calculate its time derivative. Fuzzy logic controller with triangular membership function has been designed for two case study system. By varying inertia of the study system with different types of disturbances the membership functions have been aligned. After the design of fuzzy logic controller RES has been integrated in the system which in turn reduces system inertia. The system inertia in the presence of RES has been estimated with fuzzy logic estimator. Proposed method successfully estimates system inertia with an accuracy of 99.98% - 96.13%. In comparison, to the traditional inertia estimation methods based on frequency and ROCOF measurements using swing equation, proposed PMU based fuzzy logic estimator is independent of the type of disturbance in the system. Proposed method has been tested with simulations in OPAL RT real time simulator with HYPERSIM environment.

# CHAPTER 7

# CONCLUSION, FUTURE SCOPE AND SOCIETAL IMPACT

## 7.1 Conclusion

This thesis has presented a comprehensive investigation into the impact of inverter-based resources (IBRs) on the stability, protection, and inertia estimation of modern power systems using benchmark test systems such as the IEEE 9-bus system, the single-machine infinite bus model, and Kundur's two-area system implemented in the OPAL-RT HYPERSIM real-time environment. The study examined how reduced system inertia, altered oscillatory behavior, and converter-driven fault characteristics reshape the dynamic response of the grid.

The key conclusions drawn from this research are as follows:

- Altered Dynamic and Fault Behavior: High levels of IBR penetration fundamentally change system dynamics. Reduced inertia leads to faster frequency deviations, higher ROCOF, lower frequency nadirs, and altered inter-area oscillations. Converter-interfaced generation produces limited and distorted fault currents that challenge existing relay assumptions.

- Impact on Protection Schemes: Negative-sequence-impedance-based directional relays (67Q) show reduced sensitivity and accuracy under unsymmetrical faults due to IBR control strategies. Conventional distance relays and power swing blocking (PSB) functions exhibit increased risk of under-reaching, over-reaching, and misclassification under high-IBR scenarios

- Novel Inertia Estimation Technique: A PMU-based real-time inertia estimation method was developed, exploiting bus voltage phase angle derivatives and fuzzy logic inference. This approach achieved accuracy levels between 96.13% and 99.98%, offering a robust alternative to frequency-based estimation methods and enabling dynamic monitoring of system inertia.

- Unified Framework for Modern Grids: The combined modelling, simulation, and estimation framework developed in this thesis provides practical tools for

system operators and researchers to assess stability, enhance protection coordination, and support adaptive control strategies in low-inertia environments.

Overall, the findings underscore the urgent need to adapt protection and stability assessment methods to accommodate the growing presence of renewable energy resources. They also show the value of high-fidelity real-time simulation combined with PMU-based measurement techniques and intelligent algorithms for future grid operation.

## 7.2 Future Scope

While this thesis addresses several critical challenges associated with high IBR penetration, it also reveals multiple directions for future research and development. The most promising areas include:

1. Adaptive and Wide-Area Protection: Extend the proposed methodologies to develop fully adaptive, PMU-enabled protection schemes that coordinate decisions across multiple substations and regions.

2. Integration of Grid-Forming Inverters: Grid-forming inverter technologies emulate the inertial behavior of synchronous machines and provide rapid voltage and frequency support during disturbances. Their autonomous control enhances stability in low-inertia systems but alters fault current characteristics. As a result, while they strengthen system resilience, they also challenge conventional protection schemes, requiring adaptive protection strategies.

3. Cyber-Physical Resilience: Investigate the robustness of PMU-based inertia estimation and adaptive protection against cyberattacks, data spoofing, and communication delays, ensuring secure wide-area monitoring.

4. Machine Learning for Dynamic Settings: Apply reinforcement learning and advanced AI to continuously adjust relay settings, inertia estimation parameters, and stability margins as system conditions evolve.

5. Hardware-in-the-Loop and Larger Systems: Scale up real-time simulations to larger, more complex grids with hardware-in-the-loop testing to validate the performance of protection schemes and inertia estimators under field-like conditions.

6. Market and Operational Integration: Explore how real-time inertia estimation can inform ancillary service procurement, system operator dispatch, and dynamic stability margins in electricity markets.

7. Hybrid and Multi-Energy Systems: Extend the framework to include hybrid AC/DC grids, microgrids, and integrated energy systems where distributed IBRs interact with storage, demand response, and electric vehicles.

Pursuing these research directions will build upon the contributions of this thesis and support the development of next-generation stability assessment tools, adaptive protection systems, and inertia monitoring frameworks. These advances are essential for creating a resilient, intelligent, and decarbonized power grid capable of maintaining reliability in the face of growing renewable energy integration.

## 7.3 Societal Impact

This research aligns with the global sustainability framework established by the United Nations through the Sustainable Development Goals (SDGs). The thesis addresses key technical challenges associated with the increasing integration of inverter-based resources (IBRs) into modern power systems. By investigating power system stability, evaluating conventional protection schemes, and developing a real-time inertia estimation methodology, the research contributes to reliable electricity supply, resilient energy infrastructure, and the transition towards sustainable and low-carbon energy systems. The societal relevance of this research is reflected in the following SDGs.

**1. SDG 3: Good Health and Well-being:** Reliable electricity supply is essential for healthcare facilities, emergency services, and other critical public infrastructure. By supporting improved power system stability and reducing the risk of supply interruptions, this research can indirectly contribute to the reliable operation of essential services and community well-being.

**2. SDG 7: Affordable and Clean Energy:** The research supports the integration of renewable energy sources, including photovoltaic systems, wind turbines, and battery energy storage systems, into modern power grids. The proposed real-time inertia estimation method and stability assessments provide insights into maintaining reliable grid operation under increasing renewable energy penetration. These contributions support the transition towards cleaner and more sustainable electricity generation.

**3. SDG 9: Industry, Innovation and Infrastructure:** This thesis contributes to resilient and technologically advanced electricity infrastructure through the assessment of directional and distance protection schemes, investigation of power swing blocking performance, and development of a PMU-based real-time inertia estimation method using fuzzy logic. Real-time simulation studies using OPAL-RT HYPERSIM provide a framework for evaluating system dynamics and protection performance under different operating and fault conditions. The findings can support future developments in grid monitoring, protection coordination, and power system resilience.

**4. SDG 13: Climate Action:** The research addresses technical challenges that may arise as renewable energy sources increasingly replace conventional synchronous generation. By examining the stability and protection implications of high IBR penetration, the thesis provides insights that can help reduce technical barriers to renewable energy integration. This supports the broader transition towards low-carbon electricity systems while maintaining grid stability and operational security.

Overall, the research contributes to the development of reliable, resilient, and sustainable power systems. Its findings can assist researchers, utilities, system operators, and grid planners in addressing emerging stability and protection challenges and in supporting the long-term transition towards renewable energy-based electricity infrastructure.

# REFERENCES


[1] J. Sun *et al.*, “Renewable energy transmission by HVDC across the continent: system challenges and opportunities,” *CSEE Journal of Power and Energy Systems*, vol. 3, no. 4, pp. 353–364, Dec. 2017, doi: 10.17775/CSEEJPES.2017.01200.

[2] Y. Chilukuri, A. Usman, and B. S. Rajpurohit, “Assessing the Impact of Renewable Energy Sources to Achieve Net Zero Emissions,” in *IEEE Conference on Technologies for Sustainability (SusTech)*, Portland, OR, USA, 2023, pp. 231–236.

[3] J. C. Quispe and E. Orduña, “Transmission line protection challenges influenced by inverter-based resources: a review,” Dec. 01, 2022, *Springer*. doi: 10.1186/s41601-022-00249-8.

[4] P. Kundur *et al.*, “Definition and classification of power system stability,” *IEEE Transactions on Power Systems*, vol. 19, no. 3, pp. 1387–1401, Aug. 2004, doi: 10.1109/TPWRS.2004.825981.

[5] C. He, X. He, H. Geng, H. Sun, and S. Xu, “Transient Stability of Low-Inertia Power Systems With Inverter-Based Generation,” *IEEE Transactions on Energy Conversion*, vol. 37, no. 4, pp. 2903–2912, Dec. 2022, doi: 10.1109/TEC.2022.3185623.

[6] Y. Gu and T. C. Green, “Power System Stability With a High Penetration of Inverter-Based Resources,” *Proceedings of the IEEE*, vol. 111, no. 7, pp. 832–853, Jul. 2023, doi: 10.1109/JPROC.2022.3179826.

[7] N. Nimpitiwan, G. T. Heydt, R. Ayyanar, and S. Suryanarayanan, “Fault Current Contribution From Synchronous Machine and Inverter Based Distributed Generators,” *IEEE Transactions on Power Delivery*, vol. 22, no. 1, pp. 634–641, Jan. 2007, doi: 10.1109/TPWRD.2006.881440.

[8] B. Bahrani *et al.*, “Grid-Forming Inverter-Based Resource Research Landscape: Understanding the Key Assets for Renewable-Rich Power Systems,” *IEEE Power and Energy Magazine*, vol. 22, no. 2, pp. 18–29, Mar. 2024, doi: 10.1109/MPE.2023.3343338.

[9] N. Hatziargyriou *et al.*, “Definition and Classification of Power System Stability - Revisited & Extended,” *IEEE Transactions on Power Systems*, vol. 36, no. 4, pp. 3271–3281, Jul. 2021, doi: 10.1109/TPWRS.2020.3041774.

[10] P. Mitra, L. Sundaresh, and D. Ramasubramanian, "Stability of inverter-based resource (IBR) dominated systems with different types of local loads," *CIGRE Science & Engineering*, vol. 28, pp. 1–20, Mar. 2023.

[11] Power System Operation Corporation Limited (POSOCO) and Indian Institute of Technology Bombay (IITB), "Report on assessment of inertia in Indian power system," POSOCO, New Delhi, India, Tech. Rep., Jan. 2022.

[12] M. Nagpal and C. Henville, "Impact of Power-Electronic Sources on Transmission Line Ground Fault Protection," *IEEE Transactions on Power Delivery*, vol. 33, no. 1, pp. 62–70, Feb. 2018, doi: 10.1109/TPWRD.2017.2709279.

[13] E. Ørum *et al.*, "Future system inertia PARTICIPANTS." [Online]. Available: www.entsoe.eu

[14] T. Almomani and M. Al-Momani, "Future Low Inertia Power Systems: A Comprehensive Review of Virtual Inertia Emulation Techniques and Inertia Estimation Methods," *Jordan Journal of Energy*, vol. 1, no. 2, Sep. 2023, doi: 10.35682/jje.v1i2.694.

[15] P. Kundur, *Power System Stability and Control*. New York, NY, USA: McGraw-Hill Education, 1994.

[16] J. Schiffer, P. Aristidou, and R. Ortega, "Online Estimation of Power System Inertia Using Dynamic Regressor Extension and Mixing," *IEEE Transactions on Power Systems*, vol. 34, no. 6, pp. 4993–5001, Nov. 2019, doi: 10.1109/TPWRS.2019.2915249.

[17] A. Gorbunov, A. Dymarsky, and J. Bialek, "Estimation of Parameters of a Dynamic Generator Model From Modal PMU Measurements," *IEEE Transactions on Power Systems*, vol. 35, no. 1, pp. 53–62, Jan. 2020, doi: 10.1109/TPWRS.2019.2925127.

[18] U.S. Department of Energy, "Frequency response and frequency control in the power system," U.S. Dept. Energy, Washington, DC, USA, Tech. Rep., Oct. 2010.

[19] S. Hu, J. Yang, Y. Wang, Y. Zhao, and C. Chao, "Inertia and Primary Frequency Response Requirement Assessment for High-Penetration Renewable Power Systems Based on Planning Perspective," *Sustainability*, vol. 15, no. 23, p. 16191, Nov. 2023, doi: 10.3390/su152316191.

[20] J. Jorgenson and P. Denholm, "Modeling Primary Frequency Response for Grid Studies," Golden, CO (United States), Jan. 2019. doi: 10.2172/1489895.

[21] P. Denholm, T. Mai, R. W. Kenyon, B. Kroposki, and M. O'malley, "Inertia and the Power Grid: A Guide Without the Spin," 2020. [Online]. Available: www.nrel.gov/publications.

[22] F. Gonzalez-Longatt, J. M. Roldan-Fernandez, H. R. Chamorro, S. Arnaltes, and J. L. Rodriguez-Amenedo, "Investigation of Inertia Response and Rate of Change of Frequency in Low Rotational Inertial Scenario of Synchronous Dominated System," *Electronics (Basel).*, vol. 10, no. 18, p. 2288, Sep. 2021, doi: 10.3390/electronics10182288.

[23] J. Morren, S. W. H. de Haan, W. L. Kling, and J. A. Ferreira, "Wind turbines emulating inertia and supporting primary frequency control,"*IEEE Transactions on Power System*, vol. 21, pp. 433–434, Feb. 2006.

[24] Y. Gu and T. C. Green, "Power System Stability With a High Penetration of Inverter-Based Resources," *Proceedings of the IEEE*, vol. 111, no. 7, pp. 832–853, Jul. 2023, doi: 10.1109/JPROC.2022.3179826.

[25] C. He, H. Geng, K. Rajashekara, and A. Chandra, "Analysis and Control of Frequency Stability in Low-Inertia Power Systems: A Review," *IEEE/CAA Journal of Automatica Sinica*, vol. 11, no. 12, pp. 2363–2383, Dec. 2024, doi: 10.1109/JAS.2024.125013.

[26] H. Holttinen *et al.*, "System Impact Studies for Near 100% Renewable Energy Systems Dominated by Inverter Based Variable Generation," *IEEE Transactions on Power Systems*, vol. 37, no. 4, pp. 3249–3258, Jul. 2022.

[27] M. Rezkalla, M. Pertl, and M. Marinelli, "Electric power system inertia: requirements, challenges and solutions," *Electrical Engineering*, vol. 100, no. 4, pp. 2677–2693, Dec. 2018, doi: 10.1007/s00202-018-0739-z.

[28] X. Deng, R. Mo, P. Wang, J. Chen, D. Nan, and M. Liu, "Review of RoCoF Estimation Techniques for Low-Inertia Power Systems," *Energies (Basel).*, vol. 16, no. 9, p. 3708, Apr. 2023, doi: 10.3390/en16093708.

[29] P. Moore, O. A. Alimi, and A. Abu-Siada, "A Review of System Strength and Inertia in Renewable-Energy-Dominated Grids: Challenges, Sustainability, and Solutions," *Challenges*, vol. 16, no. 1, p. 12, Feb. 2025, doi: 10.3390/challe16010012.

[30] L. Su, X. Qin, S. Zhang, Y. Zhang, Y. Jiang, and Y. Han, "Fast frequency response of inverter-based resources and its impact on system frequency characteristics," *Global Energy Interconnection*, vol. 3, no. 5, pp. 475–485, Oct. 2020, doi: 10.1016/j.gloei.2020.11.007.

[31] C. Mosca *et al.*, "Mitigation of frequency stability issues in low inertia power systems using synchronous compensators and battery energy storage systems," *IET Generation, Transmission & Distribution*, vol. 13, no. 17, pp. 3951–3959, Sep. 2019, doi: 10.1049/iet-gtd.2018.7008.

[32] M. Jafari, M. H. Shahriar, M. A. Rahman, and S. Paudyal, "False Relay Operation Attacks in Power Systems with High Renewables," in *2021 IEEE Power & Energy Society General Meeting (PESGM)*, IEEE, Jul. 2021, pp. 01–05. doi: 10.1109/PESGM46819.2021.9637969.

[33] T. P. Sari, J. Kim, A. Priyadi, V. Lystianingrum, M. H. Purnomo, and E. Muljadi, "Utilization of Supercapacitor to Extend the Critical Clearing Time in a Power System," *IEEE Open Journal of Industry Applications*, vol. 1, pp. 248–257, 2020, doi: 10.1109/OJIA.2020.3041209.

[34] F. Gonzalez-Longatt, J. L. Rueda, and D. Bogdanov, "Assessment of the Critical Clearing Time in Low Rotational Inertia Power Systems," in *2018 20th International Symposium on Electrical Apparatus and Technologies (SIELA)*, IEEE, Jun. 2018, pp. 1–4. doi: 10.1109/SIELA.2018.8447128.

[35] L. Roberts, G. Kafanas, A. Champneys, M. di Bernardo, and K. Bell, "A parametric investigation on the effects of inertia on the stability of power systems," in *2015 IEEE Eindhoven PowerTech*, IEEE, Jun. 2015, pp. 1–6. doi: 10.1109/PTC.2015.7232780.

[36] Md. S. Alam, F. S. Al-Ismail, A. Salem, and M. A. Abido, "High-Level Penetration of Renewable Energy Sources Into Grid Utility: Challenges and Solutions," *IEEE Access*, vol. 8, pp. 190277–190299, 2020, doi: 10.1109/ACCESS.2020.3031481.

[37] H. S. Samkari and B. K. Johnson, "Time-Domain Protection Scheme for Microgrids With Aggregated Inverter-Based Distributed Energy Resources," *IEEE Access*, vol. 11, pp. 13232–13242, 2023, doi: 10.1109/ACCESS.2023.3242908.

[38] A. Haddadi, E. Farantatos, I. Kocar, and U. Karaagac, "Impact of Inverter Based Resources on System Protection," *Energies (Basel).*, vol. 14, no. 4, p. 1050, Feb. 2021, doi: 10.3390/en14041050.

[39] A. Saeed, M. Jensen, M. Reno, A. Bidram, and A. Zamani, "Utilities Perspective on Protection Challenges with High IBR Penetration," Golden, CO (United States), Sep. 2024. doi: 10.2172/2458239.

[40] J. Horak, "Directional Overcurrent Relaying (67) Concepts," in *59th Annual Conference for Protective Relay Engineers, 2006.*, IEEE, pp. 164–176. doi: 10.1109/CPRE.2006.1638701.

[41] S. Liu, T. Bi, and Y. Liu, "Theoretical Analysis on the Short-Circuit Current of Inverter-Interfaced Renewable Energy Generators with Fault-Ride-Through Capability," *Sustainability*, vol. 10, no. 1, p. 44, Dec. 2017, doi: 10.3390/su10010044.

[42] A. Haddadi, M. Zhao, I. Kocar, U. Karaagac, K. W. Chan, and E. Farantatos, "Impact of Inverter-Based Resources on Negative Sequence Quantities-Based Protection Elements," *IEEE Transactions on Power Delivery*, vol. 36, no. 1, pp. 289–298, Feb. 2021, doi: 10.1109/TPWRD.2020.2978075.

[43] S. Kariyawasam and A. D. Rajapakse, "A Negative Sequence Admittance Based Algorithm for Identifying Fault Direction in the Presence of Inverter Based Resources," *IEEE Access*, vol. 11, pp. 26530–26540, 2023, doi: 10.1109/ACCESS.2023.3257137.

[44] N. Rezaei and M. N. Uddin, "An Analytical Review on State-of-the-Art Microgrid Protective Relaying and Coordination Techniques," May 01, 2021, *Institute of Electrical and Electronics Engineers Inc.* doi: 10.1109/TIA.2021.3057308.

[45] M. J. Reno, "Microgrid Protection: Advancing the State of the Art." [Online]. Available: https://classic.ntis.gov/help/order-methods/

[46] G. Custer, "Inverter Protection and Ride-Through: Today's Photovoltaic and Energy Storage Inverters," *IEEE Electrification Magzine*, vol. 9, no. 2, pp. 43–49, Jun. 2021.

[47] B. Kasztenny, M. V. Mynam, and N. Fischer, "Sequence component applications in protective relays—Advantages, limitations, and solutions," in *Proc. 43rd Annu. Western Protective Relay Conf.*, Spokane, WA, USA, Oct. 2016, pp. 1–28.

[48] G. Kou, L. Chen, P. VanSant, F. Velez-Cedeno, and Y. Liu, "Fault Characteristics of Distributed Solar Generation," *IEEE Transactions on Power Delivery*, vol. 35, no. 2, pp. 1062–1064, Apr. 2020, doi: 10.1109/TPWRD.2019.2907462.

[49] H. Aji, M. Ndreko, M. Popov, and M. A. M. M. van der Meijden, "Investigation on different negative sequence current control options for MMC-HVDC during single line to ground AC faults," in *2016 IEEE PES Innovative Smart Grid Technologies Conference Europe (ISGT-Europe)*, IEEE, Oct. 2016, pp. 1–6. doi: 10.1109/ISGTEurope.2016.7856182.

[50] "IEEE Guide for Protective Relay Applications to Transmission Lines," Dec. 05, 2015, *IEEE, Piscataway, NJ, USA*. doi: 10.1109/IEEESTD.2016.7502047.

[51] G. M. Abo-Hamad, D. K. Ibrahim, E. Aboul Zahab, and A. F. Zobaa, "Adaptive Mho Distance Protection for Interconnected Transmission Lines Compensated with Thyristor Controlled Series Capacitor," *Energies (Basel).*, vol. 14, no. 9, p. 2477, Apr. 2021, doi: 10.3390/en14092477.

[52] L. Pagnier and P. Jacquod, “Inertia location and slow network modes determine disturbance propagation in large-scale power grids,” *PLoS One*, vol. 14, no. 3, p. e0213550, Mar. 2019, doi: 10.1371/journal.pone.0213550.

[53] N. S. Gurule, J. Hernandez-Alvidrez, M. J. Reno, A. Summers, S. Gonzalez, and J. Flicker, “Grid-forming Inverter Experimental Testing of Fault Current Contributions,” in *2019 IEEE 46th Photovoltaic Specialists Conference (PVSC)*, IEEE, Jun. 2019, pp. 3150–3155. doi: 10.1109/PVSC40753.2019.8980892.

[54] A. Banaiemoqadam, A. Azizi, A. Hooshyar, M. Kanabar, and E. F. El-Saadany, “Impact of Inverter-Based Resources on Different Implementation Methods for Distance Relays—Part I: Phase Comparators,” *IEEE Transactions on Power Delivery*, vol. 38, no. 6, pp. 4090–4102, Dec. 2023, doi: 10.1109/TPWRD.2023.3301509.

[55] W. Du *et al.*, “Modeling of Grid-Forming and Grid-Following Inverters for Dynamic Simulation of Large-Scale Distribution Systems,” *IEEE Transactions on Power Delivery*, vol. 36, no. 4, pp. 2035–2045, Aug. 2021, doi: 10.1109/TPWRD.2020.3018647.

[56] J. D. Hernández-Santafé and E. Sorrentino, “Problems and Solutions Concerning the Distance Protection of Transmission Lines Connected to Inverter-Based Resources,” *Energies (Basel).*, vol. 18, no. 6, p. 1375, Mar. 2025, doi: 10.3390/en18061375.

[57] R. Chowdhury and N. Fischer, “Transmission Line Protection for Systems With Inverter-Based Resources – Part II: Solutions,” *IEEE Transactions on Power Delivery*, vol. 36, no. 4, pp. 2426–2433, Aug. 2021, doi: 10.1109/TPWRD.2020.3030168.

[58] L. S. A. Grande, R. G. Arrabé, S. Arnaltes, and J. L. R. Amenedo, “Influence of Negative-Sequence Control under Converter-Interface-based Generation in Distance Protection Relays,” in *2023 IEEE International Conference on Environment and Electrical Engineering and 2023 IEEE Industrial and Commercial Power Systems Europe (EEEIC / I&CPS Europe)*, IEEE, Jun. 2023, pp. 1–6. doi: 10.1109/EEEIC/ICPSEurope57605.2023.10194720.

[59] E. E. Omran *et al.*, “An adaptive protection scheme for an inverter-dominated grid considering Momentary Cessation,” *Electric Power Systems Research*, vol. 244, p. 111594, Jul. 2025, doi: 10.1016/j.epsr.2025.111594.

[60] M. McDonald -Chairman Demetrios Tziouvaras -Vice Chairman Apostolov *et al.*, “power swing and out-of-step considerations on transmission lines ieee psrc wg d6 power swing and out-of-step considerations on transmission lines power swing and out-of-step considerations on transmission lines ieee psrc wg d6 2 / 59 power swing and out-of-step considerations on transmission lines a report to

the power system relaying committee of the ieee power engineering society power swing and out-of-step considerations on transmission lines ieee psrc wg d6," 2005.

[61] E. E. Omran *et al.*, "An adaptive protection scheme for an inverter-dominated grid considering Momentary Cessation," *Electric Power Systems Research*, vol. 244, p. 111594, Jul. 2025, doi: 10.1016/j.epsr.2025.111594.

[62] P. Kundu, "Wide Area Backup Protection for Network Integrated with Large-Scale Solar Photovoltaic Plant," in *2023 IEEE Power & Energy Society General Meeting (PESGM)*, IEEE, Jul. 2023, pp. 1–5. doi: 10.1109/PESGM52003.2023.10252172.

[63] B. Tan and J. Zhao, "Data-Driven Time-Varying Inertia Estimation of Inverter-Based Resources," *IEEE Transactions on Power Systems*, vol. 38, no. 2, pp. 1795–1798, Mar. 2023, doi: 10.1109/TPWRS.2022.3229869.

[64] T. Kerdphol, F. S. Rahman, and Y. Mitani, "Virtual Inertia Control Application to Enhance Frequency Stability of Interconnected Power Systems with High Renewable Energy Penetration," *Energies (Basel).*, vol. 11, no. 4, p. 981, Apr. 2018, doi: 10.3390/en11040981.

[65] M. Elnasry, A. R. R. Matavalam, P. Sharma, and V. Ajjarapu, "Online Output-based Inertia Estimation of Modern Power Systems," in *2023 IEEE Power & Energy Society General Meeting (PESGM)*, IEEE, Jul. 2023, pp. 1–5. doi: 10.1109/PESGM52003.2023.10252536.

[66] B. Tan, J. Zhao, M. Netto, V. Krishnan, V. Terzija, and Y. Zhang, "Power system inertia estimation: Review of methods and the impacts of converter-interfaced generations," *International Journal of Electrical Power & Energy Systems*, vol. 134, p. 107362, Jan. 2022, doi: 10.1016/j.ijepes.2021.107362.

[67] P. System Relaying Committee of the IEEE Power and E. Society, "IEEE Standard for Synchrophasor Measurements for Power Systems Sponsored by the Power System Relaying Committee IEEE Power & Energy Society," 2011.

[68] *IEEE Std C37.118-2005 (Revision of IEEE Std 1344-1995) : IEEE Standard for Synchrophasors for Power Systems.* IEEE, 2006.

[69] P. System Relaying Committee of the IEEE Power and E. Society, "IEEE Standard for Synchrophasor Measurements for Power Systems Sponsored by the Power System Relaying Committee IEEE Power & Energy Society," 2011.

[70] A. G. Phadke and J. S. Thorp, *Synchronized Phasor Measurements and Their Applications*. in Power Electronics and Power Systems. Boston, MA: Springer US, 2008. doi: 10.1007/978-0-387-76537-2.

[71] N. Rezaei and M. N. Uddin, “An Analytical Review on State-of-the-Art Microgrid Protective Relaying and Coordination Techniques,” May 01, 2021, *Institute of Electrical and Electronics Engineers Inc.* doi: 10.1109/TIA.2021.3057308.

[72] A. Hooshyar, M. A. Azzouz, and E. F. El-Saadany, “Distance protection of lines connected to induction generator-based wind farms during balanced faults,” *IEEE Trans. Sustain. Energy*, vol. 5, no. 4, pp. 1193–1203, Oct. 2014, doi: 10.1109/TSTE.2014.2336773.

[73] A. Hooshyar, M. A. Azzouz, and E. F. El-Saadany, “Distance Protection of Lines Emanating from Full-Scale Converter-Interfaced Renewable Energy Power Plants-Part I: Problem Statement,” *IEEE Transactions on Power Delivery*, vol. 30, no. 4, pp. 1770–1780, Aug. 2015, doi: 10.1109/TPWRD.2014.2369479.

[74] M. Rezkalla, M. Pertl, and M. Marinelli, “Electric power system inertia: requirements, challenges and solutions,” *Electrical Engineering*, vol. 100, no. 4, pp. 2677–2693, Dec. 2018, doi: 10.1007/s00202-018-0739-z.

[75] S. Dong, X. Fang, J. Tan, N. Gao, X. Cui, and A. Hoke, “A unified analytical method to quantify three types of fast frequency response from inverter-based resources,” *IET Conference Proceedings*, vol. 2023, no. 20, pp. 669–674, Nov. 2023, doi: 10.1049/icp.2023.2801.

[76] A. Ulbig, T. S. Borsche, and G. Andersson, "Impact of low rotational inertia on power system stability and operation," in *Proc. 19th World Congr. Int. Fed. Autom. Control (IFAC)*, Cape Town, South Africa, Aug. 2014, pp. 7290–7297..

[77] Y. Son, Y. Ha, and G. Jang, “Frequency Nadir Estimation Using the Linear Characteristics of Frequency Control in Power Systems,” *Energies (Basel).*, vol. 17, no. 5, p. 1061, Feb. 2024, doi: 10.3390/en17051061.

[78] A. Adrees, P. N. Papadopoulos, and J. V. Milanovic, “A framework to assess the effect of reduction in inertia on system frequency response,” in *2016 IEEE Power and Energy Society General Meeting (PESGM)*, IEEE, Jul. 2016, pp. 1–5. doi: 10.1109/PESGM.2016.7741695.

[79] C. Liu and G. Cai, “Power-oscillation evaluation in power systems with high penetration of renewable power generation based on network virtual inertia,” *IET Renewable Power Generation*, vol. 13, no. 1, pp. 138–145, Jan. 2019, doi: 10.1049/iet-rpg.2018.5306.

[80] T. Xu, W. Jang, and T. Overbye, “Location-Dependent Impacts of Resource Inertia on Power System Oscillations.” [Online]. Available: http://hdl.handle.net/10125/50230

[81] S. You *et al.*, “Impact of High PV Penetration on the Inter-Area Oscillations in the U.S. Eastern Interconnection,” *IEEE Access*, vol. 5, pp. 4361–4369, 2017, doi: 10.1109/ACCESS.2017.2682260.

[82] X. Zhou, S. Cheng, X. Wu, and X. Rao, “Influence of Photovoltaic Power Plants Based on VSG Technology on Low Frequency Oscillation of Multi-Machine Power Systems,” *IEEE Transactions on Power Delivery*, vol. 37, no. 6, pp. 5376–5384, Dec. 2022, doi: 10.1109/TPWRD.2022.3177042.

[83] *U. Agrawal, J. O'Brien, A. Somani, T. Mosier, and J. Dagle, "A study of the impact of reduced inertia in power systems," in Proc. 53rd Hawaii Int. Conf. Syst. Sci. (HICSS), Maui, HI, USA, Jan. 2020, pp. 3010–3017.*

.

[84] Y. Liu, T. Xu, and T. J. Overbye, "Locational dependence of inertia's impacts on critical clearing time," in *Proc. 2018 North American Power Symposium (NAPS)*, Fargo, ND, USA, Sep. 2018, pp. 1–6.

.

[85] P.K.Agrawal, V.K.Agrawal, and Harish Rathour, “Application of PMU-Based Information in the Indian Power System,” *International Journal of Emerging Electric Power Systems*, 2013.

[86] R. Chowdhury and N. Fischer, “Transmission Line Protection for Systems with Inverter-Based Resources - Part II: Solutions,” *IEEE Transactions on Power Delivery*, vol. 36, no. 4, pp. 2426–2433, Aug. 2021, doi: 10.1109/TPWRD.2020.3030168.

[87] Y. Fang, K. Jia, Z. Yang, Y. Li, and T. Bi, “Impact of Inverter-Interfaced Renewable Energy Generators on Distance Protection and an Improved Scheme,” *IEEE Transactions on Industrial Electronics*, vol. 66, no. 9, pp. 7078–7088, Sep. 2019, doi: 10.1109/TIE.2018.2873521.

[88] P. Mishra, A. K. Pradhan, and P. Bajpai, “Adaptive Distance Relaying for Distribution Lines Connecting Inverter-Interfaced Solar PV Plant,” *IEEE Transactions on Industrial Electronics*, vol. 68, no. 3, pp. 2300–2309, Mar. 2021, doi: 10.1109/TIE.2020.2975462.

[89] L. S. A. Grande, R. G. Arrabé, S. Arnaltes, and J. L. R. Amenedo, “Influence of Negative-Sequence Control under Converter-Interface-based Generation in Distance Protection Relays,” in *Proceedings - 2023 IEEE International Conference on Environment and Electrical Engineering and 2023 IEEE Industrial and Commercial Power Systems Europe, EEEIC / I and CPS Europe 2023*, Institute of Electrical and Electronics Engineers Inc., 2023. doi: 10.1109/EEEIC/ICPSEurope57605.2023.10194720.

[90] V. Telukunta, J. Pradhan, A. Agrawal, M. Singh, and S. G. Srivani, “Protection challenges under bulk penetration of renewable energy resources in power systems: A review,” *CSEE Journal of Power and Energy Systems*, vol. 3, no. 4, pp. 365–379, Dec. 2017, doi: 10.17775/CSEEJPES.2017.00030.

[91] H. V. Padullaparti, P. Chirapongsananurak, M. E. Hernandez, and S. Santoso, “Analytical Approach to Estimate Feeder Accommodation Limits Based on Protection Criteria,” *IEEE Access*, vol. 4, pp. 4066–4081, 2016, doi: 10.1109/ACCESS.2016.2589545.

[92] M. M. Salem, N. I. Elkalashy, Y. Atia, and T. A. Kawady, “Modified Inverter Control of Distributed Generation for Enhanced Relaying Coordination in Distribution Networks,” *IEEE Transactions on Power Delivery*, vol. 32, no. 1, pp. 78–87, Feb. 2017, doi: 10.1109/TPWRD.2016.2555791.

[93] K. Jia, Z. Yang, Y. Fang, T. Bi, and M. Sumner, “Influence of Inverter-Interfaced Renewable Energy Generators on Directional Relay and an Improved Scheme,” *IEEE Trans. Power Electron.*, vol. 34, no. 12, pp. 11843–11855, Dec. 2019, doi: 10.1109/TPEL.2019.2904715.

[94] D. Chhetija, I. Khan, Z. H. Rather, and S. Doolla, “Negative Sequence Power based Fault Detection Scheme for Power Islands during Unbalanced Faults,” in *2023 IEEE International Conference on Environment and Electrical Engineering and 2023 IEEE Industrial and Commercial Power Systems Europe (EEEIC / I&CPS Europe)*, IEEE, Jun. 2023, pp. 1–5. doi: 10.1109/EEEIC/ICPSEurope57605.2023.10194733.

[95] V. Chakrapani and I. Voloh, “Impact of renewable generation resouce on the distance protection and solutions,” *IET Conference Proceedings*, vol. 2022, no. 2, pp. 238–243, May 2022, doi: 10.1049/icp.2022.0946.

[96] M. A. Azzouz, A. Hooshyar, and E. F. El-Saadany, “Resilience Enhancement of Microgrids With Inverter-Interfaced DGs by Enabling Faulty Phase Selection,” *IEEE Trans. Smart Grid*, vol. 9, no. 6, pp. 6578–6589, Nov. 2018, doi: 10.1109/TSG.2017.2716342.

[97] Y. Liang, W. Li, and W. Zha, “Adaptive Mho Characteristic-Based Distance Protection for Lines Emanating From Photovoltaic Power Plants Under Unbalanced Faults,” *IEEE Syst. J.*, vol. 15, no. 3, pp. 3506–3516, Sep. 2021, doi: 10.1109/JSYST.2020.3015225.

[98] N. S. Darwade and S. T. Nagarajan, “Investigation on Impact of Inverter Based Renewable Energy Sources on Distance Relaying,” in *Proceedings of the 3rd IEEE International Conference on Power Electronics, Intelligent Control and Energy Systems, ICPEICES 2024*, Institute of Electrical and Electronics Engineers Inc., 2024, pp. 684–689. doi: 10.1109/ICPEICES62430.2024.10719278.

[99] M. Yin, G. Li, M. Zhou, G. Liu, and C. Zhao, "Study on the control of DFIG and its responses to grid disturbances," in *Proc. IEEE Power Engineering Society General Meeting*, Montreal, QC, Canada, Jun. 2006, pp. 1–6.

.

[100] N. S. Darwade and S. T. Nagarajan, “Investigation on Impact of IBR on Negative Sequence Impedance Based Directional Protection,” in *Proceedings of the 3rd IEEE International Conference on Power Electronics, Intelligent Control and Energy Systems, ICPEICES 2024*, Institute of Electrical and Electronics Engineers Inc., 2024, pp. 615–620. doi: 10.1109/ICPEICES62430.2024.10719257.

[101] “*System Protection and Control Subcommittee*, "Protection system response to power swings," NERC, Atlanta, GA, USA, Tech. Rep., Aug. 2013. [Online]. Available: https://www.nerc.com

[102] D. Kang and R. Gokaraju, “A New Method for Blocking Third-Zone Distance Relays during Stable Power Swings,” *IEEE Transactions on Power Delivery*, vol. 31, no. 4, pp. 1836–1843, Aug. 2016, doi: 10.1109/TPWRD.2016.2520394.

[103] K. K. Thoufeer and M. K. Jena, “Revisiting Power Swing Blocking Schemes for Future Power Systems with High Penetration of Inverter Based Resources,” in *2023 10th IEEE International Conference on Power Systems, ICPS 2023*, Institute of Electrical and Electronics Engineers Inc., 2023. doi: 10.1109/ICPS60393.2023.10428747.

[104] T. Inoue, H. Taniguchi, Y. Ikeguchi, and K. Yoshida, "Estimation of power system inertia constant and capacity of spinning-reserve support generators using measured frequency transients," *IEEE Trans. Power Syst.*, vol. 12, no. 1, pp. 136–143, Feb. 1997.

.

[105] D. P. Chassin, Z. Huang, M. K. Donnelly, C. Hassler, E. Ramirez, and C. Ray, “Estimation of WECC system inertia using observed frequency transients,” *IEEE Transactions on Power Systems*, vol. 20, no. 2, pp. 1190–1192, May 2005, doi: 10.1109/TPWRS.2005.846155.

[106] IEEE Power & Energy Society and B. C. IEEE Power and Energy Society (PES) General Meeting 2013.07.21-25 Vancouver, *IEEE Power and Energy Society general meeting (PES), 2013 21-25 July 2013, Vancouver, BC, Canada*.

[107] P. M. Ashton, C. S. Saunders, G. A. Taylor, A. M. Carter, and M. E. Bradley, “Inertia estimation of the GB power system using synchrophasor measurements,” *IEEE Transactions on Power Systems*, vol. 30, no. 2, pp. 701–709, Mar. 2015, doi: 10.1109/TPWRS.2014.2333776.

[108] D. Zografos, M. Ghandhari, and R. Eriksson, “Power system inertia estimation: Utilization of frequency and voltage response after a disturbance,” *Electric Power Systems Research*, vol. 161, pp. 52–60, Aug. 2018, doi: 10.1016/j.epsr.2018.04.008.

[109] T. Kerdphol, M. Watanabe, R. Nishikawa, T. Tamaki, and Y. Mitani, “Determining Inertia of 60 Hz Japan Power System using PMUs from Power Loss Event,” in *2021 IEEE Texas Power and Energy Conference, TPEC 2021*, Institute of Electrical and Electronics Engineers Inc., Feb. 2021. doi: 10.1109/TPEC51183.2021.9384932.

[110] D. Zografos and M. Ghandhari, "Estimation of power system inertia," in *Proc. 2016 IEEE Power and Energy Society General Meeting (PESGM)*, Boston, MA, USA, Jul. 2016, pp. 1–5.

[111] K. Prabhakar, S. K. Jain, and P. K. Padhy, “Inertia estimation in modern power system: A comprehensive review,” Oct. 01, 2022, *Elsevier Ltd*. doi: 10.1016/j.epsr.2022.108222.

[112] M. A. M. Ariff, B. C. Pal, and A. K. Singh, “Estimating dynamic model parameters for adaptive protection and control in power system,” *IEEE Transactions on Power Systems*, vol. 30, no. 2, pp. 829–839, Mar. 2015, doi: 10.1109/TPWRS.2014.2331317.

[113] P. Wall and V. Terzija, “Simultaneous estimation of the time of disturbance and inertia in power systems,” *IEEE Transactions on Power Delivery*, vol. 29, no. 4, pp. 2018–2031, 2014, doi: 10.1109/TPWRD.2014.2306062.

[114] N. Petra, C. G. Petra, Z. Zhang, E. M. Constantinescu, and M. Anitescu, "A Bayesian approach for parameter estimation with uncertainty for dynamic power systems," *IEEE Trans. Power Syst.*, vol. 32, no. 4, pp. 2735–2743, Jul. 2017, doi: 10.1109/TPWRS.2016.2621072.”

[115] K. Tuttelberg, J. Kilter, D. Wilson, and K. Uhlen, “Estimation of power system inertia from ambient wide area measurements,” *IEEE Transactions on Power Systems*, vol. 33, no. 6, pp. 7249–7257, Nov. 2018, doi: 10.1109/TPWRS.2018.2843381.

[116] B. Tan, J. Zhao, V. Terzija, and Y. Zhang, “Decentralized data-driven estimation of generator rotor speed and inertia constant based on adaptive unscented Kalman filter,” *International Journal of Electrical Power and Energy Systems*, vol. 137, May 2022, doi: 10.1016/j.ijepes.2021.107853.

[117] X. Cao, B. Stephen, I. F. Abdulhadi, C. D. Booth, and G. M. Burt, “Switching Markov Gaussian Models for Dynamic Power System Inertia Estimation,” *IEEE Transactions on Power Systems*, vol. 31, no. 5, pp. 3394–3403, Sep. 2016, doi: 10.1109/TPWRS.2015.2501458.

[118] A. Schmitt and B. Lee, “Steady-state inertia estimation using a neural network approach with modal information,” in *2017 IEEE Power & Energy Society General Meeting*, IEEE, Jul. 2017, pp. 1–5. doi: 10.1109/PESGM.2017.8274640.

[119] W. Wang, W. Yao, C. Chen, X. Deng, and Y. Liu, “Fast and Accurate Frequency Response Estimation for Large Power System Disturbances Using Second Derivative of Frequency Data,” *IEEE Transactions on Power Systems*, vol. 35, no. 3, pp. 2483–2486, May 2020, doi: 10.1109/TPWRS.2020.2977504.

[120] B. Wang, D. Yang, G. Cai, Z. Chen, and J. Ma, “An Improved Electromechanical Oscillation-Based Inertia Estimation Method,” *IEEE Transactions on Power Systems*, vol. 37, no. 3, pp. 2479–2482, May 2022, doi: 10.1109/TPWRS.2022.3156441.

[121] H. Holttinen *et al.*, “System Impact Studies for Near 100% Renewable Energy Systems Dominated by Inverter Based Variable Generation,” *IEEE Transactions on Power Systems*, vol. 37, no. 4, pp. 3249–3258, Jul. 2022, doi: 10.1109/TPWRS.2020.3034924.

[122] Y. Cheng *et al.*, “Real-World Subsynchronous Oscillation Events in Power Grids With High Penetrations of Inverter-Based Resources,” *IEEE Transactions on Power Systems*, vol. 38, no. 1, pp. 316–330, Jan. 2023, doi: 10.1109/TPWRS.2022.3161418.

[123] F. Allella, E. Chiodo, G. M. Giannuzzi, D. Lauria, and F. Mottola, “On-Line Estimation Assessment of Power Systems Inertia With High Penetration of Renewable Generation,” *IEEE Access*, vol. 8, pp. 62689–62697, 2020, doi: 10.1109/ACCESS.2020.2983877.

[124] D. Al Kez, A. M. Foley, F. Ahmed, and D. J. Morrow, “Overview of frequency control techniques in power systems with high inverter-based resources: Challenges and mitigation measures,” *IET Smart Grid*, vol. 6, no. 5, pp. 447–469, Oct. 2023, doi: 10.1049/stg2.12117.

[125] Y. Zuo, M. Paolone, and F. Sossan, “Effect of voltage source converters with electrochemical storage systems on dynamics of reduced-inertia bulk power grids,” *Electric Power Systems Research*, vol. 189, p. 106766, Dec. 2020, doi: 10.1016/j.epsr.2020.106766.

[126] S. Hu, J. Yang, Y. Wang, Y. Zhao, and C. Chao, “Inertia and Primary Frequency Response Requirement Assessment for High-Penetration Renewable Power Systems Based on Planning Perspective,” *Sustainability*, vol. 15, no. 23, p. 16191, Nov. 2023, doi: 10.3390/su152316191.

[127] P. Chi, Y. Qin, Y. Tao, and R. Liang, “Research on condition assessment of XLPE cable based on signal propagation characteristics,” *Electric Power Systems Research*, vol. 195, p. 107136, Jun. 2021, doi: 10.1016/j.epsr.2021.107136.

[128] M. Wang, L. Zhang, and X. Wang, "Grid-synchronization dynamics of voltage-source converters in weak grids," *IEEE Trans. Power Electron.*, vol. 35, no. 10, pp. 10243–10255, Oct. 2020.

[129] R. W. Kenyon *et al.*, "Stability and control of power systems with high penetrations of inverter-based resources: An accessible review of current knowledge and open questions," *Solar Energy*, vol. 210, pp. 149–168, Nov. 2020, doi: 10.1016/j.solener.2020.05.053.

[130] L. Zhang, L. Harnefors, and and H.-P. Nee, "Interconnection of Power Systems via LCC-HVDC and VSC-HVDC: A Dynamic Stability Comparison," *IEEE Transactions on Power Delivery*, vol. 26, no. 4, pp. 2424–2434, Oct. 2011.

[131] S. Dulal *et al.*, "Inertia Estimation and Trend Analysis of the United States Power Grid Interconnections," *IEEE Access*, vol. 12, pp. 194436–194448, 2024, doi: 10.1109/ACCESS.2024.3520901.

[132] H. Mohsenian-Rad, M. Kezunovic, and F. Rahmatian, "Synchro-Waveforms in Wide-Area Monitoring, Control, and Protection: Real-World Examples and Future Opportunities," *IEEE Power and Energy Magazine*, vol. 23, no. 1, pp. 69–80, Jan. 2025, doi: 10.1109/MPE.2024.3403800.

[133] X. Jia *et al.*, "Real-Time Inertia Estimation Tool Implementation Based on Probing Signals," in *2023 14th International Renewable Energy Congress (IREC)*, IEEE, Dec. 2023, pp. 1–6. doi: 10.1109/IREC59750.2023.10389220.

[134] H. Saadat, *Power System Analysis*, 1st ed. Boston, MA, USA: McGraw-Hill, 1999.

[135] M. Klein, G. J. Rogers, P. Kundur, and O. Toronto, "A FUNDAMENTAL STUDY OF INTER-AREA OSCILLATIONS IN POWER SYSTEMS," 1991.

[136] G. Kou, L. Chen, P. VanSant, F. Velez-Cedeno, and Y. Liu, "Fault Characteristics of Distributed Solar Generation," *IEEE Transactions on Power Delivery*, vol. 35, no. 2, pp. 1062–1064, Apr. 2020, doi: 10.1109/TPWRD.2019.2907462.

[137] K. Zimmerman and D. Costello, "Fundamentals and improvements for directional relays," in *2010 63rd Annual Conference for Protective Relay Engineers*, IEEE, Mar. 2010, pp. 1–12. doi: 10.1109/CPRE.2010.5469483.

[138] Schweitzer, "SEL-351R RECLOSER CONTROL INSTRUCTION MANUAL IMPORTANT: Use this manual in conjunction with the SEL-351R Quick-Start Installation and User's Guide," 1997. [Online]. Available: www.selinc.com

[139] Y. Liang, W. Li, and W. Zha, "Adaptive Mho Characteristic-Based Distance Protection for Lines Emanating From Photovoltaic Power Plants Under

Unbalanced Faults," *IEEE Syst. J.*, vol. 15, no. 3, pp. 3506–3516, Sep. 2021, doi: 10.1109/JSYST.2020.3015225.

[140] A. Jalilian and D. A. Robinson, "Impact of inverter-based resources on transmission line relaying -part II: power swing protection," *Frontiers in Electronics*, vol. 4, Aug. 2023, doi: 10.3389/felec.2023.1144383.

[141] M. Jayamohan, S. Das, and S. Brahma, "Impedance Trajectories during Stable and Unstable Power Swings in Presence of PQ Control based PV Generations," in *2023 IEEE Power & Energy Society General Meeting (PESGM)*, IEEE, Jul. 2023, pp. 1–5. doi: 10.1109/PESGM52003.2023.10253031.

[142] A. Dyśko, H. Urdal, A. Roscoe, Jiebei Zhu, Ruiqi Li, and C. Booth, "Protection challenges in future converter dominated power systems: demonstration through simulation and hardware tests," in *International Conference on Renewable Power Generation (RPG 2015)*, Institution of Engineering and Technology, 2015, pp. 6 .-6 . doi: 10.1049/cp.2015.0392.

[143] J. Conto, "Grid challenges on high penetration levels of wind power," in *Proc. IEEE Power and Energy Society General Meeting*, San Diego, CA, USA, Jul. 2012, pp. 1–3

[144] V. Gevorgian, Y. Zhang, and E. Ela, "Investigating the Impacts of Wind Generation Participation in Interconnection Frequency Response," *IEEE Trans. Sustain. Energy*, vol. 6, no. 3, pp. 1004–1012, Jul. 2015, doi: 10.1109/TSTE.2014.2343836.

[145] S. Silwal and M. Karimi-Ghartemani, "On Transient Responses of a Class of PV Inverters," *IEEE Trans. Sustain. Energy*, vol. 10, no. 1, pp. 311–314, Jan. 2019, doi: 10.1109/TPWRD.2018.2804671.

[146] Z. K. Kovači´c and S. Bogdan, "Fuzzy Controller Design Theory and Applications."

# APPENDICES

## APPENDIX I

Synchronous Generator
MVA Rating = 100MVA
Voltage rating = 22 kV
Nominal power of turbine = 100 MW
Reactive power = 45 MVAR
X'd = 0.315
Shaft
H = 6.112s
Transformer
Primary connection = Star ground Secondary connection = Delta Lag
Base primary winding voltage(rmsLL) = 22 kV Base secondary winding voltage(rmsLL) = 220 kV Base
Power=100MVA Base frequency = 50 Hz
Rm = 1.081MΩ Lm = 2.8663E3
L1 = 637.00E-6H
L2 = 637.00E-6H
Three phase pi line
Line length=100km
Zero Sequence Zero seq (R0) = 0 Ω/km L0 = 10E-6 H/km C0 = 1E-9 F/km
Positive seq (R1) = 1E-9 Ω/km L1 = 3.852E-3 H/km C1 = 1E-9 F/km

## APPENDIX II

A linear Second order system can be represented as,

$$\frac{d^2\Delta\delta}{dt^2} + \frac{\pi f_0}{H}\ \mathrm{D}\ \frac{d\Delta\delta}{dt} + \frac{\pi f_0}{H} P_S \Delta\delta\ = 0$$

In state space form with,

$$x_1 = \Delta\delta\ and\ x_2 = \Delta\omega = \dot{\Delta\delta}$$

$$\dot{x_1} = x_2\ and\ \dot{x_2} = -\omega_n^2 x_1 - 2\zeta\omega_n x_2$$

$$\begin{bmatrix} \dot{x_1} \\ \dot{x_2} \end{bmatrix} = \begin{bmatrix} 0 & 1 \\ \omega_n^2 x_1 & -2\zeta\omega_n \end{bmatrix} \begin{bmatrix} x_1 \\ x_2 \end{bmatrix}$$

Which can be represented as,

$$\dot{X(t)} = AX(t)$$

If $x_1\ and\ x_2$ are desired responses output can be presented in the form of y(t)

$$y(t) = \begin{bmatrix} 1 & 0 \\ 0 & 1 \end{bmatrix} \begin{bmatrix} x_1 \\ x_2 \end{bmatrix}$$

$$y(t) = Cx(t)$$

By taking Laplace transform we have,

$$sX(s) - x(0) = AX(s)$$

$$X(s) = (sI - A)^{-1} x(0)$$

Where

$$(sI - A) = \begin{bmatrix} s & -1 \\ \omega_n^2 & s + 2\zeta\omega_n \end{bmatrix}$$

Substituting for $(sI - A)^{-1}$ we have,

$$X(s) = \frac{\begin{bmatrix} s + 2\zeta\omega_n & 1 \\ -\omega_n^2 & s \end{bmatrix}}{s^2 + 2\,\zeta\,\omega_n\; s \;+\; \omega_n^2} x(0)$$

Incase rotor is disturbed by small angle $\Delta\delta_0$, then $x_1(0) = \Delta\delta_0$ and $x_2(0) = \Delta\omega_0 = 0$ then we get,

$$\Delta\delta(s) = \frac{(s + 2\zeta\omega_n)\Delta\delta_0}{s^2 + 2\,\zeta\,\omega_n\; s \;+\; \omega_n^2}$$

Taking inverse Laplace transform results in,

$$\Delta\delta = \frac{\Delta\delta_0}{\sqrt{1 - \zeta^2}} e^{-\zeta\omega_n t} \sin(\omega_d\, t + \theta)$$

Where $\theta$ is given by,

$$\theta = \cos^{-1}\zeta$$

Therefore, motion of rotor relative to synchronously rotating revolving field is,

$$\delta = \delta_0 + \frac{\Delta\delta_0}{\sqrt{(1 - \zeta^2)}} e^{-\zeta\,\omega_n t} \sin(\omega_d\, t + \theta)$$

Where $\delta_0$ is initial rotor angle value.

# APPENDIX III

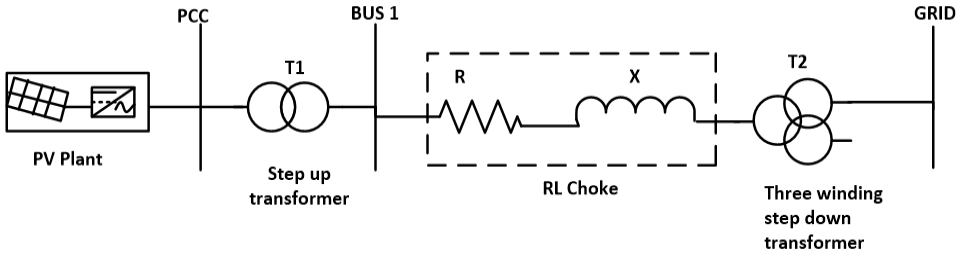


Fig.1 Schematic representation of PV farm connected to grid

MVA Rating- 750KVA
Number of modules connected in parallel Npar -270
Number of modules connected in series Nser -10
Module Data
Maximum power Pmax- 305.226W
Number of cells per module Ncell -96
Transformer

Table1. Transformer data utilized for simulation

| Two winding transformer | Three winding transformer |
|---|---|
| Star grounded/ Delta Lag | Star Floating/ Star grounded/ Delta lag |
| 0.48kV/39.664kV | 154kV/22.899kV/5.716kV |
| R1- 3.840mΩ | R1- 1.067Ω |
| L1- 61.115µH | L1- 242.726mH |
| R2 - 2.913Ω | R2 -52.44× $10^{-9}$Ω |
| L2 - 46.368mH | L2 - 139.111× $10^{-12}$H |
| | R3 - 490.00× $10^{-6}$Ω |
| | L3 - 154.4× $10^{-6}$H |

Table2. Choke data utilized for simulation

| | | Zero sequence | Direct sequence |
|---|---|---|---|
| Choke 1 & 2 | R | 443.109mΩ | 132.11mΩ |
| | L | 1.801mH | 424.55µH |
| Choke 3 | R | 3.866Ω | 972.367mΩ |
| | L | 44.162mH | 16.294mH |